Final Research Performance Progress Report

Project Title: New Fuel Cell Membranes with Improved Durability and Performance

Project Period: October 1, 2013 to September 30th, 2017

Date of Report: December 29th, 2017 (Amended November 8th, 2018)

Recipient: 3M Company, Fuel Cell Components Program, Maplewood MN, 55144

DUNS number: 00-617-3082

Award Number: DE - EE0006362

Contact: Technical: Michael Yandrasits, 651-733-5719, mayandrasits@mmm.com

Contract Manager: Steven Kays, 651-737-0853, slkays@mmm.com

Subrecipients: **General Motors Fuel Cell Activities, Pontiac MI – Craig Gittleman**

Vanderbilt University, Nashville, TN – Peter Pintaro

Submitted to: US Department of Energy Fuel Cell Technologies Office

DOE Managers: DOE Technology Development Manager: Dimitrios Papageorgopoulos

DOE Project Officer: Greg Kleen

Signature of Submitting Official: _____

Executive Summary

The objective of this project was to meet all the DOE Fuel Cell Technologies Office Multi-Year Research, Development and Demonstration Plan for membrane performance, durability and cost targets simultaneously with a single membrane. The approach was to develop new proton exchange membranes, integrate them into membrane electrode assemblies (MEA's) and then evaluate them in single fuel cells and finally fuel cell stacks. These membranes were based on Multi Acid Side Chain (MASC) ionomers containing stabilizing additives and reinforced with electrospun nanofibers.

The ionomers developed at 3M are based on a fluorinated polymer with side chains that contain one or more sulfonamide groups and a sulfonic acid group. Both of these groups facilitate proton transport and ionomers were made that show exceptional conductivity, especially at hot and dry conditions. At the same time, 3M and Vanderbilt University developed new mechanical support technology based on electrospun nanofibers. The membranes made by combining the new ionomers and nanofiber supports were evaluated at 3M and General Motors and met all the DOE technical targets except for one; the resistance at 120°C and 40 kPa water vapor pressure. A detailed analysis of the membrane requirements needed to meet this target was completed. The DOE cost target was evaluated internally but not publicly disclosed.

In the final year of the project a durability issue was identified with the sulfonimide link in the MASC polymer. Accelerated durability testing revealed a decay in performance along with an increase in membrane resistance. And, despite the fact the all but one of DOE technical targets and both Go/No Go milestones were met in the fourth and eight quarters, the membranes developed in this project could not pass the final project milestone of 2,000 hours testing in an automotive fuel cell stack at GM.

Work in the final year focused on understanding the nature of the ionomer stability. New test methods were employed such as multilayer membrane tests that allowed for detailed analysis of membranes at the end of life. Model compound studies of small molecules were initiated to investigate the stability of the sulfonimide and other functional groups present in the ionomer. At the conclusion of the project, an effective strategy to improve the ionomer stability has yet to be identified.

Despite the setback with the ionomer stability, this project has demonstrated significant advances in the field of fluorinated proton exchange membranes for automotive and other applications. The concept of multi-acid side chain ionomers had proven to be an effective strategy to reduce membrane resistance and electrospun nanofibers proven to be a viable mechanical support technology. We intend to build on these results in future membrane development efforts.

Accomplishments

The accomplishments for this project are represented in Table 1 with the summary of performance measurements for the Milestone 8 membrane compared to the DOE membrane targets for 2020. This membrane consisted of a perfluoro imide acid (PFIA) ionomer that contained an electrospun nanofiber and peroxide stabilizing additives. The membrane was optimized for performance and durability and served as the basis for additional membranes fabricated for stack testing. A discussion of the work to develop this membrane is presented in this report under Tasks 1 through 4.

In addition to the specific membrane targets, quarterly milestones where established for the project including two Go/No Go milestones at the end of the 4th and 8th quarters. A detailed summary of these millstones along with the month and date they were completed is shown in Table 2. Each milestone was successfully completed except for Milestone 12; stack testing for 2,000 hours. This is a challenging milestone, especially for an experimental membrane, however, the interim results throughout the project suggested that this target was possible. It was determined in the later stages of development that the sulfonimde group in the PFIA ionomer is subject to oxidative degradation in accelerated testing. Stack testing preceded, however, membranes fabricated with this ionomer lasted for about 830 hours, falling short of the 2,000 hour target. The oxidative stability of the ionomer is suspected to be the cause of this failure.

Nonetheless, significant advances in membrane and support technology where achieved throughout the course of this project and are detailed in the body of the report. A few notable examples include;

- The development of ionomers based on a perfluoro ionene chain extended (PFICE) side-chain and the recognition of the conductivity limits of this system.
- The development of a swell vs fiber content model based on a rule of mixing analysis of ionomer and support modulus values.
- The development of a reinforced membrane based on a single blended fiber containing ionomer and support polymer.
- Pilot scale production of perfluoro sulfonimide acid (PFIA) ionomer.
- New multi-layer membrane electrode assembly methods were developed to study the chemical changes in a membrane after accelerated aging.

Table 1. DOE Membrane Targets and results for the best membrane developed in this project.

Characteristic	Units	2020 Targets	MS#8 PFIA-S (10 um)
Maximum oxygen cross-over	mA / cm^2	2	0.6[a], 3.5[b]
Maximum hydrogen cross-over	mA / cm^2	2	1.9[c]
Area specific proton resistance at:			
120°C, P_{H2O} 40 kPa	Ohm cm^2	0.02	0.054
120°C P_{H2O} 80 kPa	Ohm cm^2	0.02	0.019
80°C P_{H2O} 25 kPa	Ohm cm^2	0.02	0.020
80°C P_{H2O} 45 kPa	Ohm cm^2	0.02	0.008
30°C P_{H2O} up to 4 kPa	Ohm cm^2	0.03	0.018
-20°C	Ohm cm^2	0.2	0.2[d]
Minimum electrical resistance	Ohm cm^2	1,000	1,635[e]
Cost	\$ / m^2	20	Not available
Durability			
Mechanical	Cycles with <10 sccm crossover	20,000	>24,000
Chemical	hrs	>500	614

a. O_2 crossover based on DOE Table 3.4.12 indicating measurement at 0.5V
b. Calculated from GM O_2 permeability data at 80°C, 100% RH, 1 atm air.
c. In cell measurements at 3M 70°C, 100% RH, 1 atm.
d. Calculated from in-plan data
e. Data provided by GM

Table 2. Milestone Summary Table

Number	Milestone	Date Completed
1	Measure conductivity and fuel cell performance on at least two different control PFSA membranes and initial samples of MASC ionomer membranes. Demonstrate MASC ionomer with conductivity of 0.1 S/cm or higher at 80°C and <50% RH.	**January, 2014**
2	Identify one or more polymer systems for further development in a nanofiber support that provides a membrane with x-y swelling of < 5% after boiling in water.	**April, 2014**
3	Develop electrospinning conditions for one or more 3M ionomers that provides fiber diameter of <1 micron.	**May, 2014**
4 **Go/No-Go**	Develop a laboratory produced membrane using an optimized ionomer and electrospun nanofiber support that passes all of the tests shown in tables D3 (chemical stability) and D4 (mechanical stability) of the FOA while still showing performance in single cell polarization experiments above state of the art, mass produced membranes (nanofiber supported 725 EW 3M Membranes) tested in the beginning of this program (not to be less than 0.5 V at 1.5 A/cm2 at 95C, 50%RH, 150 kPa inlet pressure, and 0.4 mg/cm2 total pgm catalyst loading).	**October, 2014**
5	Prepare at least one additional MASC polymer. Demonstrate conductivity of 0.1 S/cm or higher at 80°C and <40% RH. Evaluate in a supported membrane in Fuel Cell and ex situ tests.	**March, 2015**
6	Prepare dense electrospun films with and without surface treatment of the support polymer with a maximum void fraction of <5%. Prepare and characterize the resulting nanofiber composite membranes. Determine if surface treatment impacts swell, tensile or tear properties of the membrane. Select surface treatment, if any.	**April, 2015**
7	Prepare an ionomer formulation (ionomer, stabilizing additive) with optimum performance and durability that provides >500 hours in test D3 (chemical stability), and equal or better area specific resistance (ASR) to the membrane described in the Q4 milestone of the same thickness, evaluated in a 50cm2 fuel cell using the	**June, 2015**

	same MEA components and same support, to be used for development of the supported membrane described in milestone Q8.	
8 **Go/No-Go**	Produce membrane comprising a MASC Ionomer, a nanofiber support and a stabilizing additive which meets all of the 2020 membrane milestones in Table 3.4.12 (Technical Targets: Membranes for Transportation Applications) in the DOE Fuel Cell Technologies Office Multi-Year Research, Development and Demonstration Plan, section 3.4, update July 2013.	**October, 2015**
9	Develop a process for producing the membrane described in Milestone Q8 in quantities large enough to produce membranes for use in Milestone Q10 (at least 20 linear meters)	**January, 2016**
10	Manufacture for stack testing at least 30 MEAs with a minimum cell area of 250 cm2. Evaluate in fuel cells and ex situ tests. Begin stack testing.	**April, 2016**
11	Begin post mortem analysis of MEAs to determine failure mode.	**December, 2016**
12	Prepare the MEAs, the number and size to be determined by 3M and the DOE, and deliver them for testing at a DOE approved facility. Complete stack testing for a minimum of 2,000 hours.	**Test terminated after 1,000 hrs**

Project Overview

This project was led by 3M as the prime contractor with Vanderbilt University and General Motors as subcontractors. The work was split into ionomer development (Task 1), nanofiber and membrane development (Task 2), ex-situ ionomer and membrane testing (Task3), MEA fabrication and fuel cell testing (Task 4), stack testing (task 5) and project management and reporting (Task 6). This report is organized by task number and highlights are reported in each section. In addition to the tasks, milestones were developed in cooperation with the DOE program managers and reported throughout the project. The overriding objective of this work was to meet the DOE targets for fuel cell membrane set out in the DOE Multi-Year RD&D plan and the milestones were drafted with this goal in mind and results pertaining to these milestones are reported where appropriate.

Task 1 Ionomer Development

Task 1.1 Lab development

There are very few chemically stable, water insoluble, polymers capable of addressing targets set by the DOE in the Multi-Year Research and Development Plan. The approach we focused on in this project is to further develop ionomers that have multiple acids per side chain. The advantage of the multi-acid side chain (MASC) technology is the ability to use a wide range of starting EW(equivalent weight), oxidatively stable, perfluorinated polymers. This flexibility allows us to address cost, mechanical properties and fuel cell performance. The chemistry also provides an ability to disconnect the effects of starting copolymer monomer ratio - and its intrinsic EW and backbone crystallinity - on mechanical, water uptake, and conductivity properties. The resulting MASC polymer, having the original backbone crystallinity, along with the additional side chain strong acid groups, combine the best of both worlds: mechanical strength and lower water uptake with improved conductivity and performance. The main multi-acid ionomer we focused on was the perfluoro imide-acid (PFIA) material shown in Figure 1. This ionomer is produced by attaching an additional sulfonic acid group to an already polymerized ionomer through the use of a perfluoro imide functionality. The proton on the sulfonimide is very acidic and serves as an additional protogenic group. A typical fluorine nuclear magnetic resonance (F^{19}NMR) spectra is shown in Figure 2 along with the relevant peak assignments.

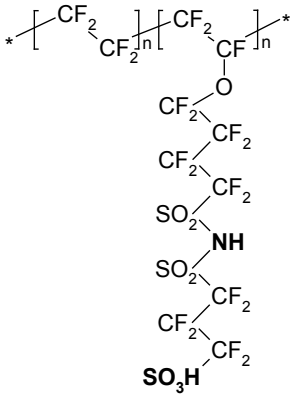

Figure 1. Perfluoro imide acid (PFIA) ionomer.

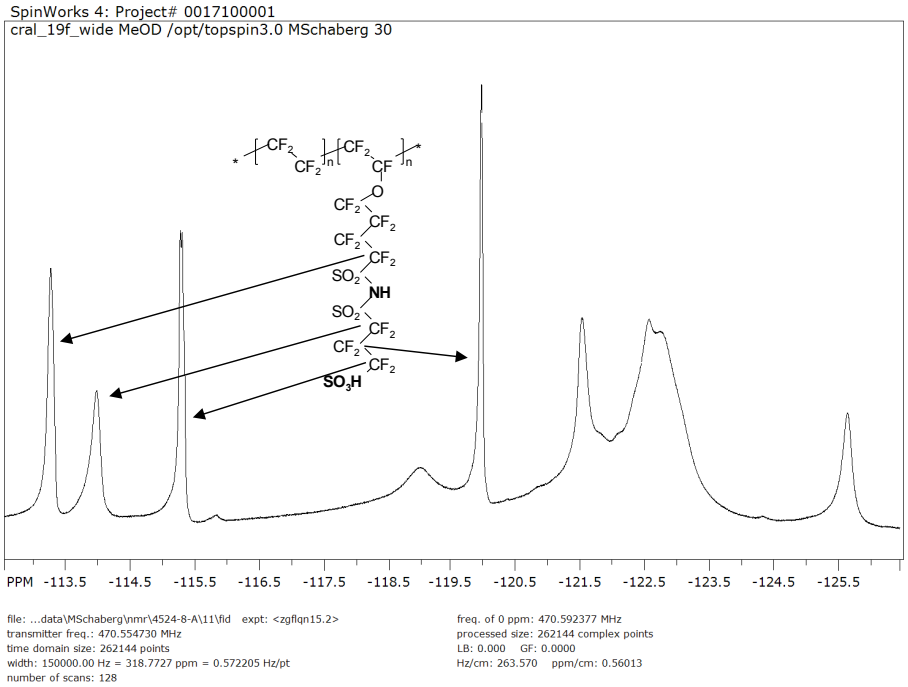

Figure 2. NMR spectra for recent pilot scale trial showing good conversion to the PFIA form of the polymer.

We have produced several different PFIA polymers using a range of backbone equivalent weights(EW) between 700 and 850 g/mol. Coated proton exchange membranes (PEMs) of these polymers have undergone conductivity testing and were compared to several different EW 3M PFSA polymers. Samples of PFIA polymer solution and PEM films were prepared and shipped to our colleagues at General Motors(GM) and Vanderbilt University for characterization in PEM testing and for use in electrospinning experiments to create new membranes.

Perfluoroionene chain extended (PFICE) development

Perfluoro Ionene Chain Extended (PFICE) polymers are the next extension of the multi-acid side chain (MASC) idea where several sulfonimde groups are added to the same side chain along with a terminal sulfonic acid group. The synthetic route employed is similar to that for the PFIA polymer but rather than hydrolyzing the terminal sulfonyl fluoride after the first bis sulfonyl fluoride is added it is further reacted with ammonia form an amide. A second bis sulfonyl fluoride is attached to form an ionene chain of two repeat units (Figure 3). The nomenclature for the PFICE-x ionomers indicates the total number of acids as x (sulfonimide plus sulfonic acid) per side chain.

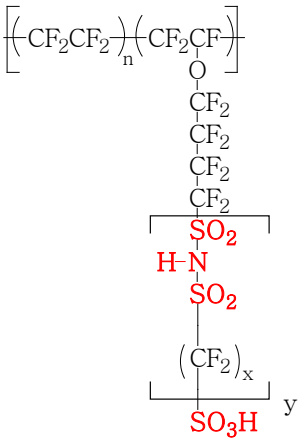

Figure 3. General structure for perfluroionene chain extended (PFICE) polymer. Typically, x = 3 and y > 1.

An important area of focus for this project was the creation of polymers to address the very difficult conductivity target of 100mS @ 40% RH & 80°C. Our aim was to push the MASC technology synthesis to produce ultra-low equivalent weight (EW) polymers by incrementally building up acid content. The PFICE polymers have been found to produce well behaved coating solutions and proton exchange membranes for testing. Note that the two-acid side chain, PFICE-2, is the same structure as the PFIA. Theoretical EWs and titration data are shown in Table 3. The average titration numbers are reasonable given the attachment efficiency is not expected to be 100% for each reaction step.

Table 3. Expected and titrated equivalent weight for new PFICE polymers

Ionomer	n	Theoretical	Titration
PFICE-2	1	501	612 ± 64
PFICE-3	2	431	503 ± 73
PFICE-4	3	397	480 ± 107

These results, however, have a larger 95% confidence interval than we would like, nonetheless, a fully fluorinated ionomer with an equivalent weight of about 480 g/mol is quite remarkable.

Model Compound Studies

Model compound studies were initiated to better understand the chemical stability of the PFIA Structure. Each functional group present in the ionomers were probed in the small molecule form to observe decomposition rates and correlate them to degradation pathways. The objective of this work is to isolate the various functionalities such as the sulfonimide and sulfonic acid groups from one another to study relative stabilities. In addition, compounds with combined functional groups can be studied to look for the impact of groups in close proximity to each other. A photo Fenton's method was chosen to best control the generation rate of peroxide radicals for these experiments. Work included screening concentrations, pH, and UV intensity. Functional group screening has started but not yet completed. 3M will continue this work

beyond the end of this project. Compounds containing perfluorocarboxylic acids, perfluorosulfonic acids, perfluorosulfonamides, perfluorosulfonimides, perfluoro ethers, and combinations will be studied. Initial degradation will be observed with ^{19}F NMR and leads will be pursued with other characterization methods. Figure 4 shows a series of model compounds that have been made in our labs for the start of this study.

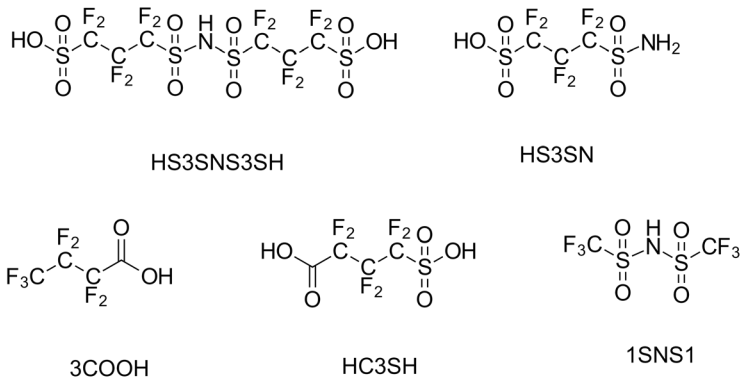

Figure 4. Model compounds studied using photo-Fenton's method.

This work assumes that hydroxyl radical is one of the main reactive species initiating degradation. To probe this process, a photo-Fenton test has been developed to a generate a high concentration of radicals from hydrogen peroxide. There is precedent for classic Fenton's testing of ionomers by adding catalytic iron to membrane and soaking in hydrogen peroxide at elevated temperatures. This method, however, is difficult to control and inconsistencies or unknowns as to the amount and rate of radical production complicated data interpretation. Photo-Fenton uses 254 nm light to photolytically cleave hydrogen peroxide without a need for metal catalysts.

The peroxide degradation rate can be quantified using a ceric sulfate titration. Initial tests standardized the peroxide loss under various conditions such as pH and UV intensity (Figure 5). The results are reliable, reproducible, and consistently show that 3% peroxide can be fully degraded within two hours at full UV intensity. Lowering UV intensity and pH slow the degradation rate.

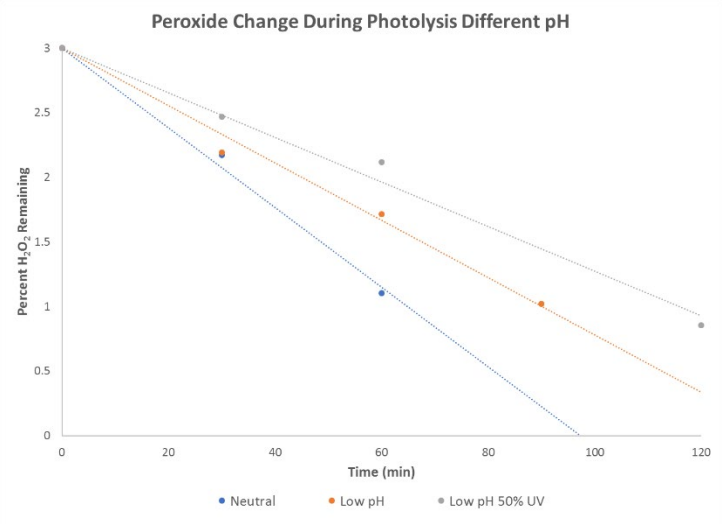

Figure 5 Titration results of photo-Fenton degradation of hydrogen peroxide.

Once initial understanding of functional group responses to the photo-Fenton conditions are gained, synthesis of other model compounds will begin to provide further detail. The reaction scheme outlined in Figure 6 shows compounds that can be synthesized based on reacting the saturated monomer (CF_3-CF_2-O-C_4F_8-SO_2F) with ammonia to make the sulfonamide as a starting material.

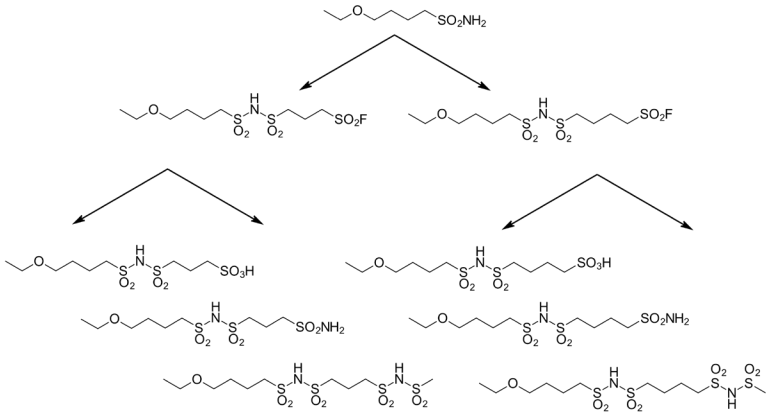

Figure 6. Reaction scheme showing the possible model compounds based on PFIA side chain chemistry. Compounds on the left have 3 CF_2's between the imide and terminal group, those on the right have 4 CF_2's.

The two main groups in the above figure correspond to a series with three carbons between the sulfonamide and the terminal functional group (left set) and a series with four carbons between these groups (right set). By changing the nature of the terminal group and the length of the spacer, we hope to better understand the roll of inductive effects on the ultimate stability of the sulfonimide functionality.

Task 1.2 Pilot Scale Development

The results for the PFIA ionomer from both this project and previous work at 3M led to the decision to pursue the scale-up of this synthesis to the pilot level. Efforts included; optimization of the synthetic process, developing quality control (QC) analytical tests suitable for pilot plant testing, and various safety and engineering reviews. Significant effort has been made to establish process and product understanding to allow for successful scale-up of the PFIA polymer. The development work and first pilot scale run were completed for this project.

A critical part of this effort is the development of QC analytical tests. These are aimed at testing reaction completion and product purity in a pilot plant setting. Fourier transform infrared (FTIR) spectroscopy methods can be used to measure the percent unreacted starting material of sulfonyl fluoride to sulfonamide (step 1) and sulfonamide to sulfonyl fluoride (step 2) were developed. In addition to setting specifications for reaction completion, we have worked to quantify the amount of residual small molecules that are used during the synthesis and must be removed upon isolation of PFIA. Inadequate removal could lead to suboptimal fuel cell performance due to catalyst poisoning or membrane degradation.

Safety and engineering reviews were conducted in accordance with 3M's safety policies. The synthetic methods developed for scale-up have been designed by a process chemist and have been reviewed by a pilot plant engineer. The process has also undergone a safety review to ensure that the proposed synthesis can be safely completed in a larger scale setting.

The first pilot scale lot was designated for use in this program while subsequent lots are not formally included as a part of this project. This distinction will allow 3M to use the additional PFIA lots for both DOE project objectives and for commercial product development. It should be noted that the quantity of material produced is still relatively small with batch sizes of about two kilograms up to tens of kilograms. Table 4 outlines the approximate production date, equivalent weight, and designated used for each batch. Lots 3 and 4 were independently synthesized but combined in the dispersion step to allow for a greater quantity for membrane experiments. The designation lot 3/4 is used for the combined ionomers.

Each pilot scale batch typically has two purposes; 1) to provide high quality polymer for characterization and membrane fabrication and 2) develop the manufacturing methods for larger scale synthesis of PFIA ionomer. One area where improvements are being made is the efficiency of the side chain attachments to the starting polymer. The ^{19}F NMR data shown in Figure 7 compares the first five lots of PFIA. These data show that the primary product is the desired PFIA as determined by the peaks in the -114 to -115.5 ppm range. However, the small peak at about -115.7 ppm represents a small portion for the polymer side chain that has not been fully reacted in lot 1 but appears to be significantly diminished or absent in lots 2, 3, and 4.

Table 4. Summary of PFIA Pilot Scale Lots

Lot Number	Date	Titrated EW	Program
1	January 2015	660	DOE

2	December 2015	652	3M
3 and 4	March 2016	625	3M
5	Sept 2016	650	3M

In addition to the NMR data, conductivity has been measured for each of the pilot scale lots. The data in Figure 8 shows the PFIA lots in red colors and a 725EW PFSA in blue. As expected, each of the PFIA membranes shows improved conductivity over the very low EW PFSA.

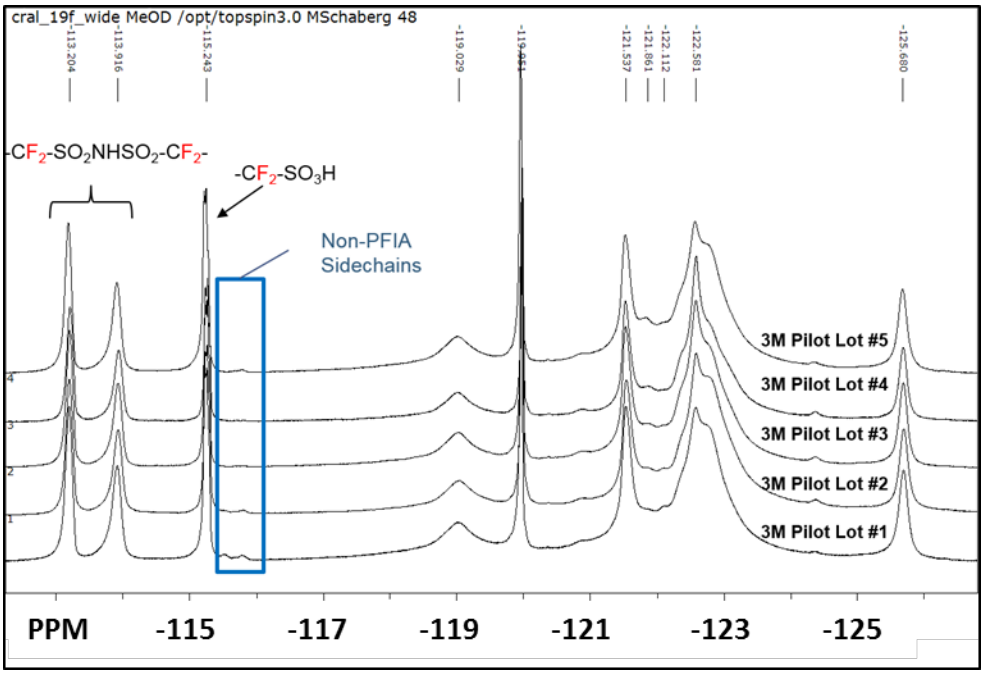

Figure 7. 19F NMR of five pilot lots of PFIA ionomer. Successful reaction is indicated by the lack of peaks in the region outlined by the blue box.

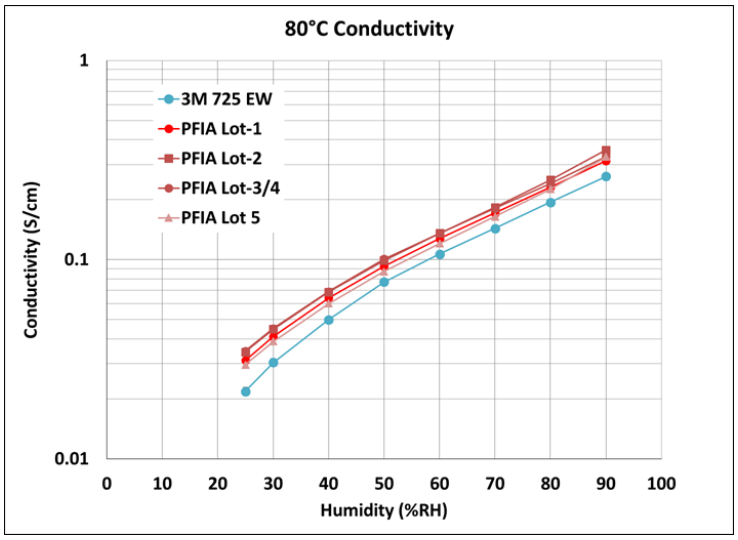

Figure 8. Four point probe conductivity for the last five pilot scale lots of PFIA (red) compared to a 725EW PFSA control (blue).

Despite the success in bringing the PFIA synthesis from lab scale to pilot scale production, we recognized in the final years of the project that there was a stability issue with this ionomer. Details of the stability concerns are explained in detail in Subtask 4.3 (Accelerated Stress Testing) of this report. In short, extensive durability testing has shown the carbon sulfur bond in bis sulfonyl imide group of the PFIA is subject to oxidative attack in a similar way as the sulfonic acid group in a traditional PFSA. The fundamental stability of these bonds may not be very different between the PFIA and PFSA but the consequences to membrane and electrode performance appear to be more severe in the PFIA case. Because of this observation, and the lack of a feasible solution to the problem, 3M has discontinued our scale-up efforts at this time. It is possible this work will be revisited if another application is identified in the future.

Task 2 Nanofiber and Membrane Development

In addition to the ionomer work, improved mechanical support is required for a commercially viable membrane. The objective of this task is to identify new nanofiber technology that improves upon the existing material and to be able to fabricate membranes from these new supports. Responsibility for this task is shared between 3M and Vanderbilt and the reporting is split between each group under according to subtask.

Subtask 2.1 Nanofiber Development

Subtask 2.2.1 3M Nanofiber Development Activities

The objective of this task is to improve the durability and strength properties of the nanofiber support used in our 3M composite membranes. In addition, it is expected that the increased

swell values measured for multi-acid side chain (MASC) ionomers will require new nanofiber constructions to counteract these swelling forces in the in-plane dimensions.

Candidate polymers must have excellent hydrolytic, oxidative, thermal stability, and be soluble in common solvents suitable for electrospinning. We have identified both fluoropolymers and fully aromatic polymers for initial experiments. These polymers will be evaluated as the sole fiber component, in polymer blends, or fiber blends. In, addition chemical modifications such as surface treatments or cross linking will be evaluated.

Early in the project we focused work on Milestone 2: "*Identify one or more polymer systems for further development in a nanofiber support that provides a membrane with x-y swelling of < 5% after boiling in water"* A first step in this effort was to review the historical swelling data for previously made supported membranes.

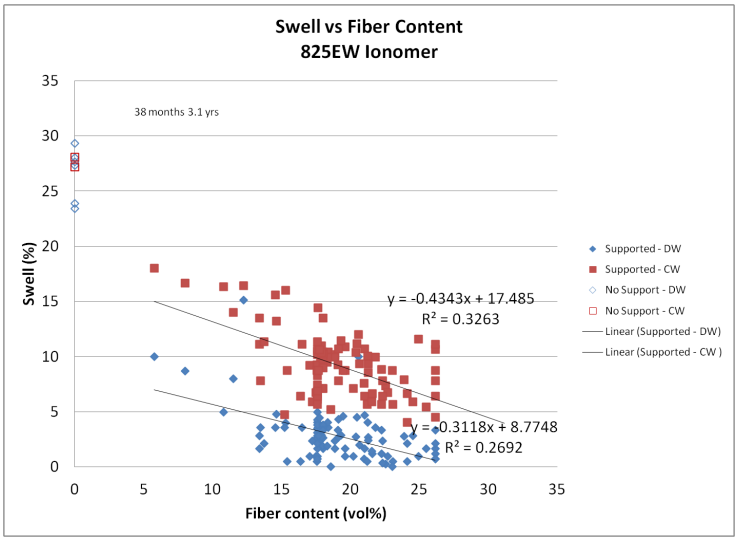

Figure 9. Historical swell data for 3M supported membranes. Red squares represent swell in the cross web direction and blue diamonds represent swell in the down web direction.

As can be seen in Figure 9, there is a clear difference in down web and cross web swelling properties as a result of the fiber manufacturing conditions. From these data, we can estimate that a fiber content of about 12% is needed to make a membrane with swell less than five percent in the down web direction and about 25% fiber contend for swell less than 5% in the cross web direction.

A comprehensive summary of all of the nanofiber development conducted at 3M is beyond the scope of this report, however a summary of the samples fabricated or obtained from outside sources, including our partners at Vanderbilt University are summarized in Table 5. Since many of the materials and sources are confidential to 3M, the polymers used and sources are reported with coded values defined at the bottom of the table. Throughout the project efforts were made to improve the nanofiber support through the use of new polymers or new processing conditions.

Table 5 Coded Nanofiber Samples Produced in Q3

Coded Sample	Form	Coded polymer	Coded Source	Basis weight (g/m2)	Objective
Q1 and Q2 samples					
S1	roll	B1	P1	4.3	Control
S2	roll	B2	P1	3.2	Improved tear strength
S3	roll	B2	P1	4.3	Improved tear strength
S4	test patch	FC3	L2	n/a	Electrospining feasibility
S5	test patch	FC4	L2	n/a	Electrospining feasibility
S6	test patch	FC5	L2	n/a	Electrospining feasibility
S7	test patch	FC6	L2	n/a	Electrospining feasibility
S8	roll	HC3	P1	4.3	Modulus study
S9	roll	FC1	P1	4.3	Modulus study
S10	roll	FC1	P1	3.2	Modulus study
S11	sheet	FC3	L1	5	Improved tear strength
S12	sheet	FC3	L1	5	Improved tear strength
S13	sheet	HC2	V	5.7	Modulus study
S14	sheet	HC2	V	14.2	Modulus study
Q3 samples					
S15	roll	FC1	P1	4.3	New polymer
S16	roll	FC1	P1	3.2	New polymer
S17	sheet	H4	L3	4.0	New polymer
S18	sheet	FC3	P1	4.1	New polymer
S19	sheet	FC4	P1	4.2	New polymer
S20	sheet	B1	P1	4.4	New process
Q4 Samples					
S21	sheet	FC1	P2	5.02	MD/TD (alternate supplier)
S22	sheet	HC1	P2	4.33	MD/TD (alternate supplier)
Q5 Samples					
S23	roll	ePTFE-1	P3	2.25	ePTFE Comparison
S24	roll	ePTFE-2	P3	5.66	ePTFE Comparison
S25	roll	ePTFE-3	P3	6.33	ePTFE Comparison
S26	roll	FC1	P1	4.4	MD/TD experiment
S27	roll	FC1	P1	4.28	MD/TD experiment
S28	roll	FC1	P1	4.36	MD/TD experiment
S29	roll	FC1	P1	4.39	MD/TD experiment

S30	roll	ePTFE-4	P3	5.40	ePTFE Comparison
Q7 Samples					
S31	roll	FC1	P2	5	MD/TD
S32	roll	FC1	P2	4.2	MD/TD
S33	roll	FC1	P2	4.9	MD/TD
S34	roll	FC1	P2	3.2	MD/TD
S35	sheet	FC1	P3	7.91	New supplier
S36	sheet	HC4	P4	5.74	New Polymer
S37	sheet	HC4	P5	4.50	New Polymer
Q7 Samples					
S38	Roll	HC4	P5	8.0	New Polymer
Polymer Codes	HC = Hydrocarbon		Source Codes	L = Lab	
	FC = Fluorocarbon			P = Pilot or production line	
	B = Blend			V = Vanderbilit	

An example of the type of results obtained in this work can be illustrated through samples S-18 and S-19. Electron microscope images are shown in Figure 10 of these two samples. Both of these materials are made with fluorocarbon polymers but the S19 sample has a lower melt point and glass transition temperature and shows significant fusing and welding of the fibers and a much denser nonwoven. The S18 sample is considered a more viable candidate.

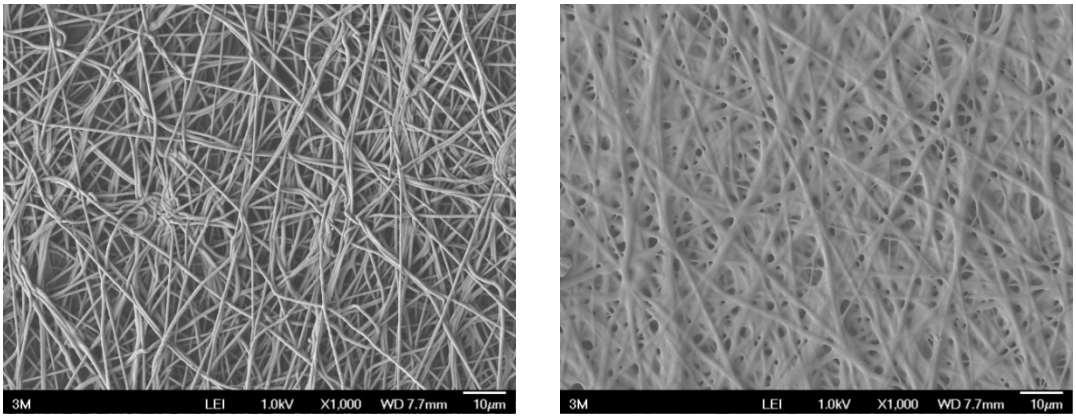

Figure 10. Electron microscope images of nanofiber samples S18 (left) and S19 (right).

Another example of work completed in this task is illustrated using a lab scale electrospinning device at 3M. As part of this work the operating ranges for gap between the spinner needle and fiber collection drum and static potential (kV) were established for one of the candidate polymers in this program (FC1). The working range were fibers are formed is given in Figure 11 for a polymer solution of 12.5 weight percent.

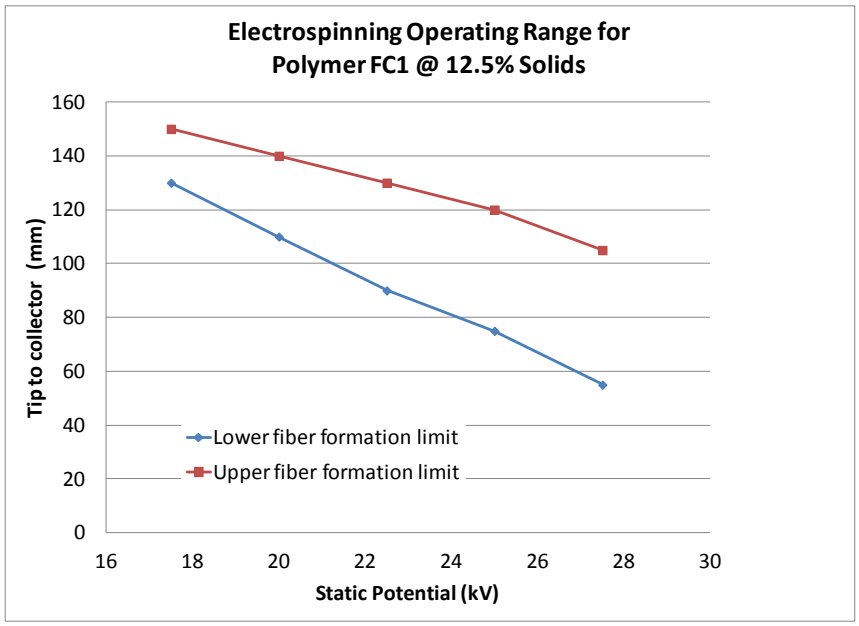

Figure 11. Example of operating range for 3M's new lab electrospinning device. The area between the upper and lower limits defines the range were fibers form for different combinations of applied potential and spinning tip to collector distance.

Machine and transvers direction nanofiber properties

One focus of our nanofiber development efforts has been to reduce or eliminate the differences in tensile properties in the machine directions (MD, also referred to as down-web) and the transverse direction (TD, also referred to as cross-web). The tensile modulus of the support material is critical in determining the linear swell of the composite membrane and, because of this, uniform properties are desired. The tensile properties are defined during production and are a result of process conditions such as line speed and other parameters. Working with our supplier, we designed an experiment where the line speed would be run at normal and half speed conditions. A second parameter, set point #2, was also varied to be 30% or 170% of the normal condition. The graph in Figure 12 shows this design space. The normal conditions are designated by “1” and the changes represented as a fraction of this value.

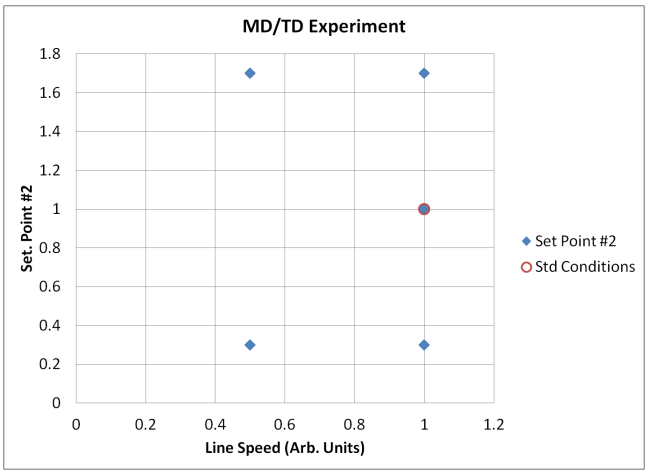

Figure 12. Parameters for a process experiment designed to reduce machine direction (MD) and transvers direction (TD) property differences in nanofiber web.

Approximately 30 meters of each condition was received and tested for tensile properties. The stress-strain data was measured five times for each sample and the curves averaged for comparison (Figure 13).

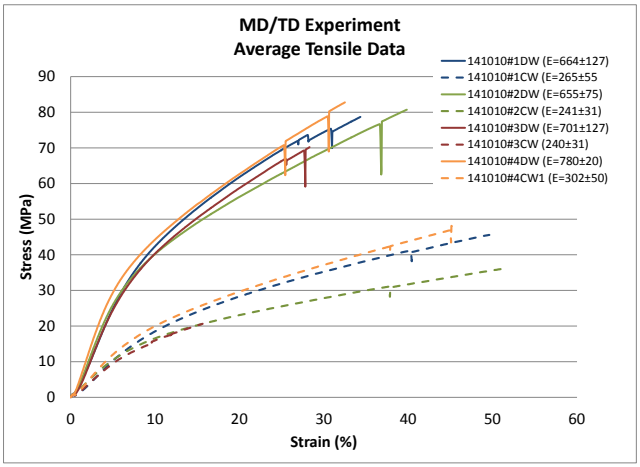

Figure 13. Tensile data for nanofiber samples from MD/TD experiment.

From this data is appears as if there is no difference between tensile properties, in particular the initial modulus, as a function of the process conditions that were varied.

Composite membranes were made from this support material and 3M's 825EW ionomer. The swell values for these membranes are listed in Table 6 along with the modulus data. Similar to the tensile data set there were no clear trends in the swell data and the machine direction or down web (DW) swell was substantially lower than the transvers direction or cross web (CW).

Table 6. Swell data for composite membranes and tensile data for nanofibers only for samples made from MD/TD experimental materials.

Swell	Tensile Modulus

Sample	DW	Stdev	CW	Stdev	DW (MPa)	Stdev	CW (MPa)	Stdev
Control	0.3	0.6	9.2	1.2				
#1	2.0	1.0	8.2	0.6	664	127	265	55
#2	0.3	0.6	10.3	1.6	655	75	241	31
#3	0.0	-	7.8	0.1	701	127	240	31
#4	1.3	1.1	9.2	1.2	780	20	302	50

It is interesting to note that the DW swell values are very nearly zero and lower than one would predict based on the nanofiber modulus and ionomer swell properties only. Additional discussion on the role of nanofiber modulus and its impact on swell will follow in Task 3.2.

Surface treatment

Surface treatment of nanofibers continues to be investigated. This quarter we explored plasma treatments in a several environments. Typical electron microscope images are shown in Figure 14. A thin layer appears to be deposited on the surface of the fibers and there is no obvious damage to the fiber structure.

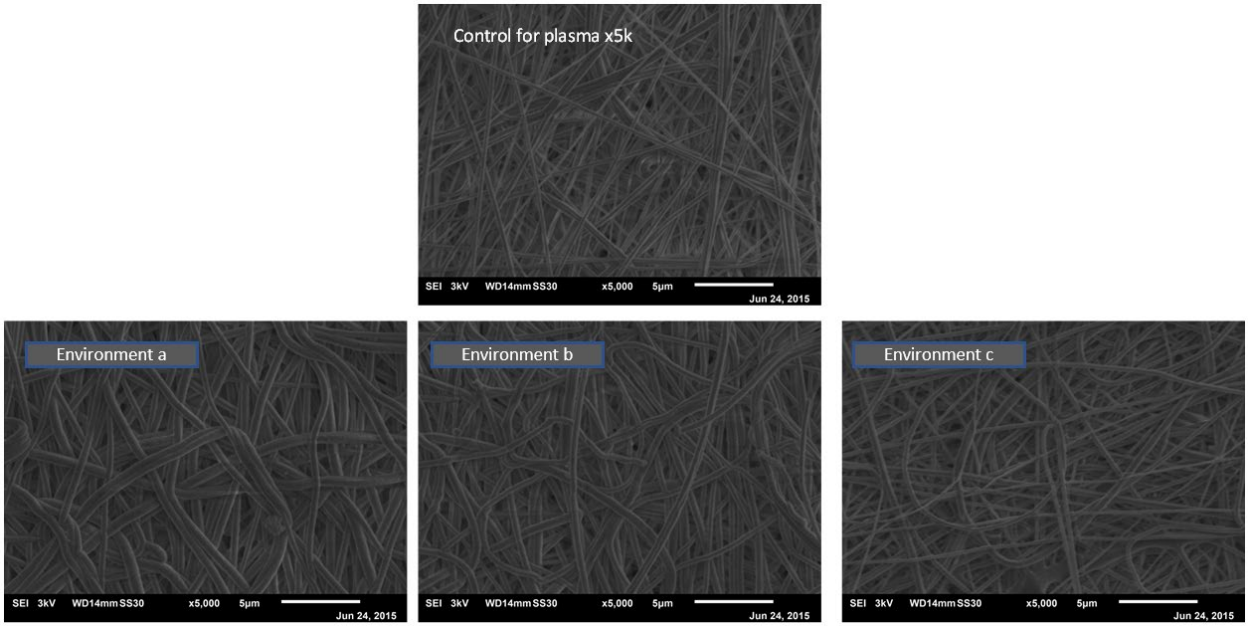

Figure 14. Electron microscope images for three plasma surface treatments compared to a control (top image).

The strength of the plasma treated films were then evaluated in a tensile test (Figure 15). It can be seen from this data that all the treated samples have significantly lower stress and strain at break despite the fact that the fibers appear intact. Exploratory work was continued in this area but to date there has been no advantage observed.

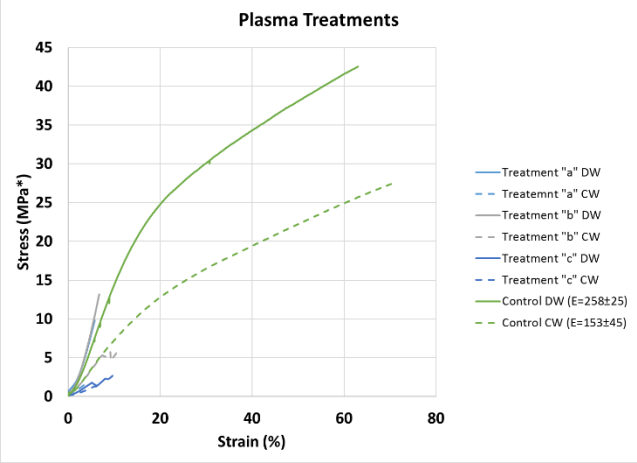

Figure 15. Stress-Strain data for samples treated with a variety of plasma conditions.

Subtask 2.1.2 Vanderbilt Activities Nanofiber Development

A main focus of this work is to identify new fiber systems for use in supported membranes. Historically, expanded polytetrafluorethylene (ePTFE) has been used for this purpose and now electrospinning provides an opportunity to expand the number of viable options. In addition, dual spinning approaches where fibers of support and ionomer are fabricated simultaneously can offer new constructions not possible with traditional fabrication methods.

Electrospinning and welding of PAI reinforcement fiber mats

Solvay's Torlon® polyamide-imide (PAI) is an exceptional polymer with a very high tensile of 152 MPa. It also has excellent resistance to wear and creep and it is table to many chemicals including acids. For these reasons, it is well-suited as the reinforcing component of high-performance fuel-cell membranes. Good quality fiber mats were obtained with a fiber diameter in the 500-1000 nm range. The raw mats show high porosity and, unfortunately, their mechanical strength was very poor. To improve the mat strength inter-fiber welding was performed by exposing the mats to DMAc vapor at room temperature for a specified period of time. This process created welds at some inter-fiber intersections and resulted in improved mat strength, with an accompanied decrease in porosity and mat thickness. Figure 16 depicts the progress of welding process as a function of exposure time to solvent vapor.

It can be seen that for exposure times up to 10 minutes, practically no welding is observed. The formation of inter-fiber welds begins at an exposure time of between 20-30 minutes.

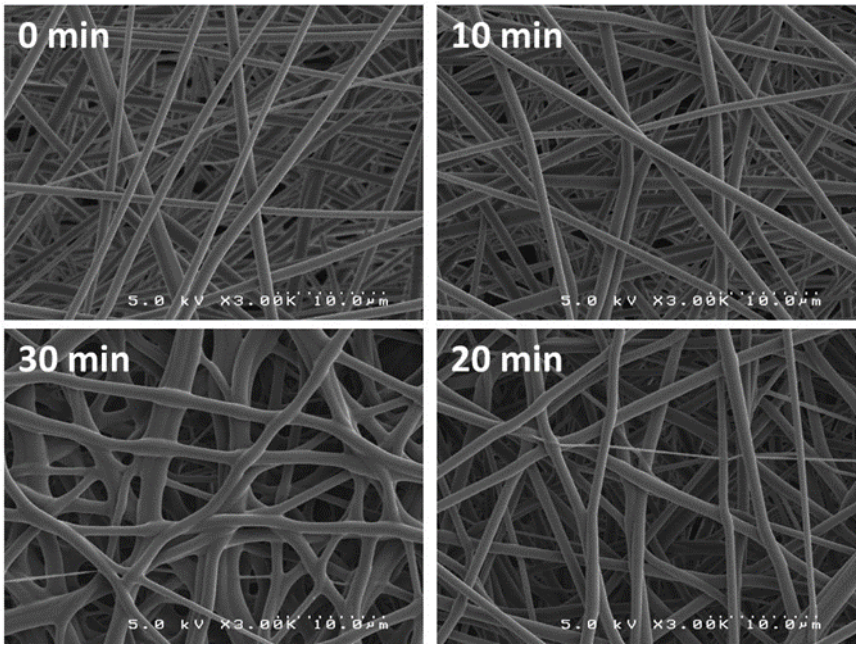

Figure 16. Fiber mat welding progress: SEM micrographs of surfaces of four mats exposed to DMAc solvent vapors for various time periods from 0 to 30 min.

The diameter of the PAI fiber was systematically changed in order to study the effect of this variable on membrane properties. The fiber diameter of an electrospun polymer is dependent on the spinning conditions used to fabricate the fibers. In order to adjust the fiber diameter of reinforcement polymers, the concentration, flow rate, spinner-to-collector (STC) distance, and voltage were varied. SEM Images of the electrospun fibers are shown in Figure 17, where the average fiber diameter is 400, 600, or 1200 nm.

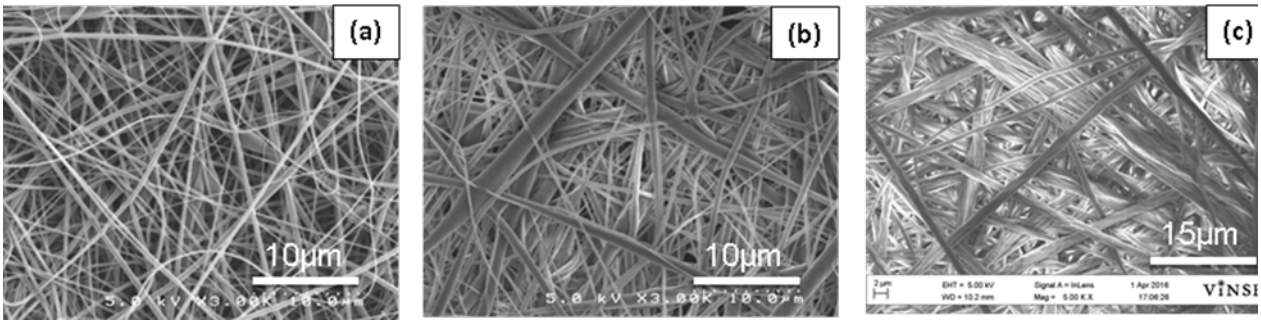

Figure 17. SEM Images of electrospun PAI fiber mats with an average fiber diameter of (a) 400 nm, (b) 600 nm, and (c) 1200 nm.

The 1200 nm PAI fibers were not evaluated for their tensile strength; however, the tensile properties from the 400 nm fibers and 600 nm fibers suggest that increasing the fiber diameters also increases the strength of the fibers. Tensile properties for the porous fiber mats, and for the fibers within a mat (correcting for fiber volume fraction) are shown in Figure 18. After spinning, the fiber mats were pressed to 70% porosity at room temperature. The fiber mat was either tested after densification or an additional processing step was applied, which was welding by

exposure to dimethyl formamide (DMF) vapors for 30 minutes. Increasing the fiber diameters show a significant increase to the strength of the mat (the mat strength nearly doubles from 6 MPa to 13 MPa with the 200 nm (50%) increase in fiber diameter. Similarly, the strength of the welded fibers increases from 17 MPa to 25 MPa in the same range of fiber diameters. In addition to the gains in strength with increased fiber diameter, there is the expected improvement in strength with fiber welding. The 400 nm fiber strengths increase from 6 MPa to 18 MPa with welding, and at 600 nm, the fiber strength increases from 13 to 25 MPa with welding. Upon adjusting for the fiber porosities, the fiber strengths are observed to be as high as 70 MPa. This value is still lower than expected (>100 MPa) and that discrepancy can be associated with the lack of sufficient number of fiber entanglements/welds for effective fiber-to-fiber stress transfer.

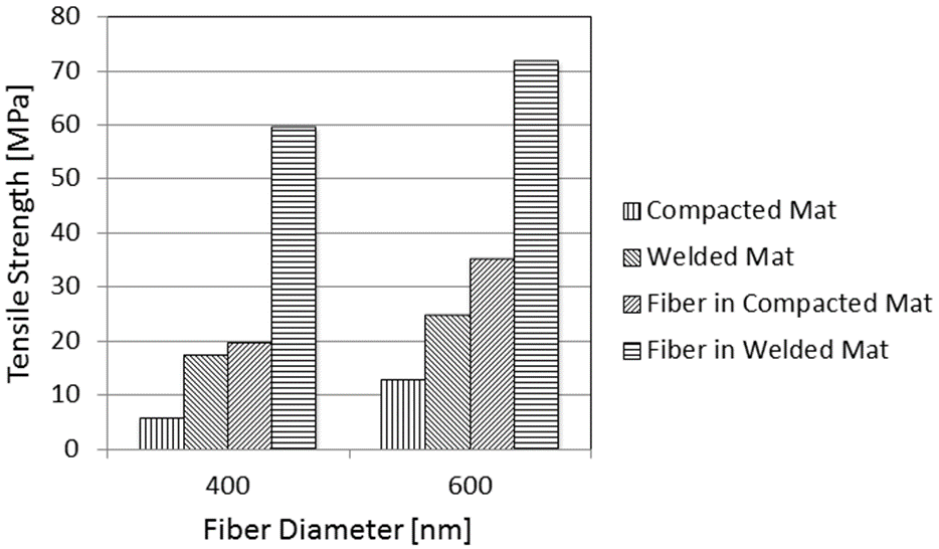

Figure 18. Tensile strength of electrospun PAI fibers

Electrospinning of PFIA ionomer

PFIA nanofiber electrospining experiments were based on our previous experience with electrospinning various PFSA ionomers. In the present study, an n-propanol/water mixed solvent was used and poly(ethylene oxide), PEO, was added as the carrier polymer (without the addition of PEO carrier, only droplet spraying was observed during electrospinning). Various factors effecting electrospinning were investigated, including solution flowrate, accelerating voltage, spinneret-target distance and humidity. Good quality fiber mats were eventually obtained with an average fiber diameter in the 500-1000 nm range. One of the most important factors studied was PEO content and molecular weight (MW). As PEO is foreign to the desired membrane composition, the goal was to minimize its content and employ a low MW PEO so that its removal after electrospinning would be simple and complete. Two PEO MWs, 400,000 and 600,000, were tested and it occurred that the former worked well. In Figure 19, the effect of PEO concentration on the structure of the electrospun mat is presented. As can be seen, the onset of fiber formation occurred at 0.25 wt% PEO. High quality fibers, however, were only

obtained at a PEO concentration of 1 wt%. At 4 wt% PEO, ribbon-type structures were formed along with fibers.

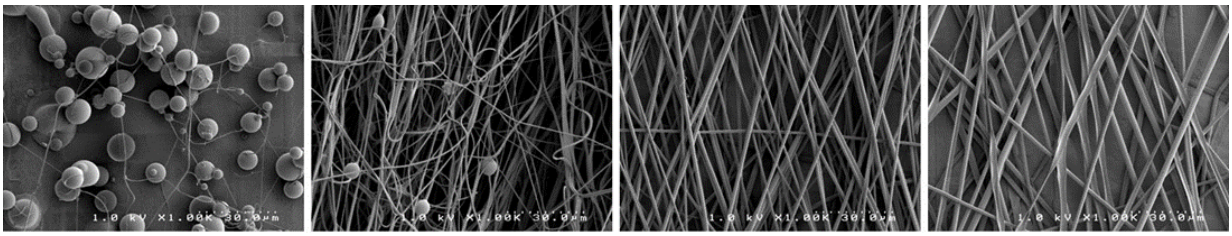

0.25wt% PEO 0.50wt% PEO 1.00wt% PEO 4.00wt% PEO

Figure 19 SEM micrographs of the surfaces of nanofiber mats electrospun with progressively higher PEO (MW=400,000) content.

Experiments were performed to verify that electrospun PFIA had retained its proton conductivity property and that the presence of PEO carrier had no detrimental effects. Two types of PFIA membranes were prepared: (1) a solution cast film and (2) a homogeneous film prepared from a nanofiber mat, where the fibers contained 20 wt% PFIA+1 wt% PEO; the mat was hotpressed which caused the fibers to melt into a homogeneous polymer film. The two membranes were kept in 1M H_2SO_4 at room temperature for 1 h and then washed with DI water. After a 24 hours room temperature water soak, the in-plane proton conductivity of the films was measured at room temperature (23°C) by AC impedance. The results are shown in Table 5.

Table 7. Proton conductivity measured in water for an electrospun and solution cast PFIA.

	Electrospun	Solution cast
Proton Conductivity (S/cm)	0.135	0.138

As can be seen, the proton conductivity of both membranes is similar so it can be concluded that the PEO carrier has been effectively removed and has no effect on PFIA conductivity.

Membranes from electrospun dual-fiber PFSA-PAI mats

One way to make nanofiber composite membranes is to electrospun fibers of support and ionomer simultaneously. This dual fiber approach was investigated to make PFIA-PAI mats. In order to demonstrate this method, Solvay's Torlon and 3M's 825 EW PFSA were concurrently electrospun on a rotating/oscillating drum target, the same as used in our previous electrospinning work. Mat composition was controlled by adjusting the relative flowrates of the PFSA and Torlon solutions during electrospinning. The resultant membranes were conditioned by boiling in 1.0 M H_2SO_4 for 1 hour followed by boiling in water for 1 hr. After storing the membranes in DI water at room temperature overnight, the membrane swelling and proton conductivity were measured. Also, to ensure proper pore closure during mat processing, selected samples were inspected by scanning electron microscope (SEM). A representative

micrograph of the membrane surface is shown in Figure 20. No pores are evident which indicates acceptable mat densification. Some Torlon nanofibers, well bonded with the PFSA matrix, can be seen at the surface.

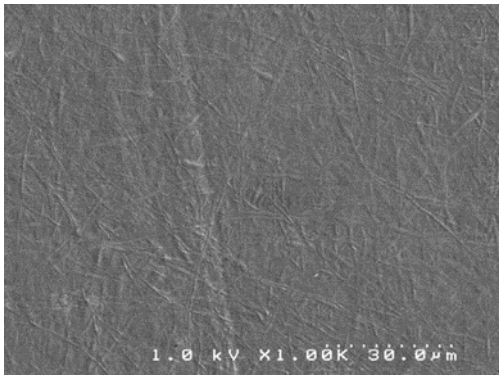

Figure 20. SEM micrograph of surface of 3M PFSA 825 EW/Torlon dual-fiber membrane after post-processing steps. Membrane contains 70 wt.% PFSA. Magnification 1,000x.

The gravimetric and lateral swelling and proton conductivity of a solution cast PFSA film and selected nanofiber composite membranes are shown in Table 8 and Figure 21. As can be seen from Table 8, the presence of Torlon fibers in a composite membrane significantly reduces both water uptake and areal membrane swelling. The significant decrease in lateral membrane swelling is particularly noteworthy. As expected, the addition of uncharged Torlon to PFSA films is accompanied by a loss in proton conductivity. It can be seen in Figure 21 that the increase of Torlon content from 0 to 50 wt.% leads to a 60% drop in conductivity: from 0.112 S/cm (pure PFSA) to 0.043 S/cm (50% Torlon).

Table 8. Swelling data obtained for the solvent cast PFSA 825EW film and the composite membranes fabricated from electrospun dual-fiber PFSA-Torlon mats.

	Water Uptake (g/g)	Lateral Swelling (cm/cm)
Cast PFSA EW825	0.548	0.167
PFSA-20 wt.% Torlon	0.397	0.045
PFSA-40 wt.% Torlon	0.301	0.019

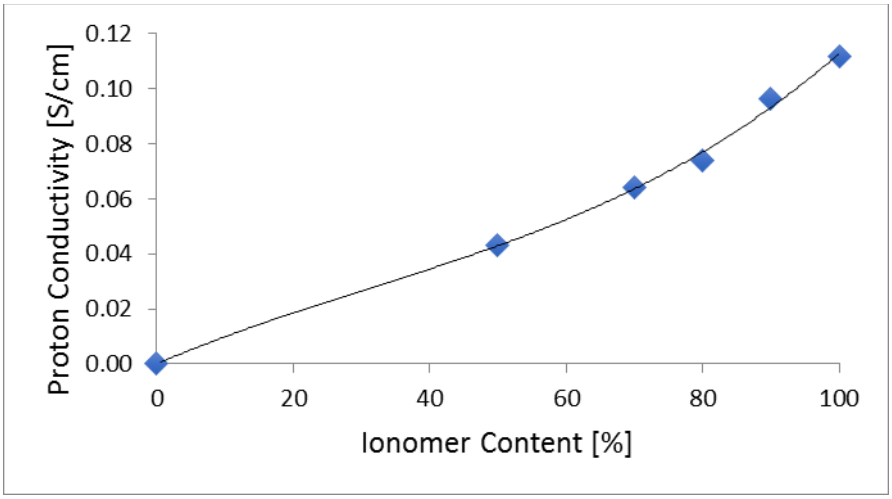

Figure 21. In-plane proton conductivity dependence on PFSA 825EW content for the PFSA-Torlon dual fiber membranes.

Fabrication of layered PFSA/PAI nanofiber composite membranes

Layering studies were initiated to evaluate a tri-layer structure on performance properties. An experimental design was completed where membrane composition (% ionomer) and layer thickness were evaluated (Table 9). The first two membranes have a total membrane thickness of 20 µm and composite layers made of 80 vol% PFSA (20 vol% Torlon); the third membrane was slightly thicker and contained the composite layers made of 60 vol%PFSA. The layer compositions were controlled by varying the flow rates of each component, and the thicknesses were controlled by electrospinning the materials for a defined period of time. Once a tri-layer fiber mat was obtained, it was densified and conditioned in the same way as that used for making single-layer composite membranes.

Table 9. Multilayer membrane design table

Membrane Composition	Layer Thickness (µm)			Total PFSA Content (vol.%)
	Top Layer	Middle Layer	Bottom Layer	
100/80/100	6.0	8.0	6.0	94.0
80/100/80	4.0	12.0	4.0	94.0
60/100/60	8.2	8.7	8.1	93.0

In order to verify pore closure and to visually verify the isolation of Torlon fibers in the tri-layer composite membrane, samples were freeze-fractured in liquid nitrogen and their cross-sections were examined under SEM.

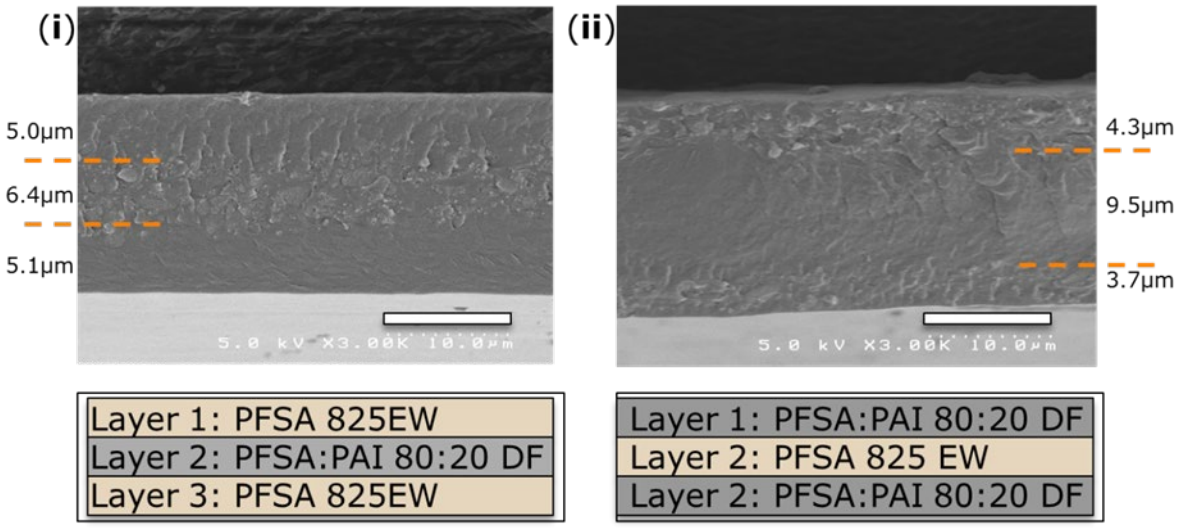

Figure 22. SEM micrographs of the actual electrospun trilayer membranes. Magnification 3,000x.

The dual fiber layers can clearly be distinguished in the cross-sections shown in Figure 22. The target structures were achieved with reasonable level of accuracy. Several other membranes were fabricated with various layer thicknesses and compositions. Membranes with reinforcing fibers in the center layer, as well as ones with reinforcing fibers on the outer layers of the membranes, were fabricated with compositions ranging from 80 – 90 vol% PFSA (20 – 10 % Torlon). The layer compositions ranged from 60 – 100 vol% PFSA. In Figure 23, the conductivity and the swelling data for the single layer and the trilayer membranes is plotted for comparison. The trilayer data follows the trend of the single layer membranes.

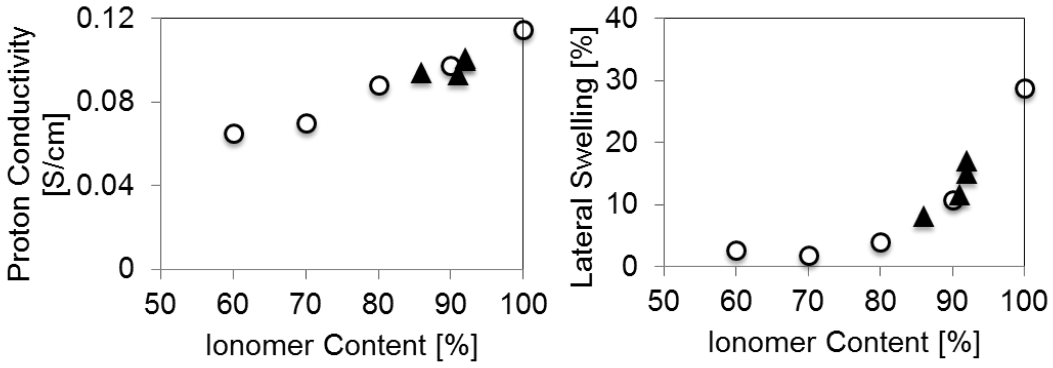

Figure 23. Comparison of the conductivity (left) and the lateral swelling (right) data for the single layer (circles) and the trilayer (triangles) membranes.

While the tri-layer membranes did not show a significant reduction of their lateral swelling, they did show improved mechanical properties (Table 10). A layered membrane with 90 vol% PFSA (10 vol% Torlon) has a tensile modulus nearly twice that of a single-layer membrane at 90 vol% PFSA. Similarly, the trilayer membrane with the 60 vol% surface layers showed superior strength, almost twice the stress at 25% strain, compared to the single layer membrane of

similar PAI content. Many of the membranes fabricated and tested showed this same trend; the presence of Torlon in the thin layers boosted the overall membrane's mechanical strength relative to a single layer membrane of similar composition.

Table 10. Tensile characteristics of selected Q5 membranes.

Membrane	*Stress at 25% Strain [MPa]*	*Ultimate Tensile Stress [MPa]*	*Tensile Mod. [GPa]*
80/100/80	16.4	20.5	0.13
90 single layer	11.9	16.7	0.09
60/100/60	20.1	21.6	0.16
Neat 825 PFSA	13.0	16.2	0.10

Dual fiber membranes PFIA/PVDF with PVDF microfibers

Composite mats of PFIA and polyvinylidene fluoride (PVDF) were fabricated by simultaneously electrospinning PFIA and PVDF from separate syringes onto a common collector. The PVDF average fiber diameter was increased from 600 nm to 1000 nm and further to 2000 nm while the total PVDF content in the final membrane was kept constant at 25 wt.%. The fiber diameter increase was achieved by increasing the PVDF concentration in the electrospinning solution and by increasing the flow rate during electrospinning. The properties of the resulting electrospun membranes are shown in Table 11. Typical fiber images from this study are shown in Figure 24.

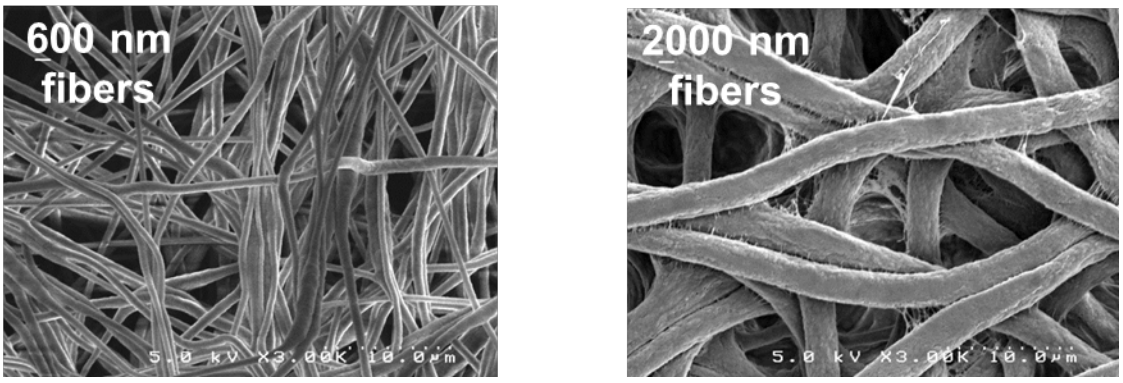

Figure 24. SEM surface images of electrospun PVDF (a) nanofiber and (b) microfiber mats. Magnification: 3,000x.

The results indicate a reduction in lateral swelling with increasing PVDF diameter. There was no PVDF fiber diameter dependence on proton conductivity and gravimetric swelling. The best membrane had 2000 nm diameter PVDF fibers. This result is due to the increase of modulus with increasing fiber size, as shown in Figure 25.

Table 11. The effect of PVDF reinforcing fiber diameter on the properties of PFIA/PVDF nanofiber composite membranes. . All membranes were 20 µm in dry thickness.

PFIA Content [wt %]	PVDF Fiber Diameter [nm]	In-Plane Conductivity [S/cm]	Gravimetric Swelling [%]	Lateral Swelling [%]	IEC [mmol/g]
100 (Cast)	---	0.125		35	1.42
75	600	0.100	59	8	1.08
75	1000	0.093	62	6	0.97
75	2000	0.100	63	4	1.07

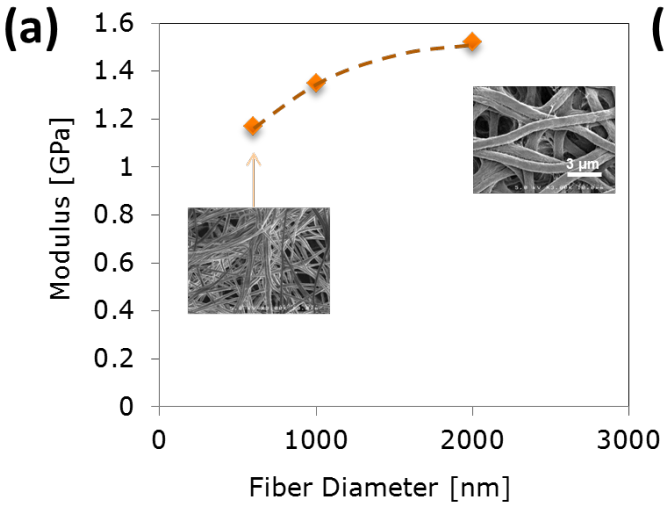

(b)

PFIA Content [wt %]	PVDF Fiber Diameter [nm]	PVDF Fiber Modulus [GPa]	Lateral Swelling [%]
75	600	**1.17**	8
75	1000	**1.35**	6
75	2000	**1.52**	4

Figure 25. The effect of fiber diameter on electrospun membrane tensile modulus (a) and on modulus and lateral swelling in water (b).

Single fiber membranes from electrospun PFIA-PVDF blend

In addition to the dual fiber approach where each of the ionomer and support fiber is spun from its own solution, another option is to use a blended polymer single fiber electrospinning. Here, the ionomer and the reinforcing polymer are dissolved in a common solvent and electrospun from a single syringe. The reinforcing polymer serves as the PFSA/PFIA electrospinning carrier so no additional polymer is added to the electrospinning solution. This strategy could simplify the membrane manufacturing process and create tighter structures due to better inter-fiber

compatibility. Single fiber mats of PFIA with either 10 wt.% or 20 wt.% PVDF (Kynar® HSV900) were successfully electrospun (Figure 26). The fiber diameter was relatively large, in the single micrometer range, with a reasonable (narrow) fiber diameter distribution. The mats were processed into dense and defect-free membranes by annealing at 200°C for 15 minutes under vacuum and then hot-pressing at 24,000 pounds and 180°C for 4x40 seconds. The resultant transparent, dense films were treated with 1.0 M H_2SO_4 at room temperature overnight and then equilibrated with DI water at room temperature. The gravimetric water uptake (g/g) and the lateral swelling (cm/cm) were determined and the in-plane proton conductivity was measured using a Bekktech four-electrode cell and a Gamry potentiostat. The results are presented in Table 12. It can be seen that the lateral swelling in both blended fiber electrospun membranes is much lower than that in a solvent cast PFIA film (7.3% for the membrane with 10% PVDF vs. 44.3% for the cast PFIA membrane).

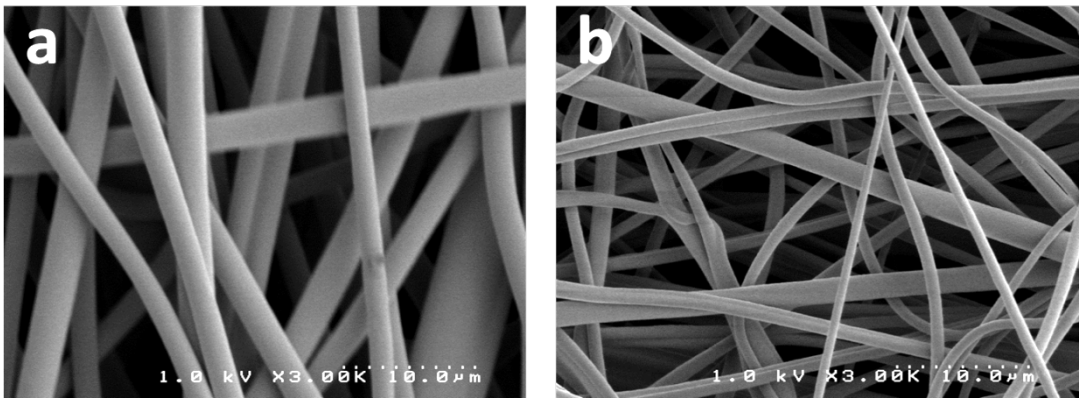

Figure 26. SEM micrographs of the surfaces of PFIA-HSV900 mats containing 90% PFIA (a) and 80% PFIA (b).

Table 12. Water uptake, swelling and proton conductivity of two single-fiber membranes containing 10 wt.% and 20 wt.% of PVDF.

	Water Uptake (g/g)	Lateral Swelling (cm/cm)	Thickness Swelling (cm/cm)	Proton Conductivity (S/cm)
Cast PFIA	-	0.443	-	0.138
PFIA_HSV_SF80 (20 wt.% PVDF)	0.552	0.073	0.756	0.099
PFIA_HSV_SF90	0.871	0.156	0.861	0.101

(10 wt.% PVDF)				

To expand on these results, four compositions were electrospun: 70, 60, 50 and 40% wt. PFIA with the balance being PVDF. The single-fiber mats were hotpressed, annealed, conditioned in boiling 1M H_2SO_4 and water, and a flexible, white mat is obtained for each composition. The summary of the conductivity measurements is given in Figure 27. As expected, conductivity increases with increasing PFIA content.

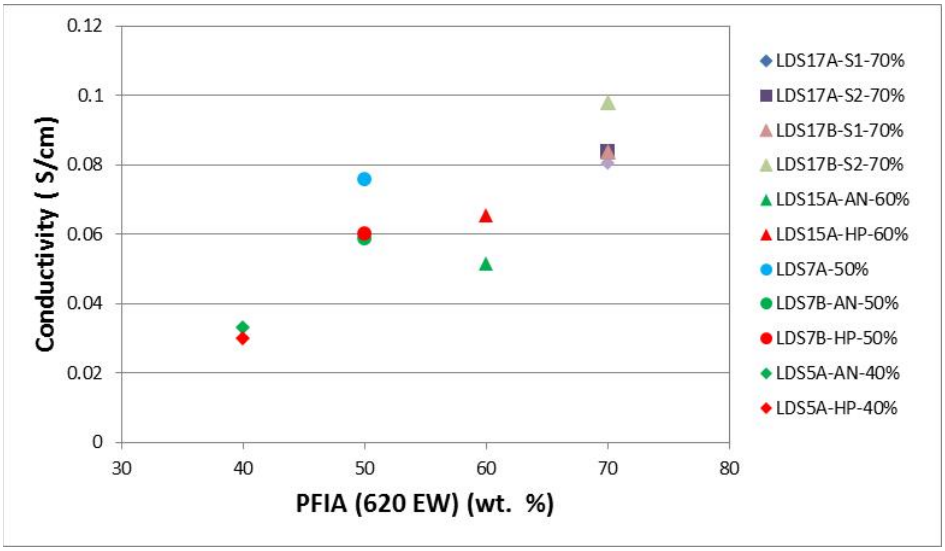

Figure 27. Conductivity of the PFIA/PVDF membranes as a function of PFIA content and mat post-treatment.

In Figure 28, in-plane conductivity and lateral swelling in water at room temperature are compared for dual fiber PFIA/PVDF membranes and for membranes prepared from blended single fibers of PFIA and PVDF.

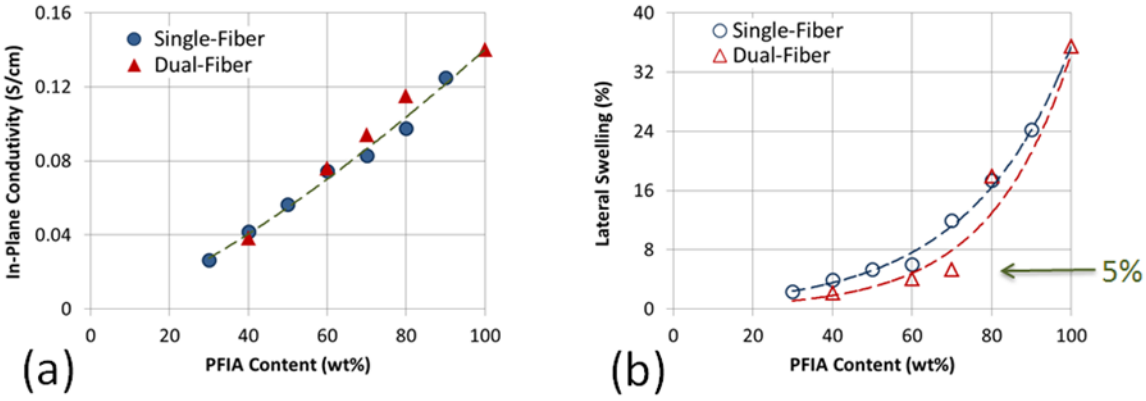

Figure 28. In-plane conductivity and lateral swelling dependence on PFIA (EW660 content for two sets of PFIA(EW660)/PVDF membranes obtained using single-fiber and dual-fiber

electrospinning. Measurements were done at room temperature with water equilibrated membrane

It can be observed that the dual-fiber membranes show slightly higher conductivity and lower lateral swelling (by a few percent), as compared to blended single-fiber membranes of similar composition. The single fiber membranes are easier to fabricate since it requires electrospinning only one polymer solution where PVDF acts as the carrier polymer and reinforcing polymer.

PFSA/PPSU membranes from electrospun, plasma treated dual-fiber mats

Surface treating polymers for improved mechanical properties or ionomer adhesion was investigated throughout this project. The experiments presented below were carried out to determine if plasma treatment of dual-fiber mats electrospun form PFSA (EW825) and polyphenylene sulfone (PPSU) will lead to membranes with better characteristics than those of untreated PFSA/PPSU mats.

The 3M PFSA 825EW was electrospun from an isopropanol/water solution, and a PPSU was spun from NMP/THF mixture. Mat composition was controlled by adjusting the relative flowrate of PFSA and PPSU solutions during electrospinning. The mats were densified by hot-pressing at 163°C and 15,000 psi for 150 sec and then annealed at 160°C for 1 hr (Figure 29). The resultant membranes were conditioned by treating with boiling 1M H_2SO_4 for 1 hour and then with boiling water for another 1 hr.

Figure 29. Transformation of the electrospun PFSA/PPSU mats into dense, defect free membranes via hotpressing.

It was postulated that adding polar groups to PPSU fiber surface could lead to improved PFSA-PPSU compatibility, which could then result in some beneficial membrane characteristics. To verify this postulate, electrospun mats from PPSU and from PFSA, were subjected to oxygen plasma (Reactive Ion Etch RF 100W) for various periods (0-300 sec), and then analyzed. Figure 30 shows SEM micrographs of the electrospun mats untreated and treated with oxygen plasma for different periods of time. Destruction of the PPSU mat is evident after 300 sec (fiber surface roughening after 30 sec) and PFSA mat degrades after 120 sec.

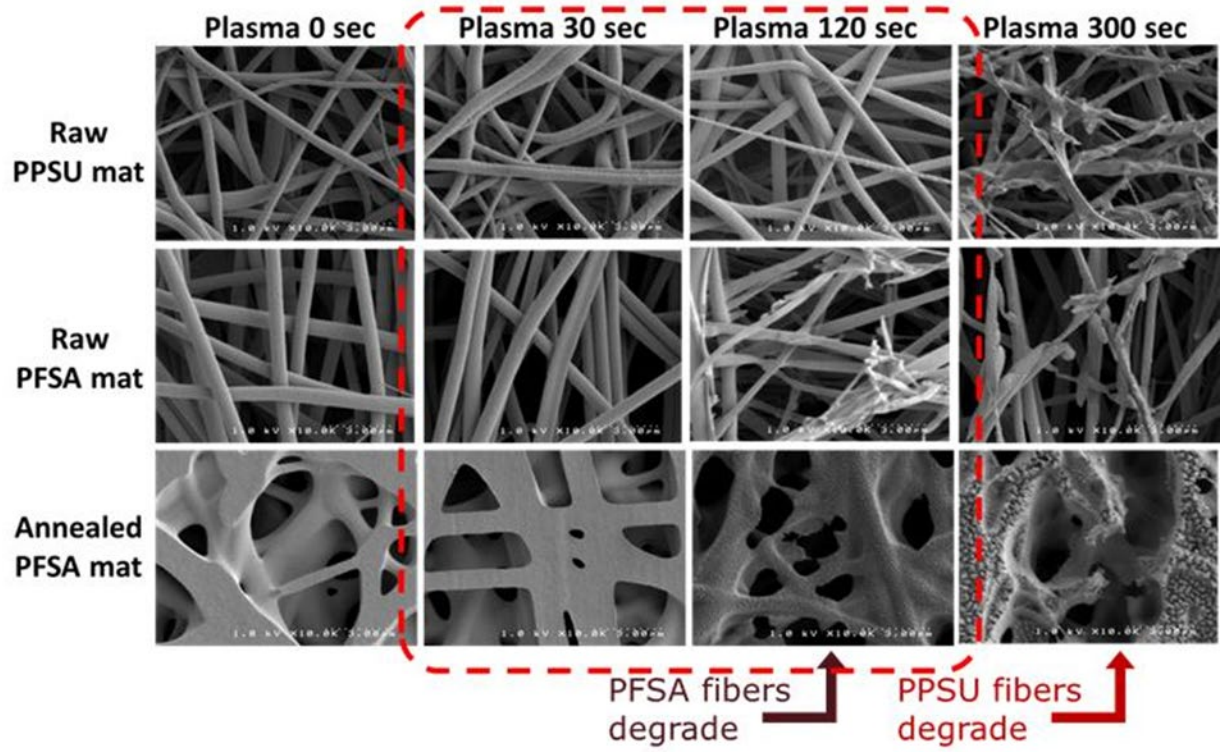

Figure 30. SEM micrographs of the surfaces of untreated (raw) and plasma treated electrospun mats from PPSU and PFSA (unannealed and annealed).

Based on these results, dual fiber PFSA/PPSU (70vol% PFSA) were exposed to oxygen plasma for 30 sec each side and then densified (hotpressing at 160°C and annealed at 160°C for 1 hr). The resultant membranes were conditioned by treating with boiling 1M H_2SO_4 for 1 hour and then with boiling water for another 1 hr. The tensile curves of the membranes hotpressed from the untreated and plasma treated dual-fiber PFSA/PAI mats are compared to that of the solution cast PFSA membrane in Figure 31. It appears that the plasma exposure increased an overall membrane hydrophilicity leading to increased swelling. The treated membrane became more ductile (elongation at break 25% vs. 5% for the untreated sample). The key characteristics of the three membranes are summarized in Table 13 below.

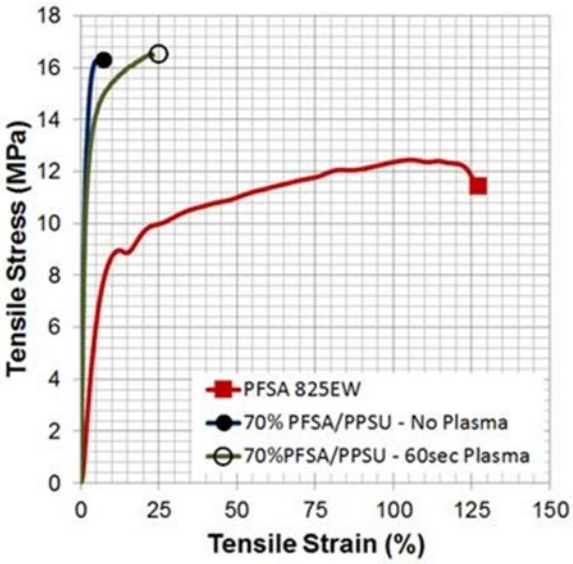

Figure 31. Tensile curves of the pristine solution cast PFSA and dual-fiber PFSA/PPSU membrane from electrospun untreated and plasma treated mat. The samples were tested in the air-dried state (45%RH).

Table 13. Key characteristics of the membranes from untreated and plasma-treated PFSA/PPSU elecrospun dual-fiber mats.

PFSA content [vol%]	Plasma 100W	Gravimetric Swelling (wt%)	Lateral Swelling [%]	In-Plane Cond [S/cm]	Modulus (Air Dry) [GPa]
100	-	58.2	28.9	0.120	0.17
70	-	39.2	6.5	0.071	0.78
	60 sec	45.7	7.9	0.079	0.56

While plasma treated membrane showed somewhat higher conductivity its modulus was lower than that of the untreated membrane. Also the lateral swelling of the treated membrane was higher than that of untreated membrane (7.9% vs. 6.5%).

Subtask 2.2 Membrane Development and Fabrication

This task covers the work needed to convert experimental nanofibers or experimental ionomers into composite membranes for evaluation. A comprehensive summary all membranes made at 3M during the course of this project along with a brief description are listed in Table 14. Lines highlighted in green indicate membranes used to meet various milestones.

Table 14. Membranes made at 3M

3M ID	QTY (ft)	Ionomer	EW	Support	Additive	Thickness (um)	Objective
Membranes Fabricated in Q1 and Q2							
A783396	30	PFSA	825	S1	yes	14	new support evaluation
A783397	30	PFSA	825	S2	yes	14	new support evaluation
A784032	10	PFIA	620	none	no	20	PFIA characterization
A785385	31	PFSA	620	none	no	20	Low EW PFSA control
A785386	9	PFSA	583	none	no	20	Low EW PFSA control
A785387	33	PFIA	620	none	no	20	PFIA characterization
1514076B	15	PFSA	825	S7	no	14	new support evaluation
1514076C	30	PFSA	825	S9	no	14	new support evaluation
1514076D	30	PFSA	825	S8	no	14	new support evaluation
Membranes Fabricated in Q3							
0514031M	10	PFIA	620	none	no	20	PFIA characterization
0514079F	31	PFSA	620	none	no	20	PFSA compasison
0514079G	9	PFSA	583	none	no	20	PFSA compasison
0514079H	33	PFIA	620	none	no	20	PFIA characterization
1514076B	15	PFSA	825	S7	no	14	new support evaluation
1514076C	30	PFSA	825	S9	no	14	new support evaluation
1514076D	30	PFSA	825	S8	no	14	new support evaluation
0514136H,I,J,K	60	PFSA	725	S16	yes	14	Membrane process evaluation
0514176B	30	PFSA	825	S15	yes	14	new support evaluation
0514176A	30	PFSA	825	S10	yes	14	new support evaluation
0514177B,C,D,E,F	30	PFIA	620	S15	yes	14	Membrane process evaluation
0514177A	15	PFIA	620	S15	yes	11	Membrane for Q4 go/no go

Membranes Fabricated in Q4							
0514206C	12	PFIA	620	none	yes	20	PFIA characterization
0514218A	35	PFIA	620	S15	yes	14	Milestone #4 Membrane
0514258A	95	PFIA	620	S15	yes	14	Support evaluation
0514261C	90	PFSA	825	none	no	20	825 EW control
0514261B	90	PFSA	825	none	no	20	725 EW control
Membranes Fabricated in Q5							
0514302H	30	PFSA	825	ePTFE - 1	no	14	Comparative membrane
0514303A	30	PFSA	825	S-15	no	14	Fiber development
0514302I	15	PFSA	825	ePTFE - 2	no	14	Comparative membrane
0514302J	15	PFSA	825	ePTFE - 3	no	14	Comparative membrane
0514342D	30	PFSA	825	S26	yes	14	MD/TD Experiment
0514342C	30	PFSA	825	S27	yes	14	MD/TD Experiment
0514342B	30	PFSA	825	S28	yes	14	MD/TD Experiment
0514342A	30	PFSA	825	S29	yes	14	MD/TD Experiment
Membranes Fabricated in Q6							
0515022A	15	PFSA	825	S30	no	10	Resistance studies
0515022B	15	PFSA	825	S30	no	15	Resistance studies
0515022C	15	PFSA	825	S31	no	20	Resistance studies
0515022D	15	PFSA	825	S31	no	10	Resistance studies
0515022E	15	PFSA	825	S31	no	15	Resistance studies
0515022G	15	PFSA	825	ePTFE - 4	no	10	Resistance studies
0515022H	15	PFSA	825	ePTFE - 4	no	15	Resistance studies
0515022I	15	PFSA	825	ePTFE - 4	no	20	Resistance studies
0515022J	15	PFSA	825	none	no	10	Resistance studies
0515022K	15	PFSA	825	none	no	15	Resistance studies

0515022L	15	PFSA	825	none	no	20	Resistance studies
0515022M	15	PFSA	825	none	no	30	Resistance studies
0515063B	65	PFIA	650	none	no	20	PFIA Pilot Scale PFIA
0515079C	60	PFIA	650	S31	yes	14	MS#7 candidate
0515079D	60	PFIA	650	S30	yes	10	MS#8 Candidate
0515079E	30	PFIA	650	ePTFE - 5	yes	14	ePTFE control
Membranes Fabricated in Q9							
0515079E	30	PFIA	650	ePTFE	Type A (1x)	14	Ionomer Stability Studies
0515324C	20	PFIA	660	ePTFE	no	14	Ionomer Stability Studies
0515324B	20	PFSA	825	ePTFE	no	14	Ionomer Stability Studies
0515324A	20	PFSA	825	ePTFE	Type A (1x)	14	Ionomer Stability Studies
0516020D	95	PFIA	660	S30	Type A (1x)	10	MS #8 repeat for MS#10
0516020C	90	PFIA	660	S30	Type A (2x)	10	MS#10 additional candidate
0516020B	82	PFIA	660	S30	Type B (1x)	10	MS#10 additional candidate
0516020A	30	PFIA	660	S30	Type B (2x)	10	MS#10 additional candidate
Membranes Fabricated in Q10							
0516081D	30	PFIA	650	S30	none	10	MS#10 additional candidate
0516081C	15	PFIA	650	S30	Typa A (1X)	10	MS#10 additional candidate
0516081B	30	PFIA	650	S30	Typa A (1X)	10	MS#10 additional candidate
0516081A	45	PFIA	650	S30	Typa A (2X)	10	MS#10 additional candidate
Membranes Fabricated in Q11							
0516139G	10	PFIA lot2	650	none	none	20	Ionomer characterization

Membranes Fabricated in Q12							
0516190A	60	PFIA-CG3/4	625	FC2	Typa A (1X)	10	Support/additive comparison
0516190B	60	PFSA	725	FC1	0	10	Support/additive comparison
0516204A	60	PFSA	725	ePTFE-5	0	10	Support/additive comparison
0516204B	60	PFIA-CG3/4	625	ePTFE-5	Typa A (1X)	10	Support/additive comparison
0516204C	60	PFIA-CG3/4	625	ePTFE-5	0	14	Vapor Phase Peroxide Testing @GM
0516204D	15	PFIA-CG3/4	625	non	0	20	Ionomer Characterization
			625				
Membranes Fabricated in Q13							
0516270C	60	PFIA lot 3/4	625	0	0	20	Unsupported PFIA membrane for lab use
0516270A	150	PFIA lot 3/4	625	FC1	Type C (1x)	10	PFIA with alternative additive
0516322A	2	PFIA - lot 2	650	0	0	30	PFIA process condition study
0516322A	2	PFIA - lot 2	650	0	0	30	PFIA process condition study
0516322A	2	PFIA - lot 2	650	0	0	30	PFIA process condition study
0516322A	2	PFIA - lot 5	650	0	0	30	PFIA process condition study
0517003F	30	PFIA lot3/4	625	ePTFE-5	Typa A (1X)	14	Low Iron
0517003E	50	PFIA lot3/4	625	FC1	Typa A (1X)	14	Low Iron

An example of the work completed in this task is a series of membranes were made with different nanofiber support basis weights and membrane thickness. Cross-section images from this series are shown in Figure 32, Figure 33, and Figure 34 for membranes with 3.2 gsm nanofiber, 4.3 gsm nanofiber, and ePTFE respectively. Initial mechanical testing was completed at GM using their blister test and is described in more detail in GM's submission to this report (Task 3.2).

Note that there were no membranes made on our pilot scale coating equipment during quarters 7 and 8. During this time we focused on evaluating previously made membranes to collect data necessary for choosing the parameters for the milestone 10 membrane constructions that were made in Q9 and Q10 of the project.

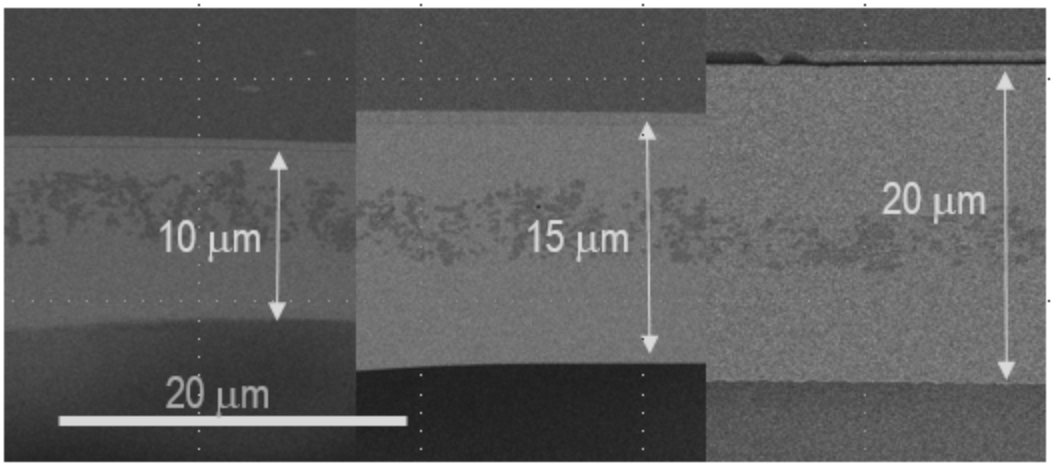

Figure 32. SEM cross section images for 10, 15, and 20 um thick membranes made with 3.2 gsm nanofiber support.

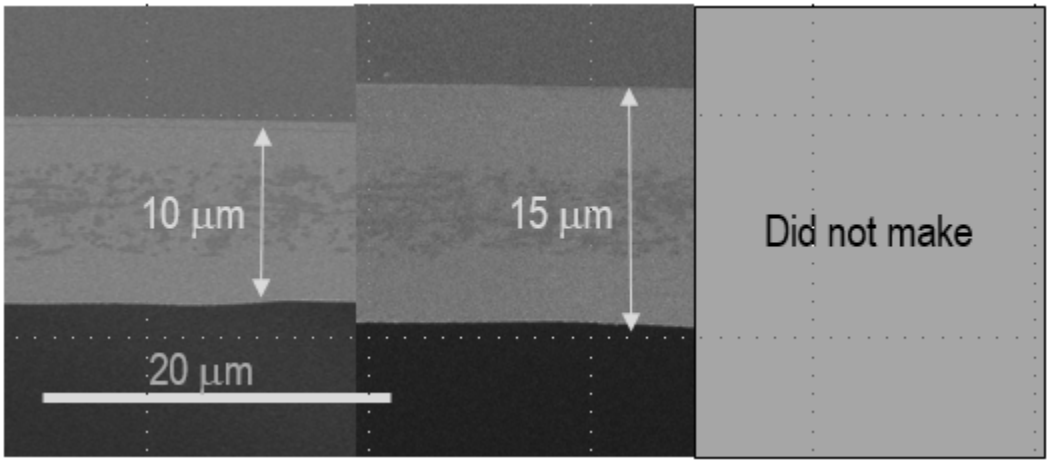

Figure 33. SEM cross section images for 10 and 15 um thick membranes made with 4.3 gsm nanofiber support.

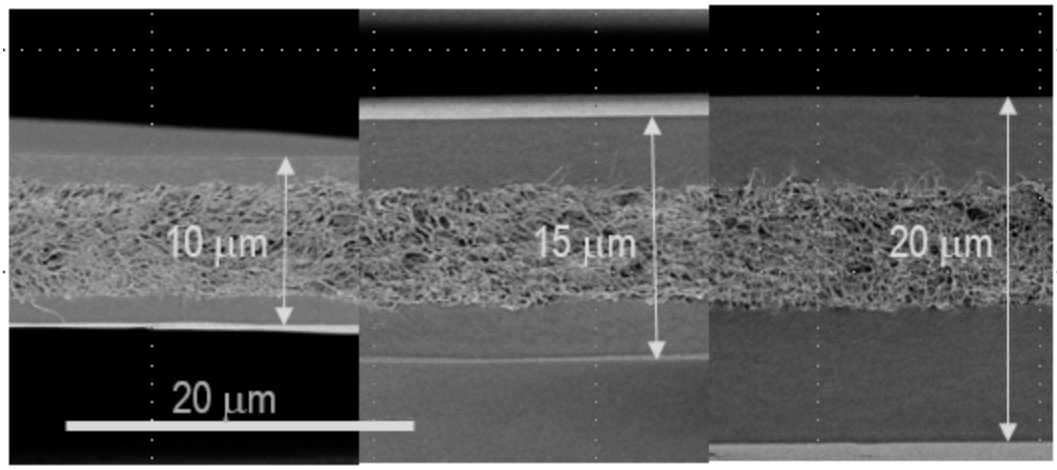

Figure 34. SEM cross section images for 10, 15, and 20 um thick membranes made with 5.4 gsm ePTFE support.

Task 3 Ex Situ Ionomer and Membrane Testing

The purpose of this task was to evaluate membrane candidates for performance characteristics such as conductivity and gas crossover as well as mechanical properties such as strength. Work was conducted at both 3M and GM and, as with other tasks, the originating organization will be designated in the section heading.

Subtask 3.1 Characterization of membrane performance properties

Subtask 3.1.1 Characterization at 3M

In-plane conductivity measurements is one of the most important tools we have to evaluate new ionomers and membrane candidates. A summary of results at 80°C that spans the last several years of ionomer development is shown in Figure 35. The two highest lines on this curve, PFIA and PFICE-4, were for ionomers synthesized in this project and show dramatic improvements over the advances from prior years.

Another good example of results from this technique is shown in Figure 36 for the PFICE series described in Task1. Data for the imide based ionomers with 2, 3, and 4 protogenic groups are plotted along with a 725EW PFSA membrane for comparison. The milestone 5 target of 100 mS/cm at 40% RH is shown with a blue dot. The dramatic increase in conductivity as a result of this series is evident where the PFICE-4 sample exceed the milestone 5 target and has conductivities of over double the already exceptional 725EW ionomer.

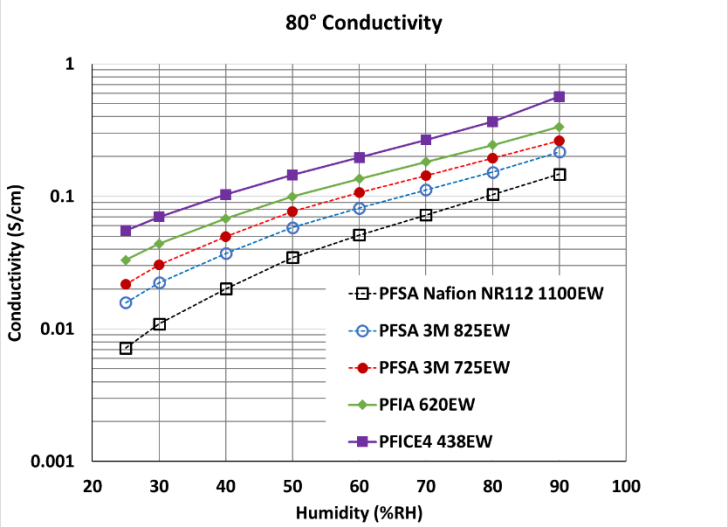

Figure 35. Conductivity as a function of relative humidity for membranes made without additive or support.

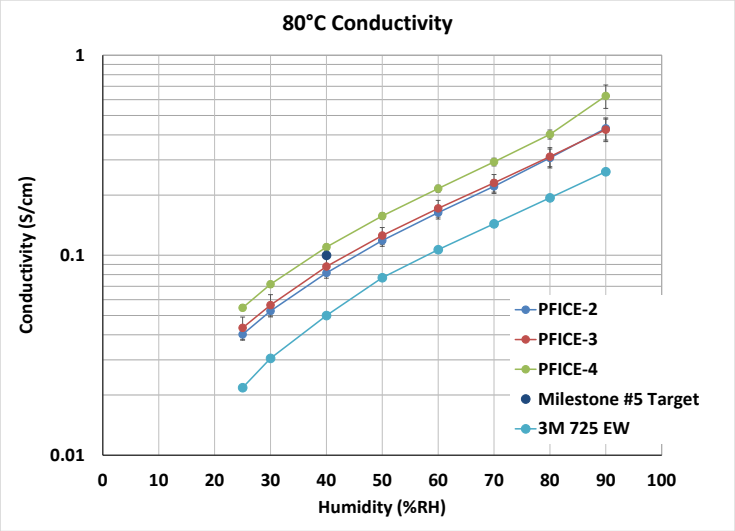

Figure 36. Average conductivity vs relative humidity for PFICE-2,3, and 4 samples and a 725EW control. Samples measured using low clamp force.

Other characterization in this task included titration for equivalent weight determination. Table 15 shows the values for the PFICE series compared to the theoretical values expected if 100% attachment were obtained at every step.

Table 15. Titration values for PFICE series

Ionomer	# Imides	Theoretical (EW)	Titration (EW)
PFICE-2	1	501	534 ± 7
PFICE-3	2	431	475 ± 5
PFICE-4	3	397	438 ± 3

Data from these tests was used to examine the dependence of conductivity on the ionomer equivalent weight. Figure 37 shows a plot of the conductivity at 80°C and 50% RH of PFSA, PFIA, and PFICE ionomers as a function of their measured EWs. As expected, the lower EW samples had higher conductivity and form a reasonably good line. The limit of conductivity, in this system, is shown with the red dashed line. This is designated the "ionene limit" since a PFICE-x polymer with an indefinitely long side chain would effectively be an ionene with an EW of 293 g/mol. In other words, a little over 200 mS/cm is the maximum conductivity one would expect from this polymer system.

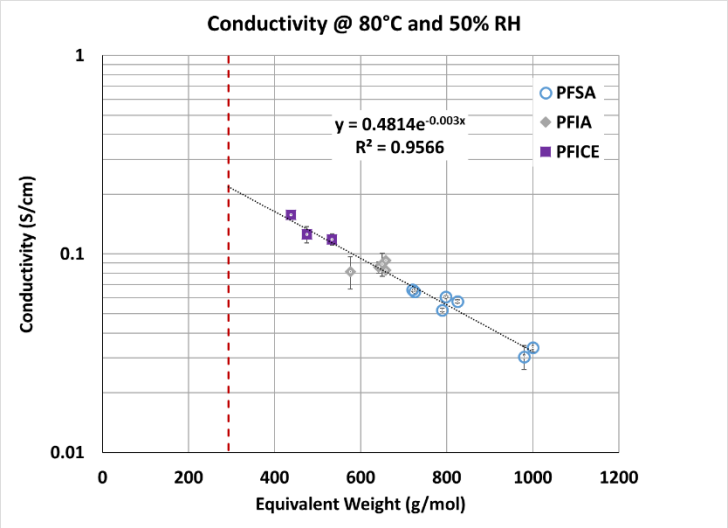

Figure 37. Conductivity versus EW at 80°C and 50% RH for PFSA, PFIA, and PFICE ionomers. The red line indicates the "ionene limit" of 293 g/mol.

This idea was applied to a series of composite membranes consisting of various PFSA equivalent weights and fiber fractions. For this analysis, the "apparent equivalent weight" (*EWa*) was calculated by the following equation that takes into account the non-conductive, fiber fraction (*f*) of the membrane.

$$EWa = \frac{1}{\left(\frac{1}{EW}\right) * (1 - f)}$$

A plot of the conductivity from this series vs EWa is shown in Figure 38. The fit is remarkably good and virtually the same as that of the ionomer only data discussed above. The combination of these two sets of data is shown in Figure 39.

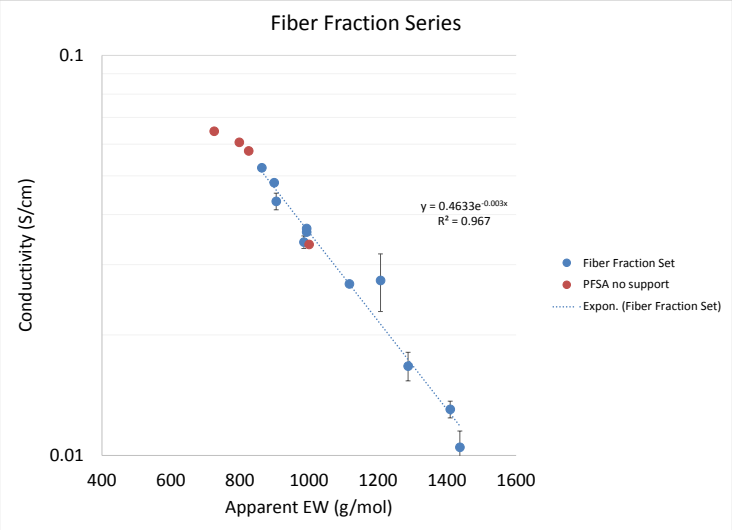

Figure 38. Conductivity at 50% RH and 80°C as a function of apparent equivalent weight for a series of membranes where the fiber fraction was varied. Red symbols show the data for 100% PFSA are reference.

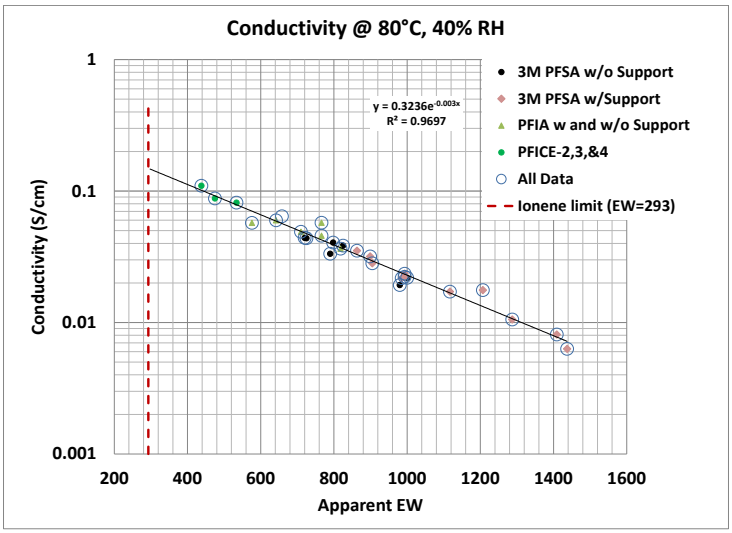

Figure 39. In-plane conductivity as a function of apparent equivalent weight (see Q4 and Q5 reports for more detail).

Conductivity data of this type, in combination with the through-plane resistance measurements from Task 4 were used to evaluate progress towards the DOE targets for resistance at 80°C and 120°C at the specified water partial pressures. The in-plane conductivity data has been converted to resistance and shown in Figure 40 along with the through plane measurements for the same membrane. The DOE water partial pressure targets are converted to RH and shown with dashed lines for each temperature. For the milestone 8 membrane, the targets are meet at all humidities in the 80°C case but are outside the desired range in the 120°C case.

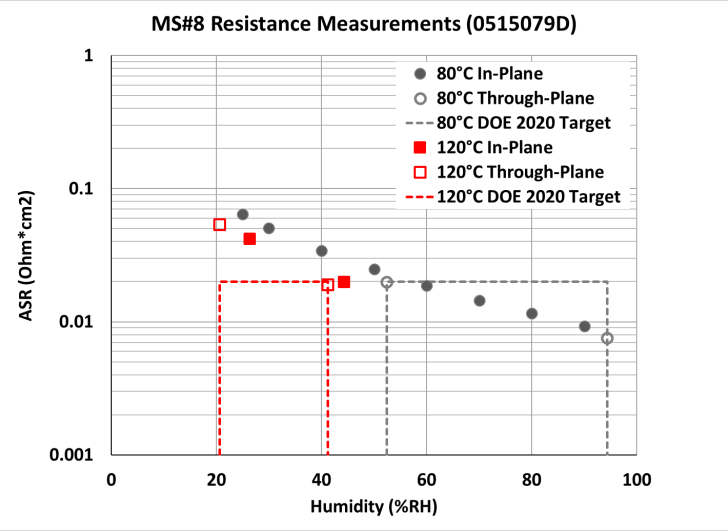

Figure 40. Area Specific Resistance (ASR) as a function of relative humidity for the milestone 8 membrane. Both In-plane (solid symbols) and through-plane (open symbols) data are shown. The dashed lines represent DOE targets for 120°C (red) and 80°C (grey).

The significant shortfall at the 120°C dry conditions suggests a closer look at the basic ionomer properties and membrane construction. Since the 10 micron, PFIA based, Milestone #8 membrane could not reach this target the question becomes; what would it take to make a membrane with a resistance of 20 mOhm*cm^2 at 120°C and 40 kPa water pressure? The two variables that most affect resistance are thickness and conductivity. Assuming a commercially viable membrane needs to be in the thickness range of 10-14 microns then conductivity becomes the main variable to investigate. The conductivity versus equivalent weight for several membranes at 120°C and low humidity is plotted in Figure 41. In this analysis, the equivalent weight is represented as “apparent equivalent weight” in order to account for the presence of reinforcing fibers that effectively “dilute” the acid concentration in the membrane. The blue symbols in this figure represent non-supported membranes where the green symbols have the EW adjusted to reflect the fiber content.

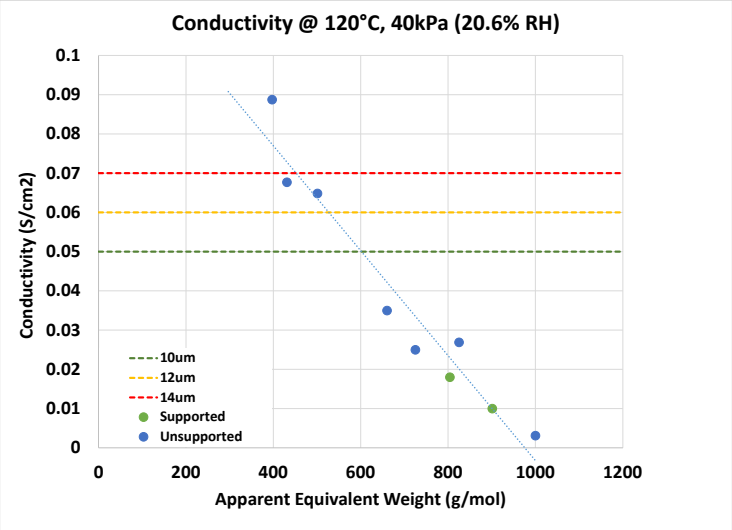

Figure 41. Conductivity vs apparent equivalent weight where the lines show the value required for a 10 (---), 12 (---) and 14 (---) um membrane to achieve 20 mOhm*cm2.

As expected, the conductivity increases with decreasing equivalent weight over an EW range of about 400-1000 g/mol with a correlation coefficient of 0.94. The dashed lines represent the conductivity threshold required for a 10, 12, or 14 micron membrane to meet the 20 mOhm*cm^2 target. For example, an ionomer with equivalent weight of about 607 g/mol is needed to make a 10 micron thick membrane that would meet this target. Similarly, EWs of 537 and 466 g/mol are necessary to make membranes that are 12 and 14 microns respectively. However, the need for reinforcing fiber supports must be taken into consideration. A fiber loading of about 20% by volume would be reasonable in order to meet the mechanical and chemical durability tests. The addition of a support therefore requires that the ionomer EW be reduced about 486 g/mol in order to have the *apparent* EW meet the requires 607 g/mol in the 10 micron case. If a 12 or 14 micron membrane were needed the ionomer EW would have to be 429 and 373 g/mol respectively in order to accommodate a 20% fiber fraction and still meet the resistance target.

Table 16. Thickness, conductivity, and equivalent weight requirements needed to meet the 20mOhm*cm2 target at 120°C and 40 kPa water pressure.

Thickness (um)	Conductivity (S/cm)	Apparent EW (g/mol)	Ionomer EW if 20% fiber (g/mol)
10	0.05	607	486
12	0.06	537	429
14	0.07	466	373

It is clear from this table and Figure 41 that the target is not possible with PFIA based membranes with equivalent weights as low as 620 g/mol. The perfluoro ionene chain extended (PFICE-x) polymer system, however, may allow EWs in this necessary range for the case.

Subtask 3.1.2 - Characterization at GM

Resistance and crossover testing

Several membranes were sent to GM through the course of this project. Basic characterization was completed and examples of these results are described here. Through-plane proton transport resistance was measured using AC impedance spectroscopy in a 50cm^2 H_2/N_2 Cell.[i] H_2 gas permeability was measured using a limiting current experiment in a 50cm^2 H_2/N_2 Cell.[ii] The proton transport resistance as a function of RH at 80°C is shown in Figure 42. Several trends can be seen from the proton transport resistance results. The support causes an increase in the proton transport resistance of both the 825 and 725EW membranes, even though the supported PEMs are thinner (14μm) than the non-supported PEMs (20μm). The supported PFIA membranes have significantly lower resistance than do the supported PFSA membranes, and the 725EW supported PEM has slightly lower resistance than the supported 825EW PEM. One sample of PFIA (0514218A) has lower resistance than a previously received sample (05123102A), especially at dry conditions.

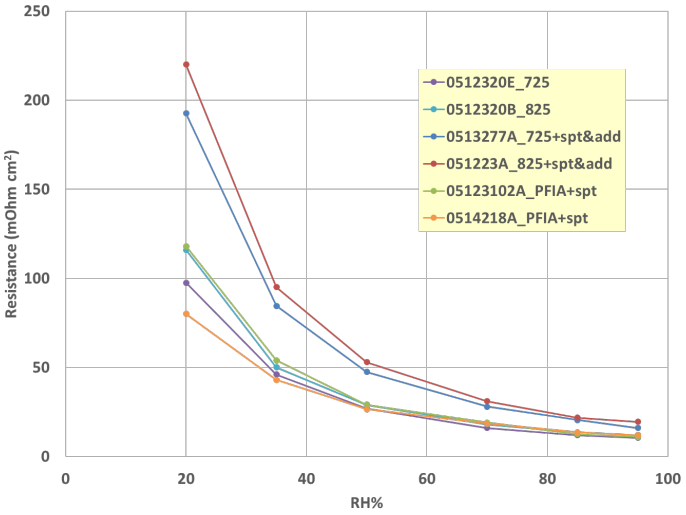

Figure 42. Through plane proton transport resistance at 80°C

GAS Permeability

H_2, N_2 and O_2 gas permeability measurements at 80°C we run for all membranes using a procedure described elsewhere[iii]. The H_2 and O_2 gas permeabilities for five PFIA membrane samples are shown in Figure 43 and Figure 44, respectively. Each measurement was done in triplicate. For both gases, permeability expectedly increases with RH for all membrane types. The permeabilities of both gases is reduced by including a support. Membranes with the FC1-nanofiber supports do seem to exhibit slightly lower permeability than those with ePTFE

supports. Within the FC1-nanofiber supported PEMs, permeability appears to decrease with increasing fiber fraction, and the impact appears greater for H_2 than for O_2. Annealing temperature has a negligible impact on the permeability of both gases.

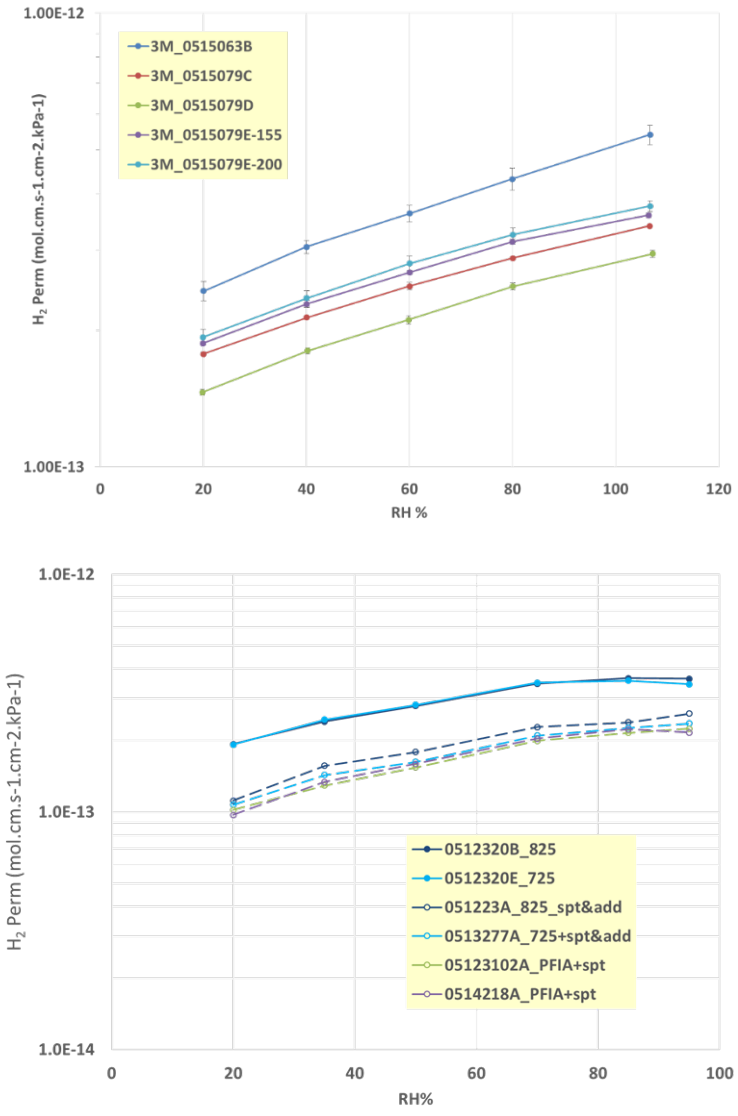

Figure 43. H2 gas permeability of PFIA membranes at 80°C. Top graph shows only PFIA samples for both supported (0515079C, 079D, 079E-155 and 079E-200) and unsupported(0515063B) membranes. Bottom graph shows a comparison of supported PFIA (0512310A and 0514218A), supported PFSA (0512233A and 0513277A) and unsupported PFSA (0512320B and 320E).

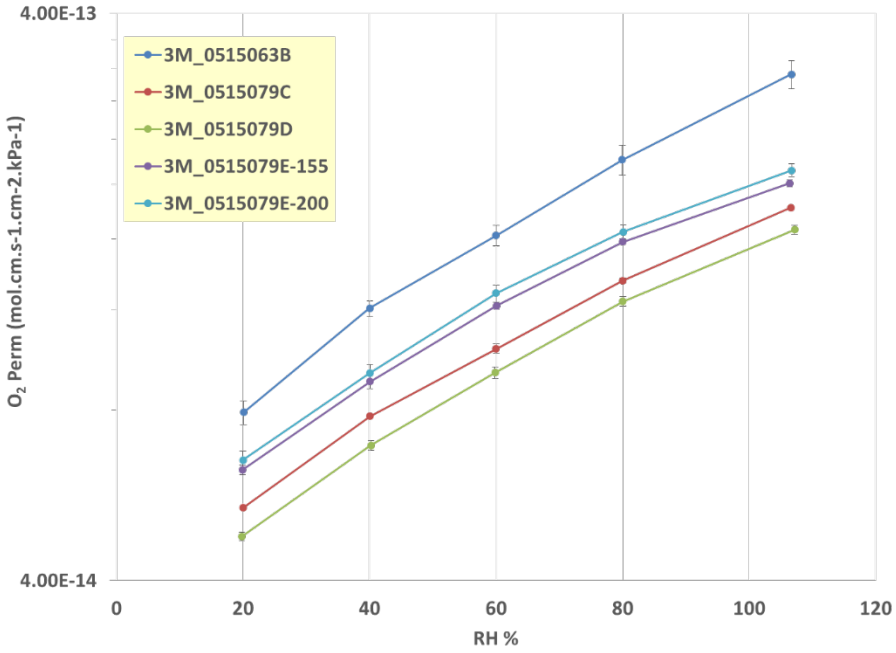

Figure 44. O2 gas permeability of PFIA membranes at 80°C (O2 permeation data not available for PFSA but expected to be similar to PFIA shown above)

Based on the data shown in Figure 43, supported membranes have lower hydrogen permeation than the comparable supported membranes. It is also clear that PFIA membranes as not significantly more permeable in this test.

Subtask 3.1.3 Characterization at NREL

The National Renewable Energy Lab (NREL) was enlisted to do rotating disk electrode (RDE) work under a purchase agreement. The objective of this work was to understand the impact that unique PFIA decomposition fragments might have on the fuel cell electrode performance.

Using NREL's developed oxygen reduction reaction (ORR) experimental procedures, NREL was tasked to perform a series of systematic rotating disc electrode (RDE) experiments on three model compounds that 3M provided (see Table 17). These model compounds were intentionally selected to systematically study the effect of the functional groups (sulfonamide and sulfonic acid compared to carboxylic acid) and the perfluoro chain. For each model compound, three replicate experiments were carried out for a fixed concentration, using glassy carbon (GC) RDE electrodes with a catalyst ink. The ink was identical in all experiments and prepared using 5wt% perfluorosulfonic acid (PFSA) ionomer and TKK Pt on carbon [Pt/Vu TEC10V50E]. The ORR activity after contamination was compared to baseline measurements with no impurity present in a 0.1 M perchloric acid ($HClO_4$) electrolyte.

Table 17. List of materials provided by 3M for this RDE study.

Material	CAS #	Molecular Weight (g/mol)	Form	% Solids	Label	Notes
Sulfamic acid	5329-14-6	97.09	White crystalline powder	100 (pure)	SX1140-3	No ORR RDE experiments were carried out
1. Trifluoromethane-sulfonamide (TFMSAM)	421-85-2	149.09	White crystalline powder	100 (pure)	T1290	Irritant, hazardous; 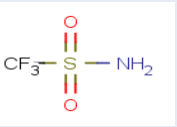
2. Hexafluoro-propane disulfonic acid (HFPDSA)		198.19	Light orange solution	56.7% in 0.1M HClO4	4533-25	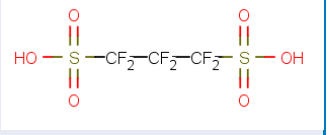
3. Hexafluoropropane Sulfonamide sulfonic acid (HFPSAMSA)		197.2	Light yellow solution	33.8% in 0.1M HClO4	4531-30-13	**Priority 1** 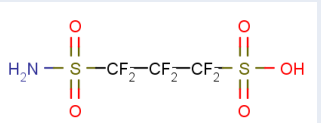
Perfluorinated imide acid (PFIA)		1089	Colorless solution	9.93% in 0.1M HClO4	3M 798bb PFSAmide	Polymer form; MW is for repeat unit No ORR RDE experiments were carried out

Hexafluoropropane sulfonamide sulfonic acid (HFPSAMSA) is the highest priority material to study since it has been identified as a decomposition product from accelerated stress tests (ASTs) for the PFIA ionomer, but in very small amount. Its chemical structure is also similar to the perfluoro (4-sulfonic butanoic) acid (DA-3M) compound that has been identified as a decomposition product of a 3M perfluorosulfonic acid (PFSA) ionomer studied previously by NREL. The only difference is the carboxylic acid group in DA-3M vs. the sulfonamide group in hexafluoropropane sulfonamide sulfonic acid.

The goals of the first set of experiments were: (1) to demonstrate that we can reproduce previous NREL results (Jason Christ) with the DA-3M compound (0.01 mM) on Pt/Vulcan catalyst, and to baseline the contamination effect of DA-3M model compound on the current state-of-the art catalyst, Pt/HSC. We were able to demonstrate that our new results (slides 5-8) for the DA-3M compound on Pt/Vu were similar to Christ's. Compared to Pt/Vu, the effect of DA-3M on Pt/HSC was similar, more reproducible, but less dramatic. For this reason, we in agreement with 3M decided to study the effect of the PFIA degradation model compounds on Pt/Vu.

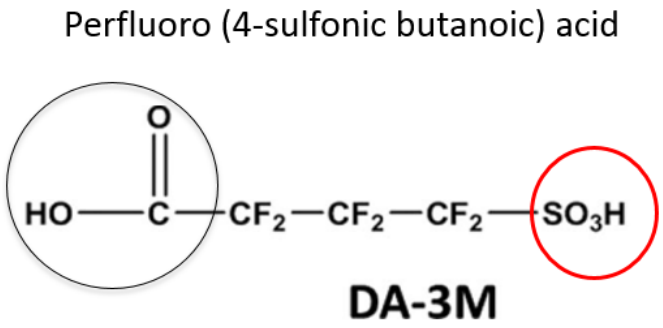

Figure 45. The chemical structure of perfluoro(4-sulfonic butanoic) acid (DA-3M)

The effect of three PFIA degradation model compounds on ORR activity was studied. The trifluoromethane-sulfonamide (TFMSAM) material behaved differently than DA-3M in that it goes into $HClO_4$ very easily and no foaming or loss of electrolyte was observed during the RDE experiment. Both HFPDSA and HFPSAMSA materials behaved similarly to the DA-3M baseline in that foaming and small loss of electrolyte were observed in 0.1 M $HClO_4$. At 0.01 mM, TFMSAM showed minimal effect on the ORR activity, about 10% (a in Figure 46 and Figure 47) and is partially recoverable. It is suggested that a higher concentration of TFMSAM be studied to determine if a greater impact is observed at higher concentration. Both HFPDSA (d in Figure 46 and Figure 47) and HFPSAMSA (c in Figure 46 and Figure 47) model compounds have a clear negative impact on the ORR activity, with HFPSAMSA having the biggest effect on ORR mass activity (63% vs. 53%loss). The mass activities for HFPSAMSA and HFPDSA model compound are almost fully recoverable (only 2-3% of the mass activity was not recovered), while the mass activity for TFMSAM is only partially recoverable (b in Figure 46 and Figure 47). It can be inferred that although the sulfonamide and sulfonic group may have the highest impact on ORR mass activity, the activity can be almost fully recovered. The effect of the carboxylic acids appears to be more detrimental in that the mass activity is not recoverable, at least not by simply rinsing the electrode and transferring it to a clean cell.

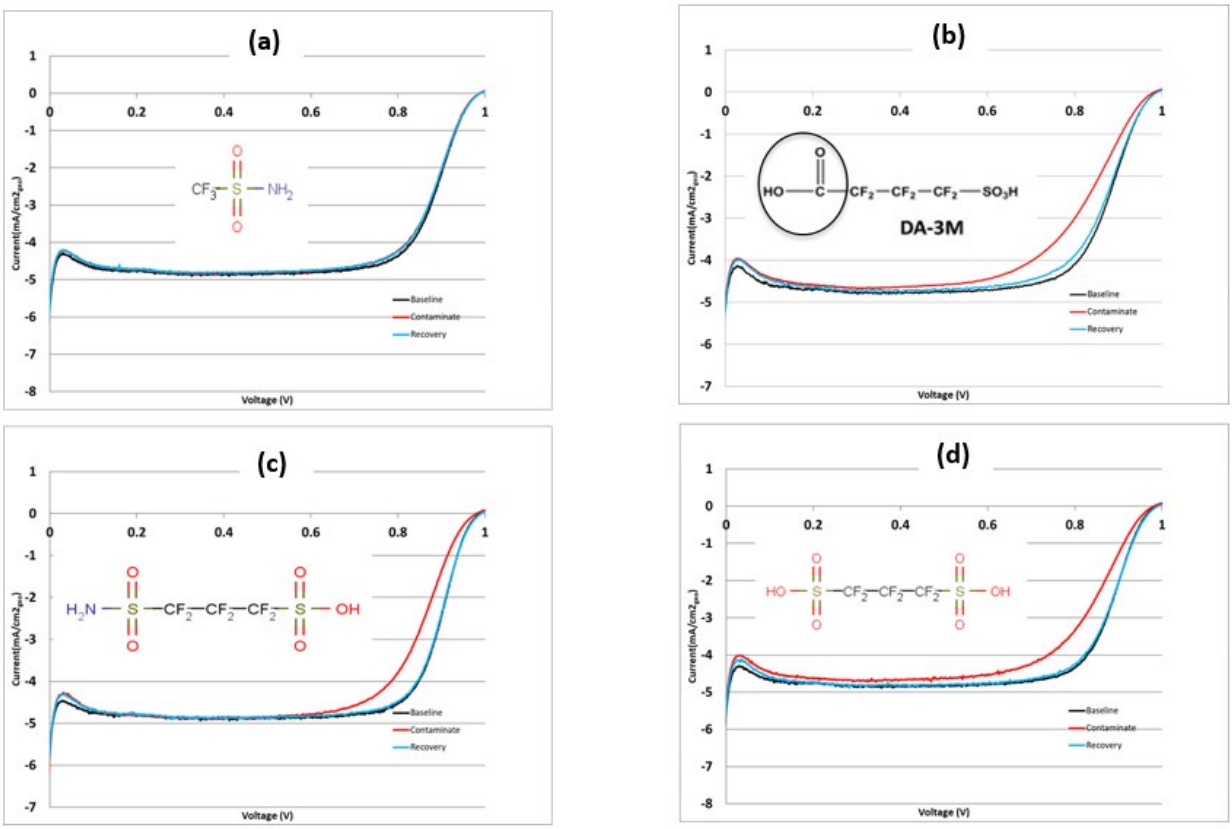

Figure 46. The contamination and recovery effects of different model compounds on ORR curves. A) TFMSAM, B) DA-3M C) HFPDSA, D) HFPSAMSA

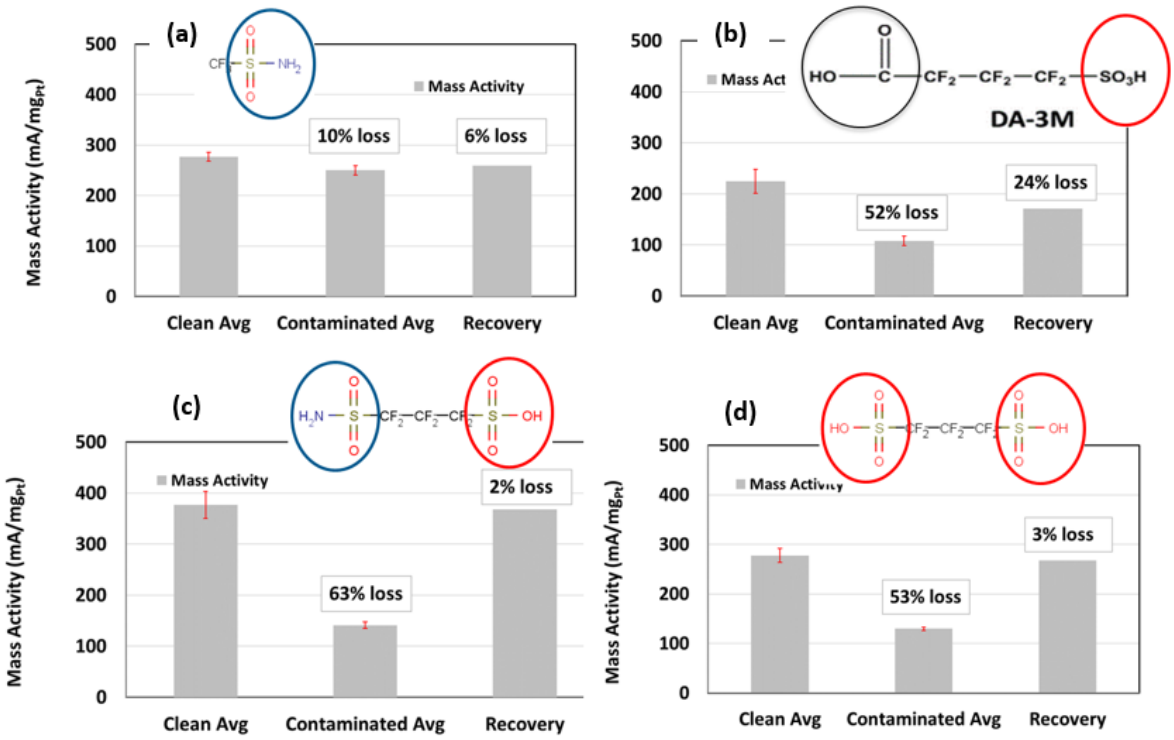

Figure 47. The contamination and recovery effects of different model compounds on ORR mass activity. A) TFMSAM, B) DA-3M C) HFPDSA, D) HFPSAMSA

Figure 48 shows that the compounds with a sulfonamide group (TFMSAM and HFPSAMSA, a and c) hinder the onset of Pt oxide formation more than the compounds with a carboxylic or sulfonic acid group (e.g., DA-3M and HFPDSA). The sulfonic and carboxylic acid groups appear to hinder the hydrogen underpotential deposition (HUPD) region more than the sulfonamide. Furthermore, the results suggest that recovery from the contamination of a di-acid with a carboxylic acid group and a sulfonic acid group (DA-3M) is more difficult than a di-acid with only sulfonic acid groups (HFPDSA). This is the case for both the recovery of mass activity and ECA.

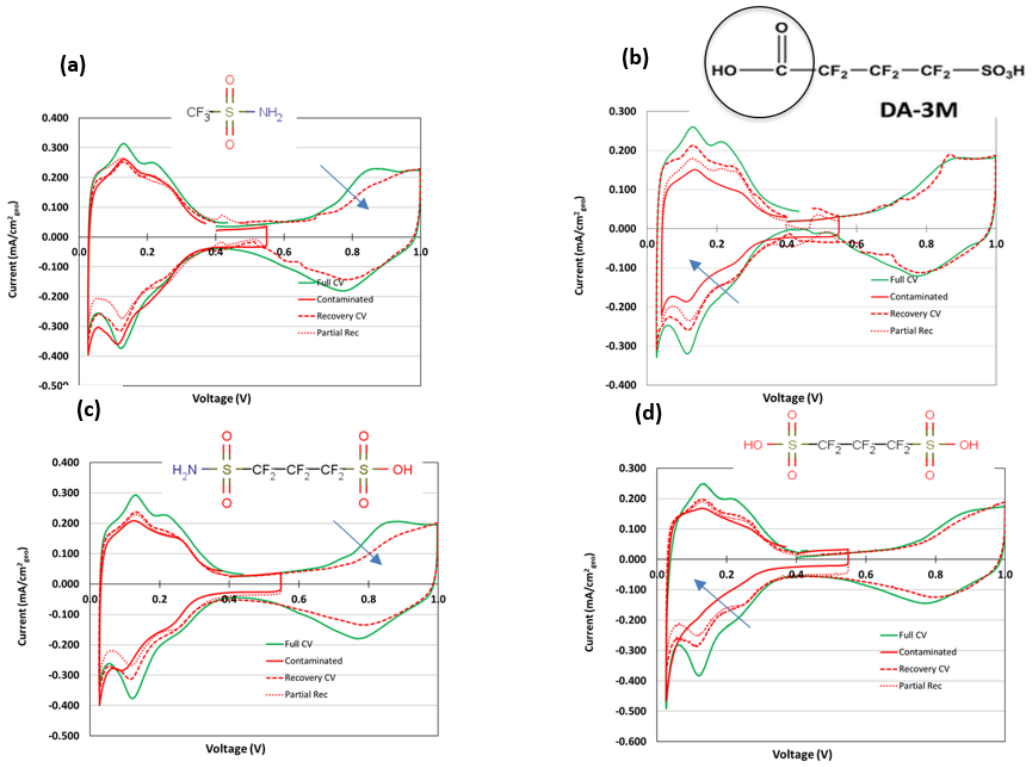

Figure 48. The contamination and recovery effects of different model compounds on Pt CV. A) TFMSAM, B) DA-3M, C) HFPDSA, D) HFPSAMSA

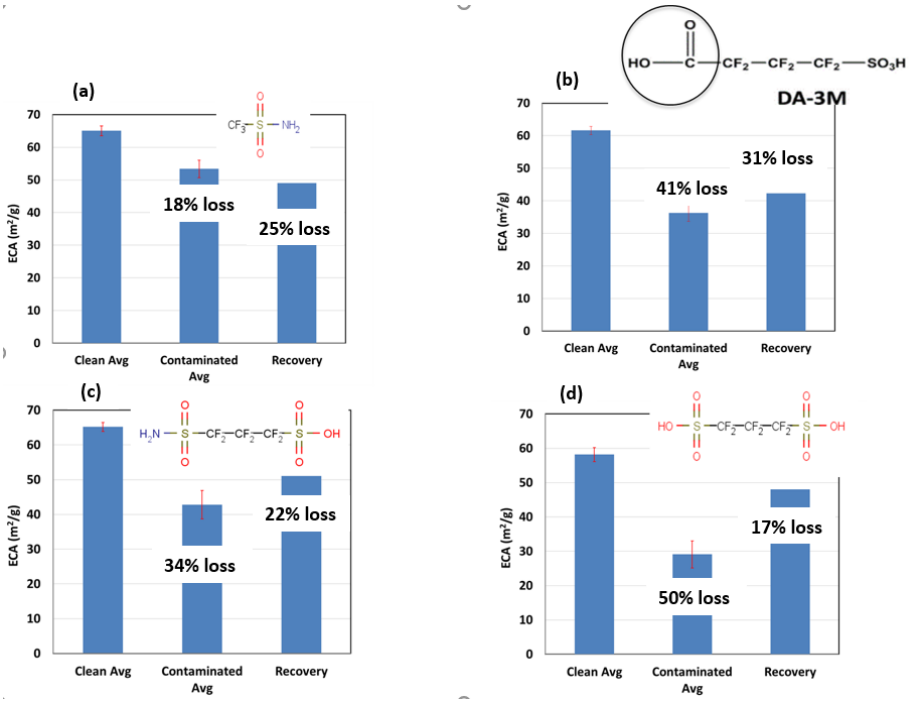

Figure 49. The contamination and recovery effects of different model compounds on the electrochemical surface area (ECA). A) TFMSAM, B) DA-3M, C) HFPDSA, D) HFPSAMSA

It is interesting to note that the loss of ECA due to TFMSAM contamination of the HUPD region was not recoverable (Figure 49 a). It can also be argued that the mass activity was not recoverable either. Perhaps it is because TFMSAM is a relatively small molecule with a sulfonamide functional group that adheres to Pt strongly enough that it cannot be removed easily. Perhaps it is because TFMSAM is not a di-acid and/or does not have a sulfonic acid group and/or it does not have a perfluoro chain and hence it does not behave like a surfactant (i.e., it did not foam like the other compounds did in perchloric acid during RDE experiment). As a result, TFMSAM adsorbs and desorbs on Pt differently than the compounds studied here.

In a previous experiment, NREL's RDE results showed that sulfate decreased both the ORR mass activity and ECA. This may partially be due to sulfate/bisulfate anion adsorbing onto Pt and blocking ORR active sites. The Pt CV showed that sulfate/bisulfate anion adsorbed onto Pt and hindered the onset of Pt oxide formation. The sulfuric acid molecule is like TFMSAM in that it is a small molecule with perfluoro chain and one functional group. In contrast to TFMSAM, sulfuric acid has a different functional group and no -CF3 attached to it. Also in contrast to TFMSAM, the majority of the ECA and mass activity from sulfuric acid contamination was recoverable.

In summary, compounds with a sulfonamide group (TFMSAM and HFPSAMSA) hinder the onset of Pt oxide formation more than the compounds with carboxylic or sulfonic acid group (e.g., DA-3M and HFPDSA). Furthermore, the sulfonamide and sulfonic group appear to have the highest impact on ORR mass activity and the activity can be mostly recoverable. The detrimental effect of the carboxylic acids, however, is that it is only partially recoverable by the simple recovery steps used, i.e. rinsing the electrode and transferring it to a clean cell. The sulfonic and carboxylic acid groups appear to hinder the hydrogen underpotential deposition (HUPD) region more than the sulfonamide.

Subtask 3.2 Characterization of membrane mechanical durability properties

Subtask 3.2.1 Mechanical characterization at 3M

Dynamic Mechanical Analysis

In an effort to better understand the physical properties of the perfluoro ionene chain extended (PFICE) ionomers, we completed a series of dynamic mechanical analysis (DMA) experiments. Storage modulus (E') versus temperature is shown in Figure 50 for a series of PFICE ionomers and a PFSA control. In this set the starting backbone polymer was about 700 g/mol for the PFICE set.

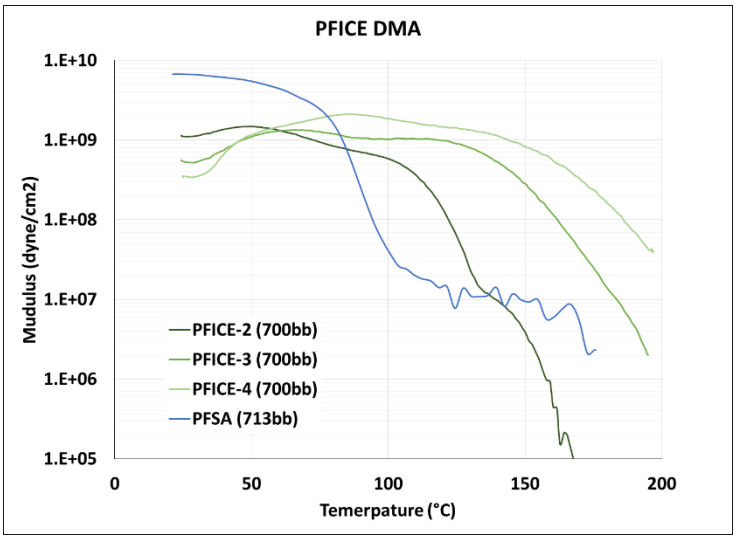

Figure 50. Storage Modulus (E') vs. temperature for PFSA control and PFICE series.

There are a number of notable features in this data that differ from the traditional PFSA modulus vs. temperature behavior. First, the initial modulus at room temperature of the PFICE ionomers are lower than the corresponding PFSA and decrease with increasing acid content. Next, the modulus appears to increase with temperature between room temperature and about 100°C with the most noticeable increase occurring for the PFICE-4 ionomer. Both of these effects are likely due to absorbed water in the ionomer. In effect, the water bound to the acid groups is plasticizing the polymer resulting in the lower modulus at the beginning of the experiment and, as the temperature increases, the modulus increases due to the loss of this water. It is unclear from this data if the lower values are due solely to adsorbed water or if the polymers are softer even when fully dehydrated.

The other notable feature in this data is the increase in the alpha transition as characterized by the maximum in tan delta (graph not shown).

Table 18. Alpha Transition for PFICE Series

Sample	Alpha transition (°C)
PFSA 713EW	95
PFICE-2 (700bb)	130
PFICE-3 (700bb)	154
PFICE-4 (700bb)	173

The alpha transition is similar to a glass transition but rather than being associated with the cooperative motion of the backbone it is associated with the loss of ionic aggregation of the side chains. The increase in this transition is therefore not surprising as the ionic character of the side chain increases. It should be noted that these data reflect the properties of a very dry ionomer. It is expected that the increased water absorption of these materials will result in much lower modulus material when hydrated.

Swell and Solubility

Ionomer swell is an important property relating to the potential durability of a membrane. The PFIA based ionomers have historically had lower swell than the same equivalent weight PFSA. This apears to be the case for the most recent measurements shown in Figure 51. The pilot scale PFIA lot 1 is also shown in this graph. The PFICE series shown on the same plot has significantly higher swell as the EW decreases. This trend is to be expected due to the higher acid content of the PFICE ionomer but also the polymers were made with a 700 EW starting backbone which, in the PFSA form, is the EW where the swell values start to rapidly increase as the EW is decreased.

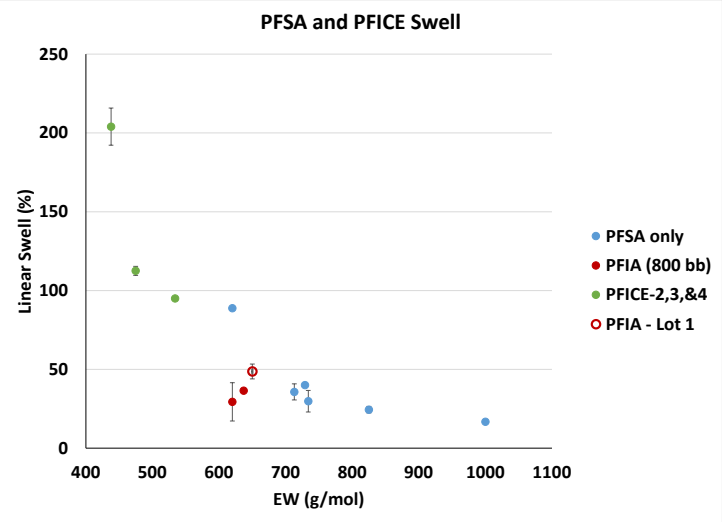

Figure 51. Liner swell as function of equivalent weight.

While the swell data can be managed by incorporating a nanofiber support, the water solubility of the ionomer is a much more fundamental limitation for practical use in membranes. Figure 52 shows the water solubility data for several PFSA, PFIA, and PFICE polymers after refluxing in a Soxhlet extractor for 4 hours. It can be seen that below an equivalent weight of 600 g/mol the PFSA polymers become essentially soluble. The PFIA materials made with a starting backbone polymer of 800 remain mostly insoluble as the 600 g/mol rage is approached. Furthermore, the PFICE series, which was made with the 700 starting backbone, has remarkably low water solubility despite the very low EW of 438 g/mol for the PFICE-4 ionomer.

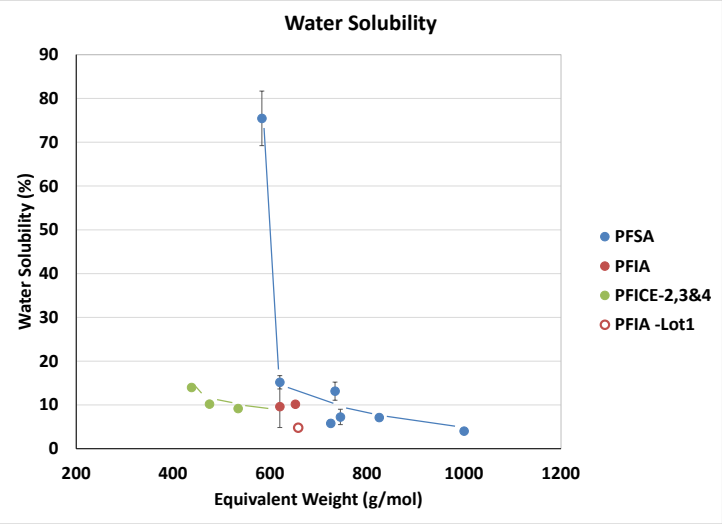

Figure 52. Water solubility for PFSA, PFIA and PFICE ionomers after refluxing for 4 hours in a Soxhlet extractor.

Rule of Mixing model for Swell

An important role of the nanofiber support in a composite is its ability to reduce the membrane swell when hydrated with water. Empirically we know that the stiffness of the fiber material and the total fiber content effect the swell but as part of this project we developed a way to predict if a new support would be suitable for use in a fuel cell membrane. Building on work started at General Motors, we have developed the following relationship (Equation 1) based on the rule of mixing for composite properties. This relationship describes the swell of the composite in terms of the fiber fraction, ionomer swell, and the modulus of both the fiber support and the ionomer. Figure 53 shows a simple schematic that outlines the basis of this approach. To consistently account for the fiber contribution to a composite membrane we assume that the thickness of the fiber layer can be reduced to the thickness of that same mass of fibers in the form of a dense film. This has the mathematical advantage of removing any measurement error from the fiber thickness and allows for the fibers to be accounted for regardless of the void volume of the support. The result of this analysis is shown in Equation 1

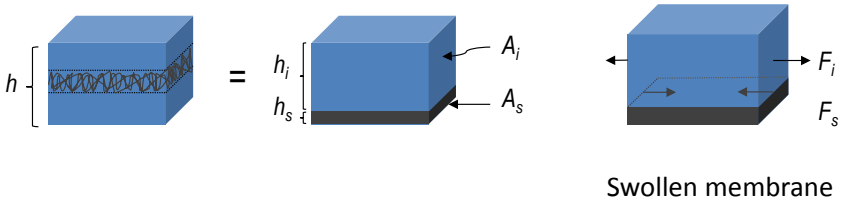

Figure 53. Schematic for force balance used in deriving predictive swell equation.

.

$$\varepsilon_c = \frac{E_i*(1-f)*\varepsilon_i}{E_i*(1-f)+E_s*f}$$

Equation 1. Rule of mixing model for composite membrane swell (□) as a function of Ionomer modulus (E_i), support modulus (E_s) and fiber fraction (*f*).

Where:

E_i	Modulus of ionomer at the wet condition
E_s	Modulus of support at the dry condition
ε_i	Swelling strain of the free-standing ionomer
ε_c	Swell strain of the composite membrane
f	Fiber fraction (vol%)
h	Thickness
A	Area
F_i	Force due to swelling ionomer
F_s	Force of support resisting swell

A key input to this model is the modulus of the ionomer when in the swollen state (E_i). This value is obtained from a tensile test on the unsupported ionomer while still immersed in water. We preconditioned the membrane under the same conditions as the swell measurement by boiling in water for three hours prior to the tensile test. Figure 54 shows the averaged stress-strain curves for these measurements when pre-boiled, soaked in water without boiling, and a control at room conditions. The pre-boiling, hydrated ionomer, has a modulus of about 35 MPa.

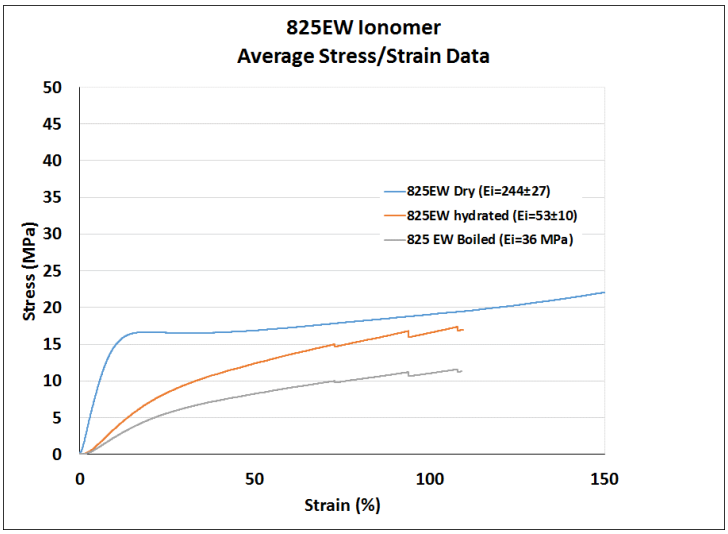

Figure 54. Stress vs. strain curves for 825 EW ionomer at room conditions, after soaking in water, and after boiling in water for 3 hours. The hydrated and boiled membranes were measured while immersed in water.

The modulus of the fiber support is also need for the model. In this case, however, we need to define how the support cross sectional area is calculated. For solids materials like neat membrane, the measured width and thickness of the sample provide the cross-sectional area use to determine the stress applied to the sample. In the nanofiber case, however, the measured thickness of the sample is a combination of fiber volume and pore volume. Furthermore, the sample is compressible and its thickness will depend upon the amount of force applied during the measurement. A more consistent value for the thickness (*h*) is to use effective thickness of the sample as determined by the basis weigh (g/m^2) divided by the density, *p* (g/cm^3).

$$h\ (cm) = \frac{bw(\frac{g}{m^2})}{\rho\ (\frac{g}{cm^3})} \times \frac{10{,}000\ (m^2)}{cm^2}$$

Equation 2. Effective support thickness calculation.

The sample thickness now represents only the fiber contribution to the material and does not include the pore volume.

This convention was used to measure the stress-strain properties for a series of electrospun nanofiber supports of differing basis weights. As an example, the data shown in Figure 55 is for a series of supports with basis weights varying between 8 and 16 grams per square meter (gsm) where the down web and cross web properties are clearly different but the shapes of the curves and, therefore, the modulus are quite similar. This is what one might expect when the data is normalized for thickness correctly.

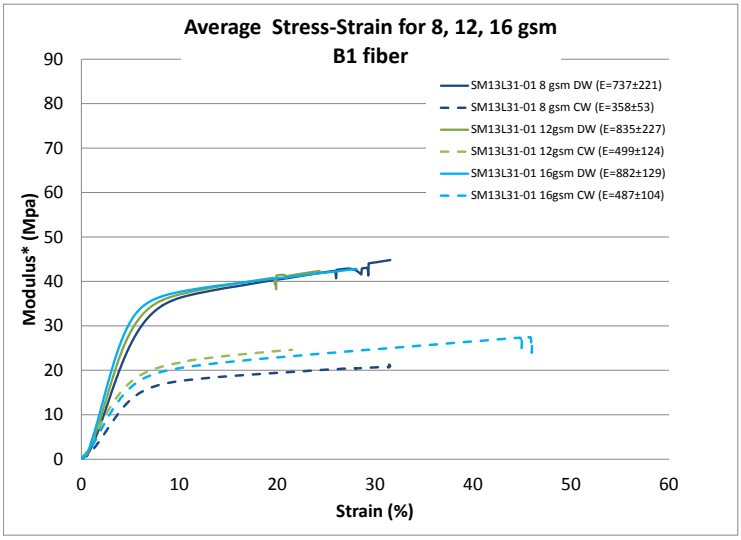

Figure 55. Average stress/strain plot for three different basis weight support materials. Cross sectional area determined from basis weight and fiber density.

This relationship was applied to a variety of composite membranes made in this project. In addition to the nanofiber candidates, membranes made using expanded polytetrafluroethylene (ePTFE) were also evaluated. The stress-strain data for three ePTFE supports are shown in Figure 56. Interestingly, these materials show a very distinct-down web (DW) and cross-web (CW) difference but with the stiffer measurements in the cross-web direction.

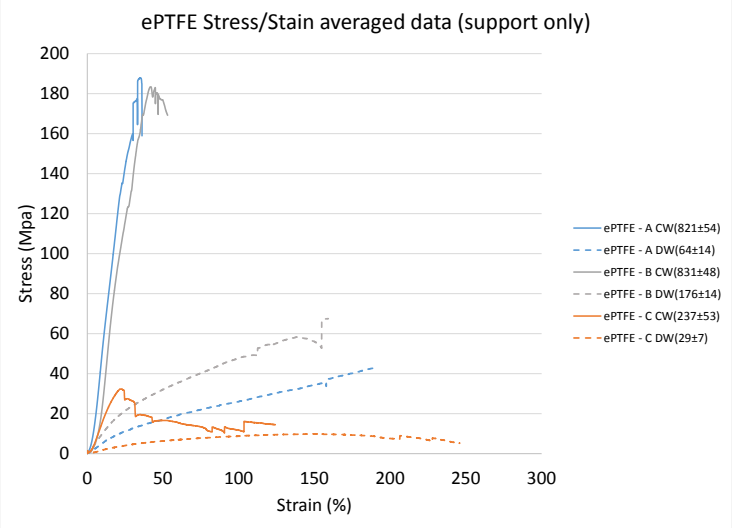

Figure 56. Average stress/strain data for three different ePTFE support materials.

Using the pre-boiled modulus value for the ionomer in the model, along with the measured modulus for a series of nanofiber supports with differning basis weights, we can contruct the predicted swell curves. Figure 57 shows swell as a function of fiber content for one type of fiber (hydrocarbon-fluorocarbon belnd, B1). The lines represent the expected values based on the input from the fiber and ionomer modulus measurements and the symbols represent actual measured data. It can be seen that the model predicts the swell of the composite remarkably well in both down web and cross web directions.

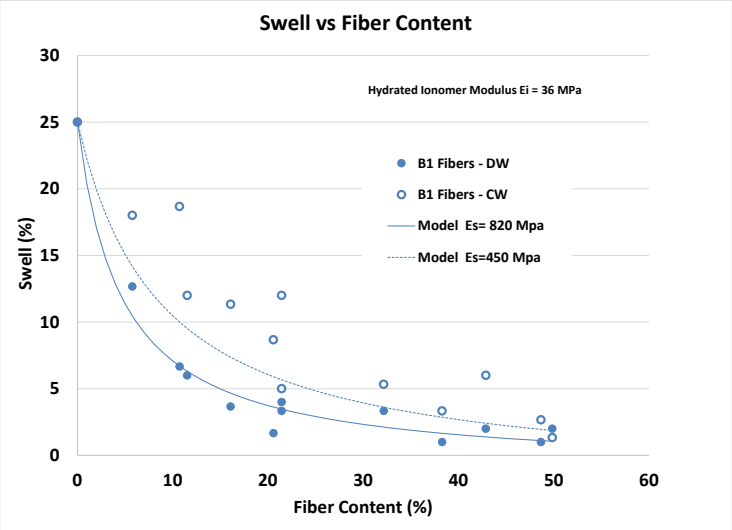

Figure 57. Swell vs Fiber content for a series of membranes made with the same fiber type.

It would be most useful to apply this model to a variety of fiber reinforcing materials in order to understand the trade offs between increased fiber modulus and increased fiber content in a composite membane. Figure 58 shows swell as a function of the product of fiber support modulus (E_s) and fiber fraction (f). This allows us to construct a curve that incldes several materials with differning down web and cross web properties. From this analysis we are able to predict the potential for new fiber support candidates without having to fabricate composite membanes and do the indivdual swell measurements.

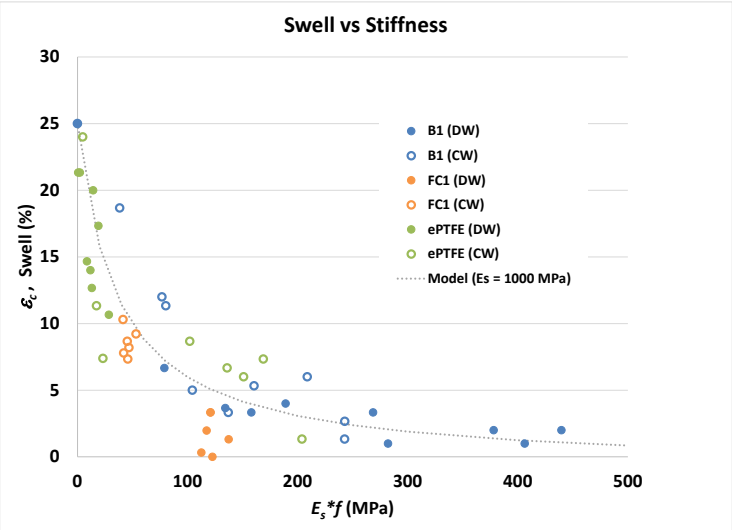

Figure 58. Swell vs. the product of the fiber modulus (E_s) and fiber fraction (f). Solid symbols represent down web (DW) data and open symbols represent cross web (CW) data.

Another test of the model is to plot the predicted swell versus the measured swell values (Figure 59.) Interestingly, the model appears to predict higher swell than was actually measured for several samples. This implies that the model will provide a conservative estimate of the swell when used as a guide for establishing material targets such as fiber modulus of fiber fraction.

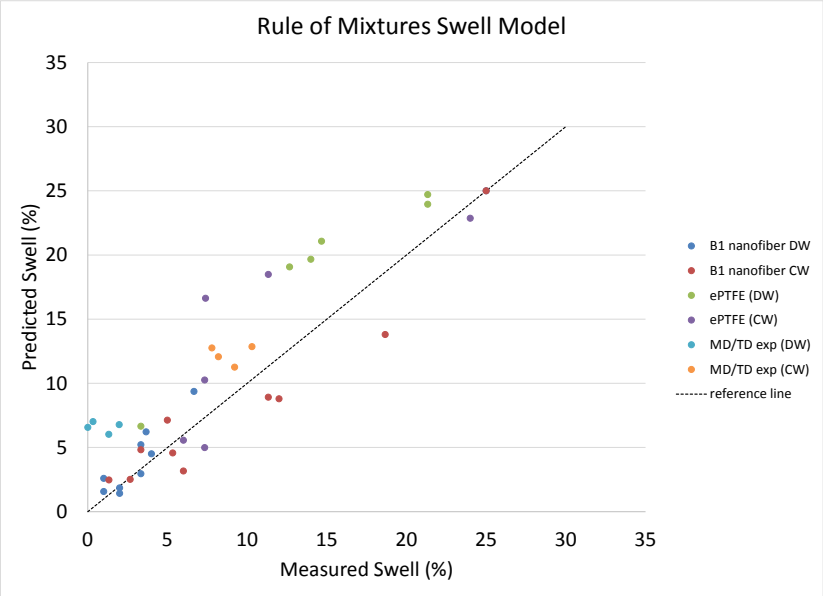

Figure 59. Comparison between measured swell data and predicted data based on rule of mixing model. Reference line represents the ideal case (45° line) and not a curve fit.

Subtask 3.2.2 Mechanical characterization at GM

Mechanical Testing

To evaluate the mechanical stability of the 3M membranes, a blister test was used to generate stress life curves[iv] for the various membrane types. For each sample, 16 blister samples were used at a total of six different pressure ramp rates: 1, 0.2, 0.1, 0.05, 0.02, and 0.01 kPa/sec. The test condition for all samples was 90°C and 10%RH. For comparison with non-supported PEMs, blister tests were also run for a commercial 25µm DuPont™ NR-111 Nafion® PEM, and a 12µm thick non-supported PEM of DuPont™ DE2020 Nafion® coated at GM.

The stress at which a blister burst is determined by the Hencky equation (Equation 3);

$$\sigma = \frac{1.724}{4}\left(\frac{E(t,T,RH)p^2a^2}{h^2}\right)^{1/3} \qquad \sigma_{ij}(\sigma,t,T,\lambda) = \int_0^t E(t-\xi,T,\lambda)\frac{d[-\delta_{ij}\beta(T,\lambda)\Delta\lambda]}{d\xi}d\xi$$

Equation 3. Hencky equation

where σ is the stress at the center of the blister; E is the relaxation modulus; p pressure at which an individual blister burst (the point at which the blister could no longer retain pressure); a is the blister radius; T is temperature; and h is the membrane thickness. The relaxation modulus for the various membranes was not measured. Thus, assuming that the modulus of each supported PEM is governed by the support properties, which is the same for all of the 3M PEMs, the burst stress for each blister was simply reported as the Hencky normalized pressure (Equation 4).

$$\sigma \propto (p/h)^{2/3}.$$

Equation 4. Hencky normalized pressure.

Typical results are plotted in Figure 60. The time and stress at which each individual blister bursts are indicated by the data points in the plot. A power law curve was used to fit the data for all the different ramp rate conditions, creating stress-life curves for each membrane type, as indicated by the lines in Figure 60. The stronger the membranes, the higher a burst stress and the longer the times to break. Thus, the strongest membranes have stress-life curves toward the upper right corner of the graph.

In this example, it is clear that all of the 3M supported PEMs are stronger than the non-supported Nafion® PEMs made by either DuPont or GM. Both supported PFSA PEMs are significantly stronger that the supported PFIA PEM, exhibiting lifetimes about 100 times higher than the PFIA PEM at a given stress. Among the supported PFSA PEMs, the 825EW PEM appears to be slightly stronger than the 725 EW PEM.

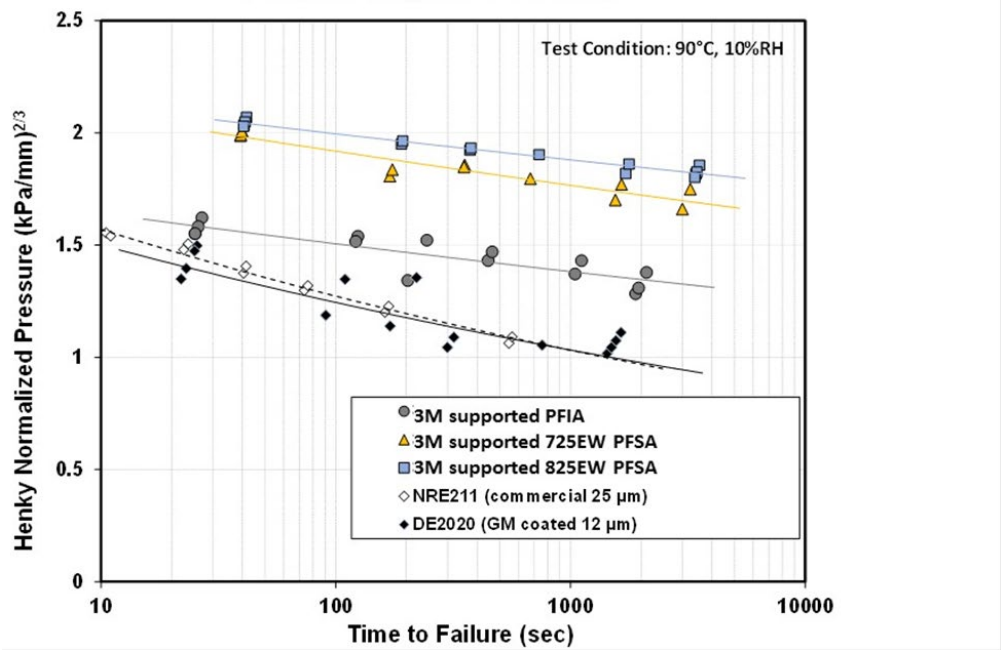

Figure 60. Pressure Ramp to Burst Blister Tests

Figure 61 compares the Hencky normalized burst pressure stress-life curves for PEMs of selected ePTFE and nanofiber FC1 supports at 90°C and 10% RH. The ePTFE supported PEMs have dashed lines and the solid lines represent the FC1 supported PEMs.

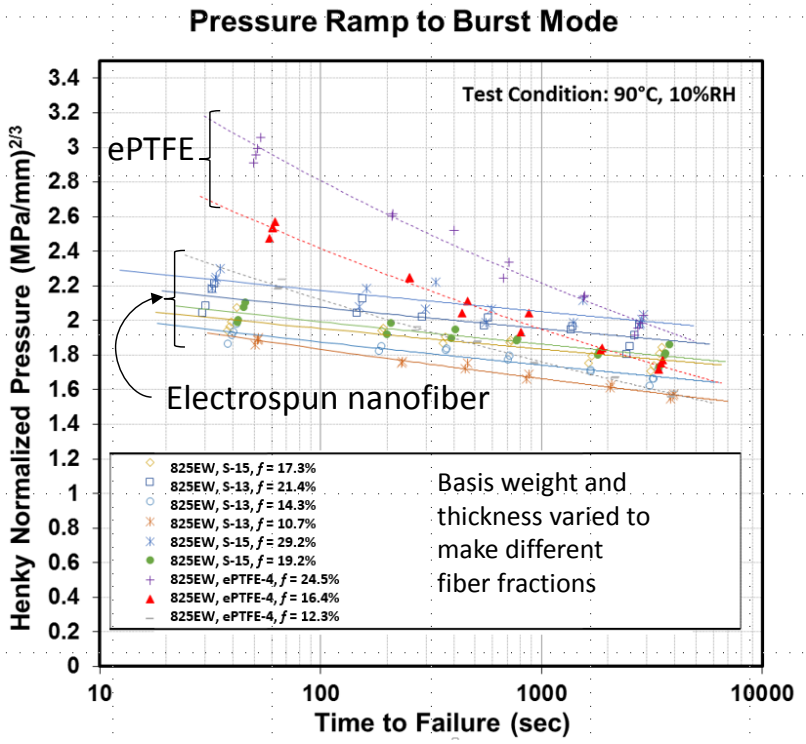

Figure 61. Pressure ramp to burst blister tests of supported PFSA membranes at 90°C & 10% RH.

One thing that is immediately noticeable is that the slopes of the stress-life curves for the ePTFE-supported PEMs are greater than those for the nanofiber FC1-supported PEMs. Within each family of supported PEMs, the slopes of the stress-life curves are similar. This relative difference in the slopes of the stress-life curves suggest that there is a stronger viscoelastic contribution from ePTFE than from the nanofiber FC1 supports.

To better interpret the stress-life data, we plotted the Hencky normalized pressures as a function of support fiber weight fraction for both types of reinforcement. Figure 62 and Figure 63 show plots of the Hencky normalized pressures at 200 and 2000 sec, respectively for both the FC1 and ePTFE supported membranes. In these plots, all membranes were annealed at the same temperature, except for the gray filled diamonds, which were annealed at a higher temperature. From these data, we see that for a given support, the Hencky normalized burst pressure at both short (200s) and long (2000) burst times increases linearly with fiber weight fraction. The lines for both the ePTFE- and FC1-supported PEMs intercept the x-axis (0% fibers) at the same point, which is, expectedly, close to the Hencky normalized pressures for the non-supported PEMs. We also see that the Hencky normalized burst pressures are lower for the membranes annealed at the higher temperature as compared to those annealed at lower temperatures. This is similar to what we observed in earlier studies reported in 2014.

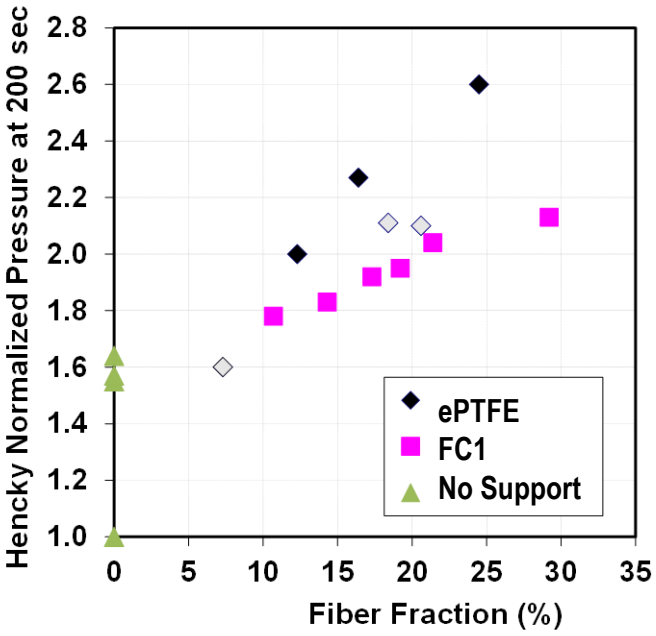

Figure 62. Hencky normalized pressure at 200 sec for supported and non-supported PEMs. All membranes were annealed at 155°C, except for the gray filled diamonds, which were annealed at 200°C.

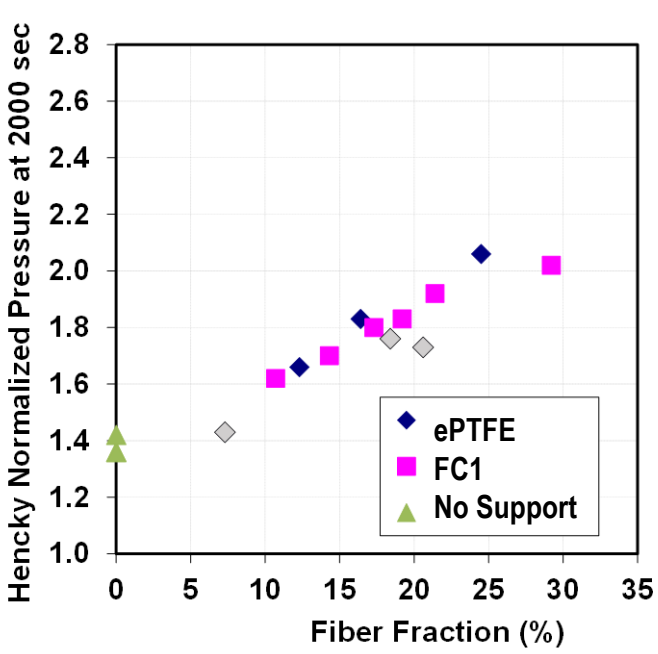

Figure 63. Hencky normalized pressure at 2000 sec for supported and non-supported PEMs. All membranes were annealed at 155°C, except for the gray filled diamonds, which were annealed at 200°C.

Another key observation is that the two different supports show different behaviors and long and short burst times. At short burst times of 200s, the ePTFE-supported PEMs have higher Hencky normalized burst pressures than the FC1-nanofiber supported PEMs do. However, at longer times (2000s) PEMs made using both supports have similar Hencky normalized burst pressures. It is expected that at even longer times (i.e. lower stresses) that the FC-1 nanofiber supported PEMs will be superior to the ePTFE-supported PEMs. Further analysis is required to fully assess the implications of the time dependent behavior.

Membrane Swell

Water swelling tests for a series of PFIA membranes made with the FC-1 nanofiber support and ePTFE were conducted at GM. Tests were done by placing membrane samples in liquid water and heating the samples in pressure vessels at elevated temperatures for 24h. Separate samples of each membrane were heated at 25, 60, 80, 100 and 120°C. After 24h the samples were removed from the water filled vessels, quickly hand-dried to wipe of any excess liquid water, weighed, and measured for length width and thickness. The dimensions were compared with a dried membrane to determine the percent dimensional swelling and water uptake at each temperature. The percent mass, length and width increases after 24h at 60°C are shown in Figure 64. In these experiments, the length is the down-wed direction and the width is the cross-web direction. As expected, the supported membranes swell less than the non-supported PEMs. For the supported membranes, the cross-web (width) swelling is lower than the down-web (length). Another key observation is that the membranes with the 3M FC1 supports swell less than the ones made with ePTFE supports. Of the FC1 supported samples, the one with the higher basis weight has lower mass uptake. However, basis weight has little effect on the in

plane swelling. Additionally, the membrane annealed at higher temperature swells less than the lower temperature annealed samples.

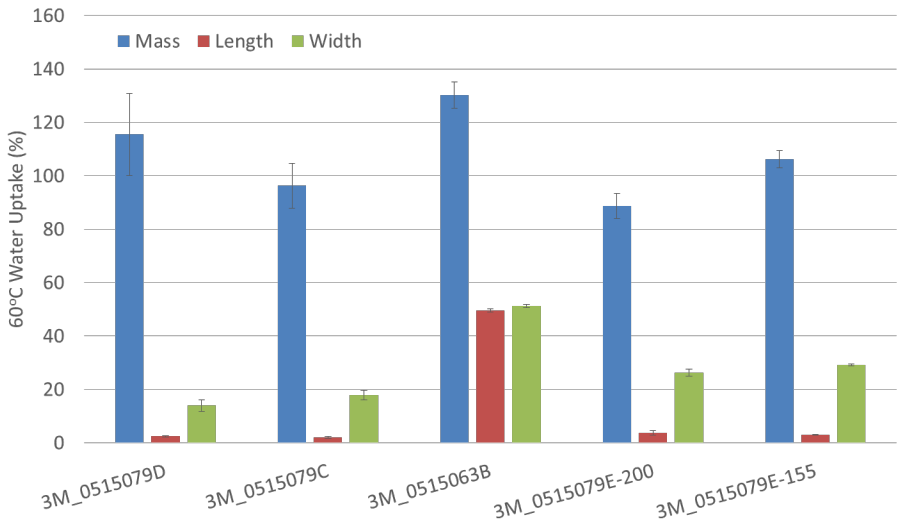

Figure 64. Percent Swelling of PFIA membranes after 24h in liquid water at 60°C

Figure 65 and Figure 66 show the percent swelling and mass uptakes for a FC1 nanofiber-supported and an ePTFE supported PEM, respectively, as a function of temperature. Both membranes contain 17.3-17.5 volume % support, are 14μm thick and were annealed at the same temperature, so it is a good comparison of the support type. These plots show the percent increase in all three dimensions, the mass uptake of water, and the calculated mass uptake based on the volumetric swelling and the density of water. Note the excellent agreement between the measured and calculated mass uptakes, with the exception of the highest temperature (120°C) for the ePTFE-supported sample. We were unable to get a good measurement for the FC1-nanofiber supported membrane at 120°C because the sample started to come apart as the ionomer came off the support. PFIA membrane with both support types exhibit increased swelling with higher temperature. At all temperatures, the ePTFE-support PEM swells more than the FC1-nanofiber supported PEM, with the difference between the two types increasing with higher temperatures.

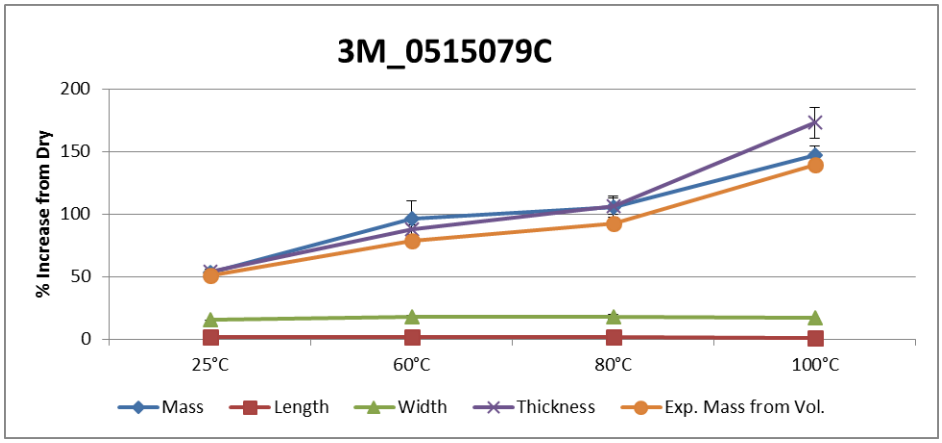

Figure 65. Percent Swelling and Mass Uptake of FC-1 supported 3M_0515079C PFIA membranes after 24h in liquid water at various temperatures.

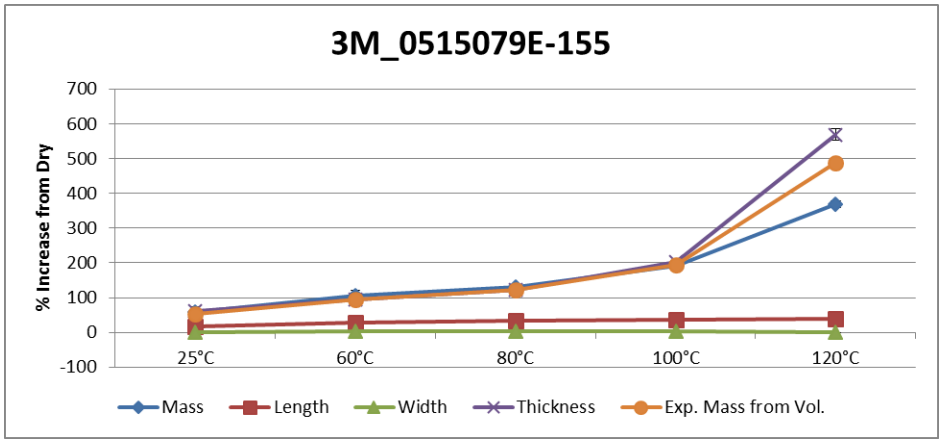

Figure 66. Percent Swelling and Mass Uptake of ePTFE supported 3M_0515079E-155 PFIA membranes after 24h in liquid water at various temperatures.

Subtask 3.3 Characterization of membrane chemical stability properties

Introduction and Background to Peroxide vapor stability test

Ionomeric membranes used in PEM fuel cells must have adequate durability for the intended application. For example, membranes used in automotive applications have target life times of approximately 8000 hours of operation. Chemical durability of isolated membranes can be assessed using ex-situ methods such as the solution phase Fenton's test which employs ferrous ion in a hydrogen peroxide solution to generate the aggressive hydroxyl radical. Fenton's tests of perfluorosulfonic acid (PFSA) ionomers induce membrane damage from the ends of the polymer chains in the so-called unzipping mechanism (Figure 67). Solution phase

Fenton's tests do not, however, induce polymer main chain scission reactions which can rapidly reduce both average molecular weight and mechanical strength of the polymer film.

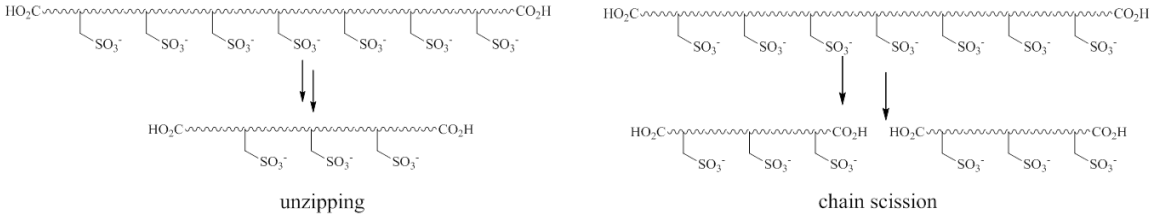

Figure 67. Ionomer degradation modes

Previous studies have shown that hydrogen peroxide (H_2O_2) vapor treatment of PFSA membranes does, indeed, induce main chain scissions that are also believed to occur during in-situ fuel cell operation.[v,vi] GM has developed a versatile H_2O_2 vapor test that allows the testing to be performed over a range of RH values at constant peroxide concentration.[vii,viii] A summary of a typical three-step 200 ppm H_2O_2 vapor test is show in Figure 68. In this test, both chemically stabilized NRE212 and unstabilized N112 are employed while the rates of degradation are monitored by the fluoride evolution rate (FER). The initial, 20 hour step of the test is conducted at 90ºC and 95% RH. After stabilization, the degradation rates maintain constant values that reflect the relative amounts of carboxylate end groups present in the two ionomers. Because NRE212 is chemically stabilized by fluorination, its carboxylate content is much lower than that of unstabilized N112. The second step of the test is conducted at 90ºC and 25% RH where the degradation rates of both ionomers increase significantly. In the final step, the RH value is returned to the original 90ºC, 95% value. Here, the degradation rates are again stable but their values have increased relative to the original 95% phase. The increased degradation rates after the low RH excursion of step two reflect changes in the carboxylate content of the ionomers which are associated with chain scission events. The increased carboxylate content of the ionomers are shown in Figure 69. The carboxylate content is assessed by FTIR analysis of the potassium salt form of the membranes. Initially, NRE212 has no detectable carboxylate signal at 1693 cm^{-1} but after the three-step test, the carboxylate signal has increased substantially, reflecting the damage that occurs during the low RH excursion. Unstabilized N112 has a carboxylate signal initially and undergoes a similar increase of its signal after the low RH excursion reflecting a similar degree of scission. Importantly, long term, 95% control studies show that no increase in carboxylate occurs over 60 hours indicating that the chain scission damage is incurred during only the low RH excursion.

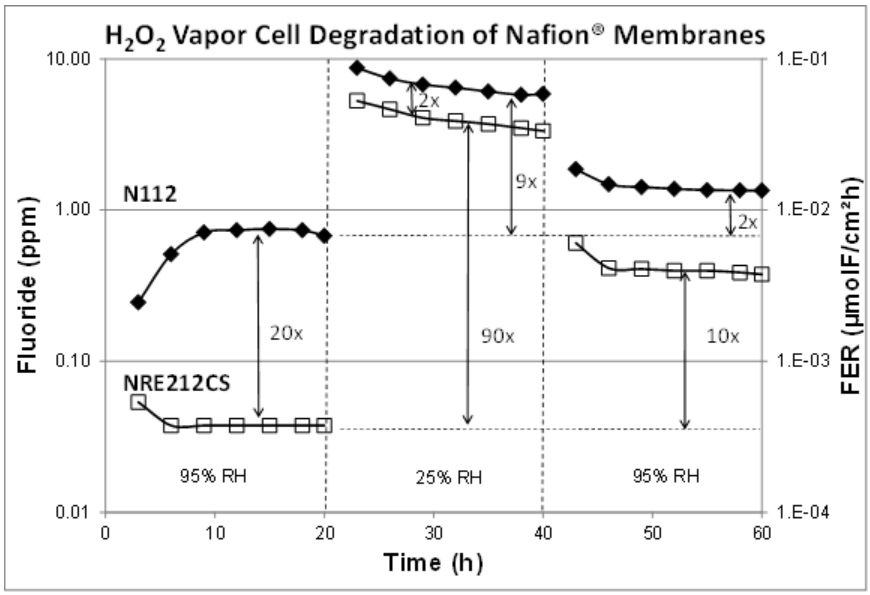

Figure 68. FER values obtained from N112 and NRE212CS while subjected to 200 ppm of H2O2 vapor using 95-25-95 RH test

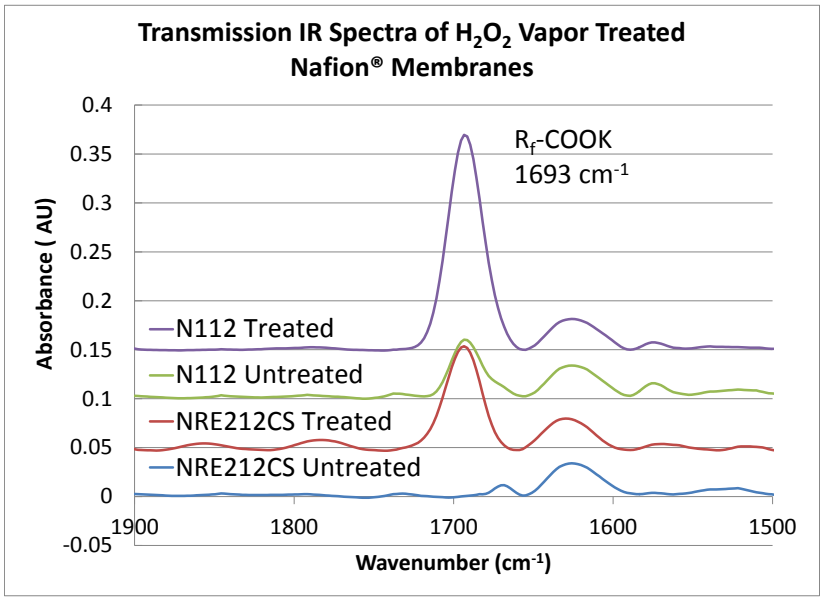

Figure 69. Intensities of COOK infrared bands of N112 and NRE212CS at 1693 cm 1 after treatment shown in Figure 1

Tests of 3M Membranes

Several PFSA and PFIA samples were run using this test. All samples were supported with ePTFE or a nanofiber in order to maintain membrane integrity throughout the test. One set consisted of membranes made with and without peroxide scavenging additives. The results of the peroxide vapor cell tests are shown in Figure 70. There a several clear observations from

these series of experiments. Firstly, both PFSA and PFIA membrane classes show a benefit from the stabilizing additive, both at low and high RH. Secondly, the 3M825 EW PEMs are more robust than PFIA PEMs, both with and without stabilizer. Finally, the stabilizer additive appears to suppress chain scission of the PFSA PEMs. This is evidenced by a similar FER for both the first and third stages of the test where the RH is 95%. These results are similar to what has been seen for commercially available end group-stabilized Nafion® membranes[2]. The PFIA seems to have a higher rate of unzipping degradation at both 95% RH and 25% RH, as evidence by the higher, flat FER profiles during those stages of the H_2O_2 vapor cell tests. Surprisingly, even without the stabilizer, there doesn't appear to be a great deal of chain scission for the PFIA PEM. The FTIR data showing the changes in carboxylate groups is seen in Figure 71.

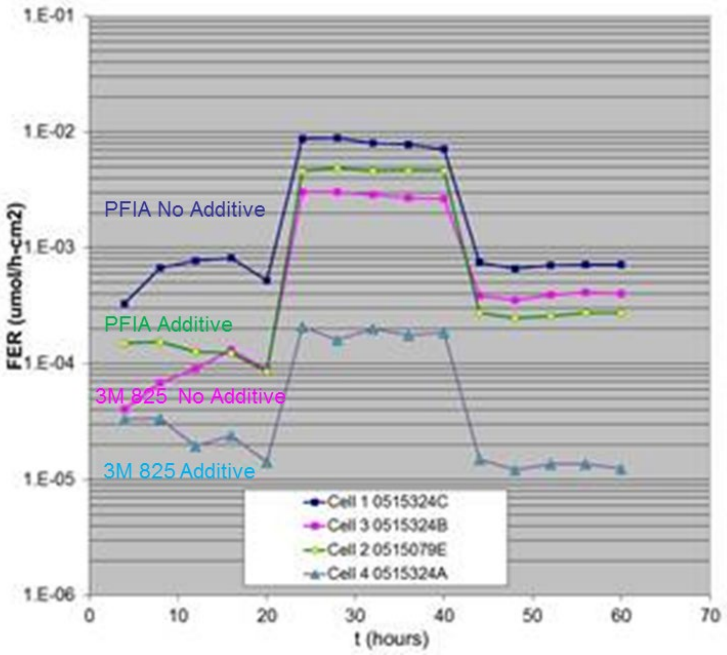

Figure 70. Three-step H2O2 vapor test (30 ppm) of 3M membranes. The test is done at 90ºC: 95%RH for the first 24h, 25% RH for the next 24h and 95%RH for the final 24h.

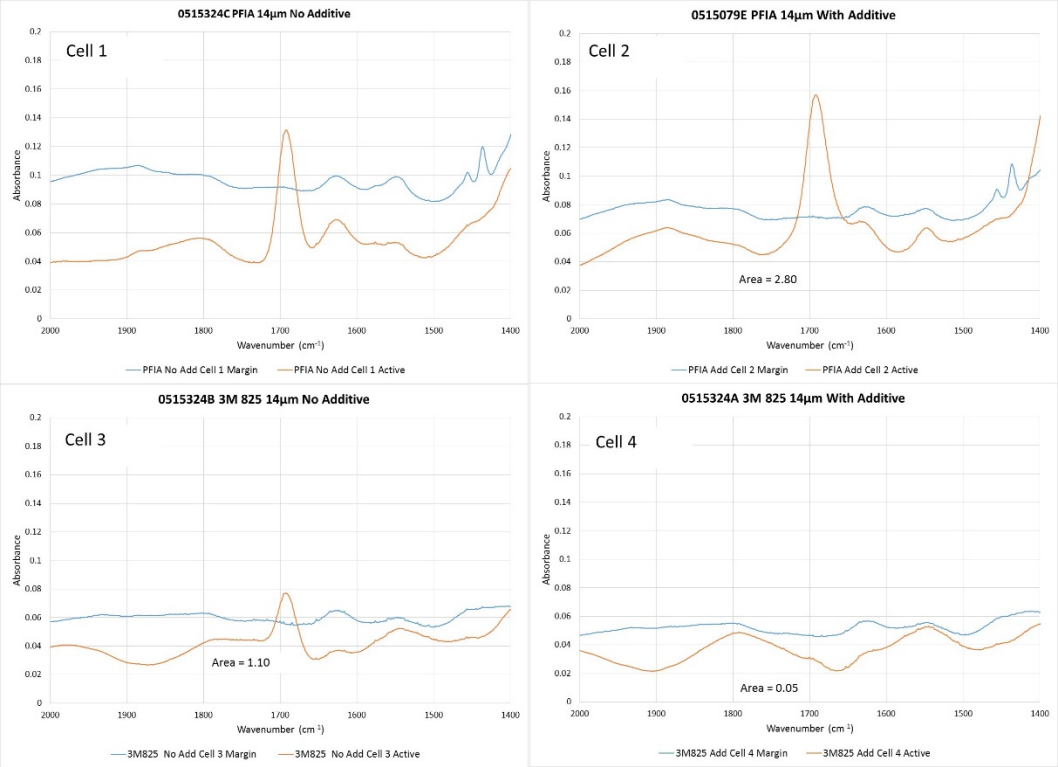

Figure 71. FTIR spectra of K+ - exchanged membranes after H2O2 vapor degradation.

Compared to stabilized 3M PFSA, all stabilized PFIA variants exhibit increased fluoride release rates and carboxylate growth when subjected to a 60 hour, variable RH H_2O_2 vapor test. Even PFIA samples that contain lower levels of iron contamination than the earlier PFIA sample show qualitatively similar degradation behavior. That is, the lower iron levels did not prevent H_2O_2 induced damage.

Task 4 MEA fabrication and Fuel Cell testing

Subtask 4.1 MEA preparation

MEAs for fuel cell testing under Task 4 were fabricated in subtask 4.1. Standard methods were used at 3M and GM, however, the details of these processes are proprietary and not disclosed in this report.

Subtask 4.2 50cm2 performance testing

Subtask 4.2.1 50cm2 performance testing at 3M

A large number of fuel cell tests were completed during the course of this project and of those, a few of the key results will be discussed in this section. Figure 72 shows one particular result

that highlights the effect of increase operating temperature and decreased humidity on cell voltage and resistance for a series of PFSA and one PFIA membranes (supported membranes are denoted with a “-S” extension). In this test, the hydrogen and air dew points are held constant at 80°C and the cell temperature is increased up to 120°C. As expected, the performance, as measured by voltage at 0.4A/cm2, decreases as the inlet humidities decrease. However, the lower equivalent weight samples show higher performance at the hotter, drier conditions. Likewise, the resistance is lowest for the PFIA sample and highest for the supported PFSA membranes. The performance of the PFIA hand spread sample was compromised in this test likely due to edge failure and crossover (orange circle symbols). However, the exceptionally low resistance of the MEA with the PFIA membrane at the hottest and driest conditions is a clear advantage over the PFSA membranes.

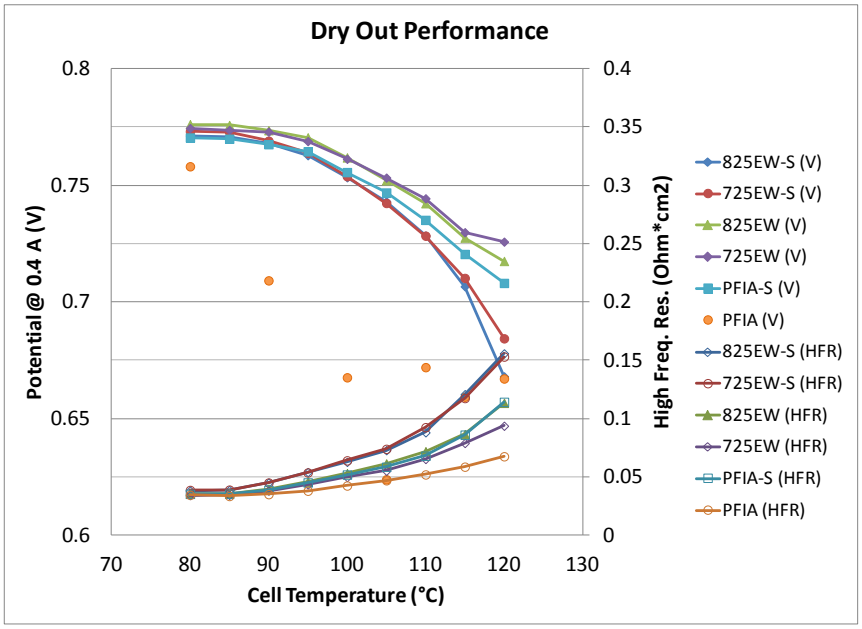

Figure 72. Fuel cell performance and HFR for samples run with 80°C dew points on anode and cathode as a function of cell temperature.

Another example of this type of data is shown in Figure 73 where the high current RH sensitivity for various supported membranes including some benchmark PFSA membranes as well as two PFIA membranes. One PFIA membrane is composed of 80% PFIA and 20% PFSA. The other PFIA membrane was identified as passing the program's fourth milestone. All membranes contain reasonable quantities of chemical stability additives. As expected, the PFIA membranes showed some benefit compared to the PFSA membranes.

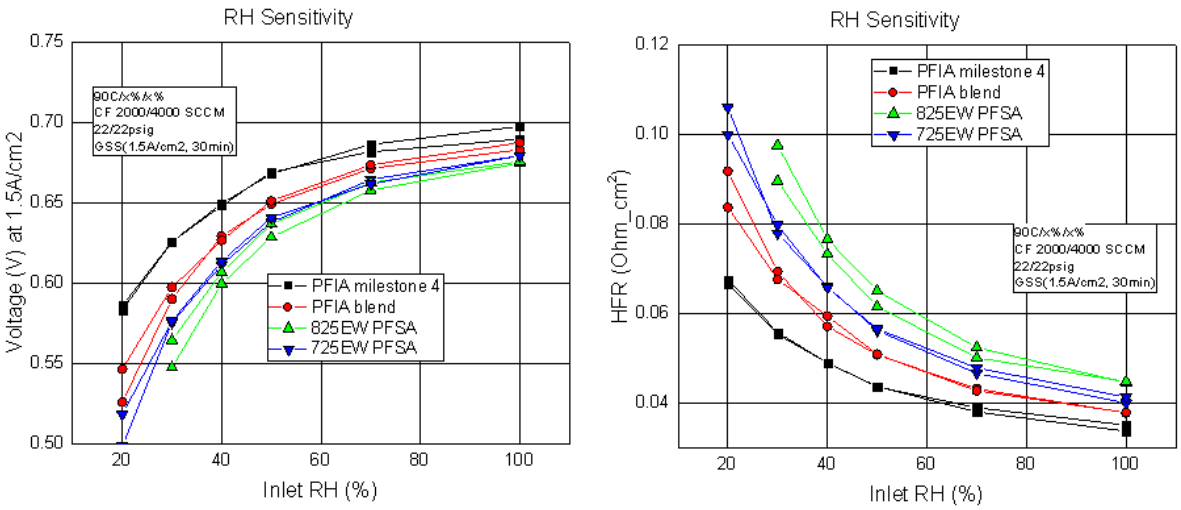

Figure 73. High current RH sensitivity for 3M supported membranes

In Cell Conductivity Measurements

A study was completed to determine the membrane through-plane resistance in a cell and its relationship to the ex-situ in-plane conductivity measurements. The transmission line approach was based on testing membranes of different thicknesses and extrapolating the cell resistance to zero thickness in order to determine the "non-membrane" resistance values. Measurements were taken at 80°C as a function of inlet RH. The test protocol and analysis was conducted on 3M 725EW PFSA membrane MEAs with standard commercially available 3M electrodes.

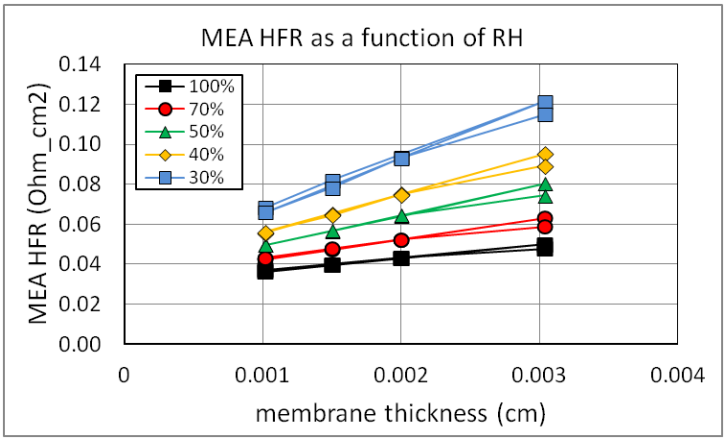

Figure 74. Measured HFR as a function of thickness at various RH's. The linear relationship between HFR and thickness allows the calculation of conductivity, in this case simply the inverse of the slope. The intercept values are indicative of non-membrane component contributions to HFR.

Figure 74 illustrates the high frequency resistance (HFR) versus thickness at each RH where the slope of each line is the resistivity of the membrane in Ohm_cm. Figure 75 shows the conductivity as a function of RH calculated from this data along with our traditional four-point probe conductivity. There is some discrepancy between the in-cell through-plane conductivity and the in-plane measured conductivity that is likely due to the changes on dimension of the membrane when hydrated in these different environments.

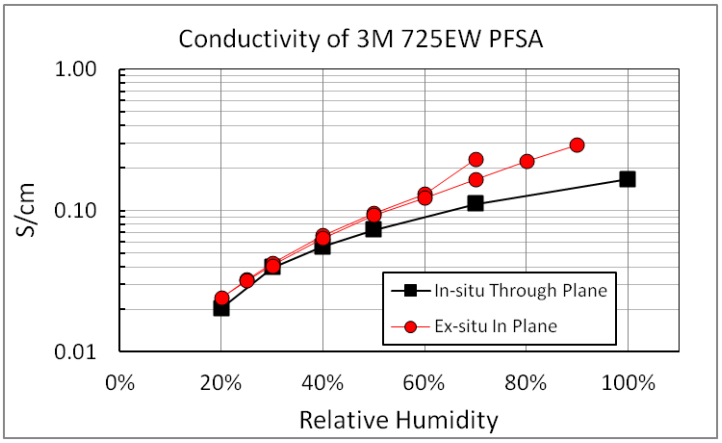

Figure 75. Reasonable agreement in measured conductivity of 3M 725EW PFSA ionomer membranes when measured through plane (in cell) versus in plane (out of cell) especially at low RH's.

In an effort to determine the conductivity of the ionomer filled support composite, transmission line analysis was conducted for a series of supported membranes as a function of neat ionomer skin thickness. Figure 76 shows the plot of HFR versus thickness for a series of unsupported and membranes supported with low basis weight standard 3M support. We expect the slopes of these lines to be similar since the neat ionomer skin is the only change in both the unsupported and supported membranes. However, the impact of the ionomer-filled support composite is captured and can be calculated from the intercept value as outlined below in Figure 77.

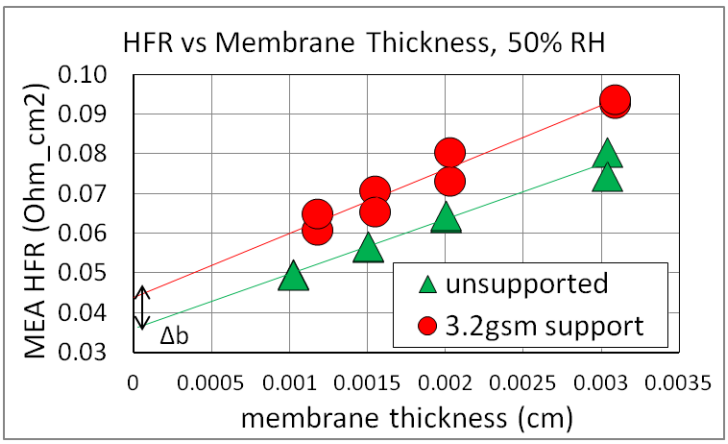

Figure 76. Transmission line data for unsupported 3M 725EW PFSA membrane MEAs compared with membranes with the same ionomer plus the addition of standard low basis weight 3M support.

- Supported Membranes as Resistors in Series
  - $R_{total} = R_{skin} + R_{composite}$
    - $R_{skin} = l_{skin} / \sigma_{skin}$
    - $R_{composite} = l_{composite} / \sigma_{composite}$
    - $L = l_{skin} + l_{composite}$
  - $R_{total} = L(1/\sigma_{skin}) + l_{composite} / \sigma_{composite} - l_{composite} / \sigma_{skin}$
- From a linear fit of MEA HFR (R_{total}, Ohm_cm2) versus membrane thickness (L, cm)
  - $\sigma_{skin} = 1 / m$
  - $\sigma_{composite} = l_{composite} / (\Delta b + (l_{composite} / \sigma_{skin}))$

Figure 77. Series of equations used to calculate the conductivity of the neat ionomer skin and fiber filled composite layers in a supported membrane

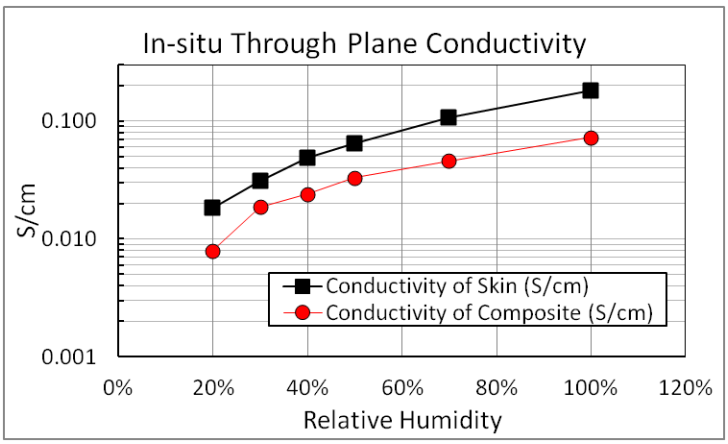

Figure 78. Transmission line analysis of 3M 725EW PFSA ionomer membranes containing standard low basis weight 3M support.

The data in Figure 78 shows the ionomer-filled 3M support composite layer has roughly a 2x decrease in conductivity compared to the neat ionomer. Since the void fraction of the low basis weight standard 3M support is roughly 50%, first approximation suggest that the impact of the support is solely a dilution effect with minimal impact from effects like tortuosity or lambda restriction.

Trilayer membrane performance testing

Throughout the course of this program we have sought to understand the effect that nanofiber support has on the performance and durability of a composite membrane. These experiments are often designed to assess the impact of fiber content on through-plane resistance. One important question is whether the fiber location within the membrane will influence this resistance either positively or negatively. In the following study, we fabricated three membranes; the first was made using 3M's traditional method of filling an existing nanofiber non-woven support with an ionomer dispersion followed by drying and annealing (left most image in Figure 79). The next two were fabricated at Vanderbilt University using their dual fiber method. For these membranes, one was made to mimic the 3M construction by depositing only ionomer fibers on the outer layers and a 50 vol% layer in the center using a polyamide imide (PAI) supporting fiber (Figure 79, center). The other was made by depositing ionomer and PAI support evenly throughout the membrane (Figure 79, left). The ionomer in the dual fiber membranes were then fused to form dense layers with the PAI support. In all cases the membranes used 825EW 3M ionomer, no additive, and are 20 um thick with fiber contents between 14 and 20%.

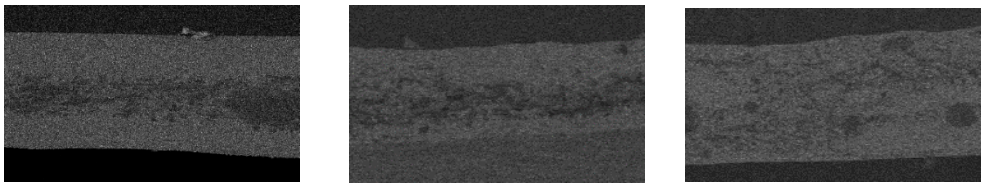

Figure 79. SEM cross section images after focused ion beam polishing for typical 3M three layer membrane (left) and Vanderbilt's 3 layer membrane (center) and one layer membrane (right) based on dual spinning methods.

Performance of all three membranes at 80°C with 100 % RH and 95°C with 50% RH are shown in Figure 80 and Figure 81 respectively. In both cases the performance and resistance are nearly identical. These results suggest that, for this study, the location of the fiber does not significantly affect the through-plane resistance, and therefore performance. It is important to note that this was not an exhaustive study and that there may be other circumstances where the fiber location can impact performance. In addition, the durability and mechanical property differences between constructions may warrant a specific fiber location. However, the observation that fiber content does not negatively impact membrane resistance beyond what one would expect due to reduced ionomer content is a significant finding that should allow a wide range of reinforced membrane constructions.

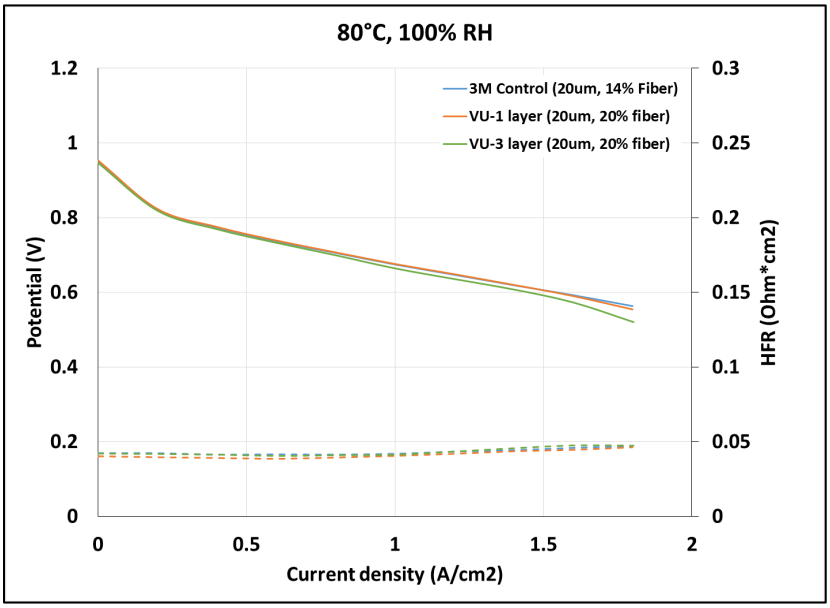

Figure 80. Polarization and HFR curves for membranes based on 3M or Vanderbilt fabrication methods at 80°C and 100% RH.

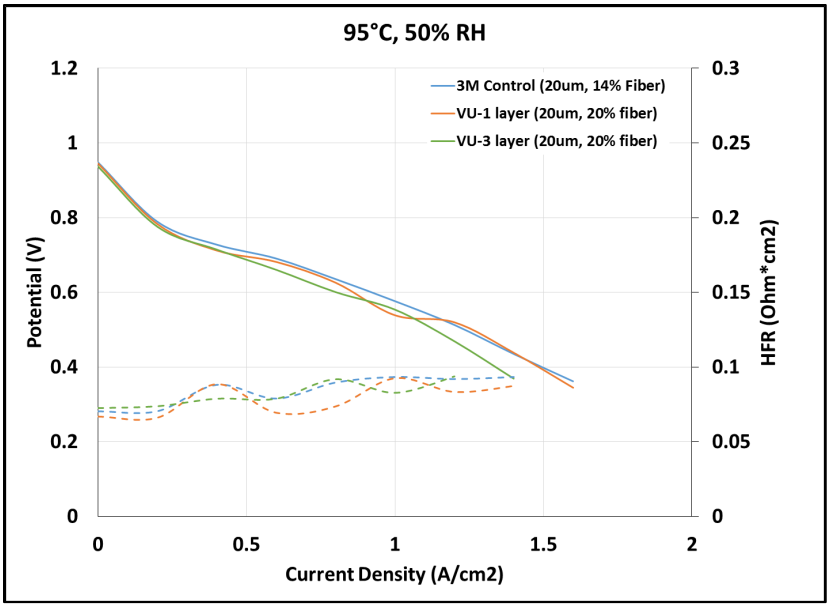

Figure 81. Polarization and HFR curves for membranes based on 3M or Vanderbilt fabrication methods at 95°C and 50% RH.

Fuel cell evaluation of PFICE materials

Fuel cell evaluations on the experimental PFICE materials were completed once samples were available and simple, unsupported membranes were fabricated. Membranes made for these experiments were hand-cast in the laboratory and subject to variation in thickness, defects, and other related quality issues. Two different activation methods were employed prior to the performance evaluations. One set of materials were activated using 3M's thermal cycling protocol while a second set of materials were activated using solely load cycling between 0.25V and 0.85V, twenty times. While the thermal cycling protocol is known to provide very good activation of the MEA upon initial start-up, we are concern that the unsupported PFICE material may not be able to withstand the extreme hydration cycling resulting in membrane failure.

During activation, as shown in Figure 82, all samples initially exhibited the expected increase in kinetics. However, after the tenth load cycle, the PFICE materials exhibited an unexpected decline in kinetics. This decline persisted for the remainder of the load cycling portion of activation. The samples that were then subsequently thermal cycled showed some recovery of this lost kinetics.

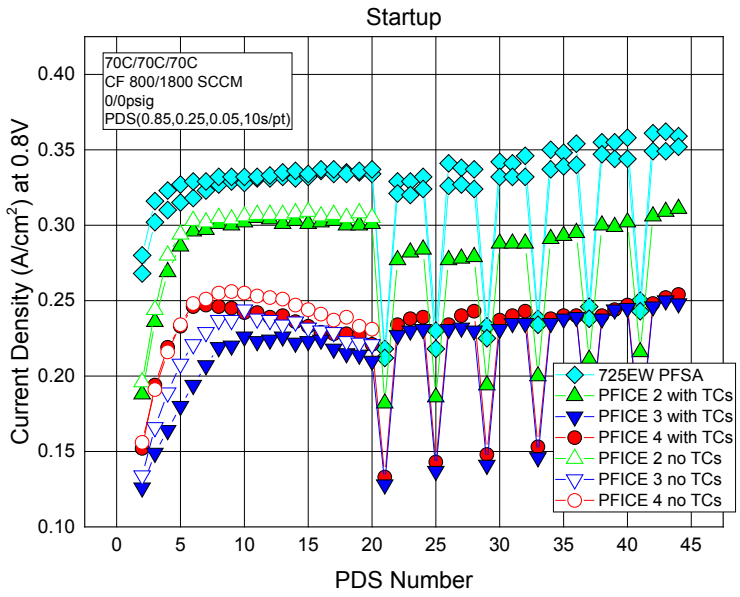

Figure 82 – Activation process for PFICE materials as well as 725EW PFSA material. PDS Number reflects the number of load cycles performed. After 20 load cycles, either activation is completed or 6 thermal cycles are performed. Between each thermal cycle, 4 load cycles are performed.

Fuel cell performance was evaluated first at 80°C with saturated hydrogen and air. It was observed that the PFICE materials exhibited reduced performance compared to a 725EW PFSA membrane of similar thickness (Figure 83). It was also evident that there was a significant benefit to performance with thermal cycling with all PFICE materials. This benefit was observed both in the kinetics region as well as an additional benefit at higher current densities. It should be noted that the 725EW PFSA membrane samples were activated using the thermal cycling procedure.

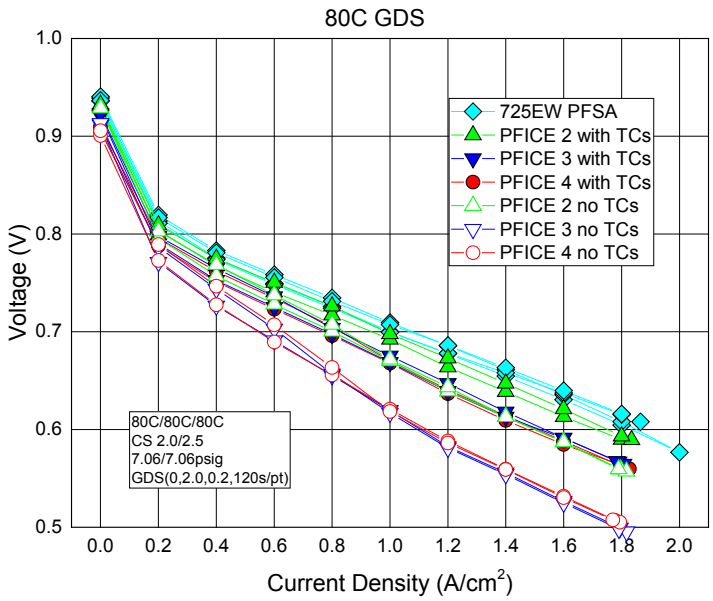

Figure 83 – Performance of PFICE materials compared to 725EW PFSA. Open symbols represent MEAs that did not receive thermal cycles during activation. Filled symbols represent MEAs that received six thermal cycles during activation.

Fuel cell performance was then evaluated with decreasing RH. It was observed again that the PFICE materials showed reduced performance compared to the 725EW PFSA membrane, as seen in Figure 84. In fact, the performance rank opposite of expected with the observation being that PFICE 3 and 4 < PFICE 2 < 725EW PFSA. Again, there was a large benefit to performance with thermal cycling.

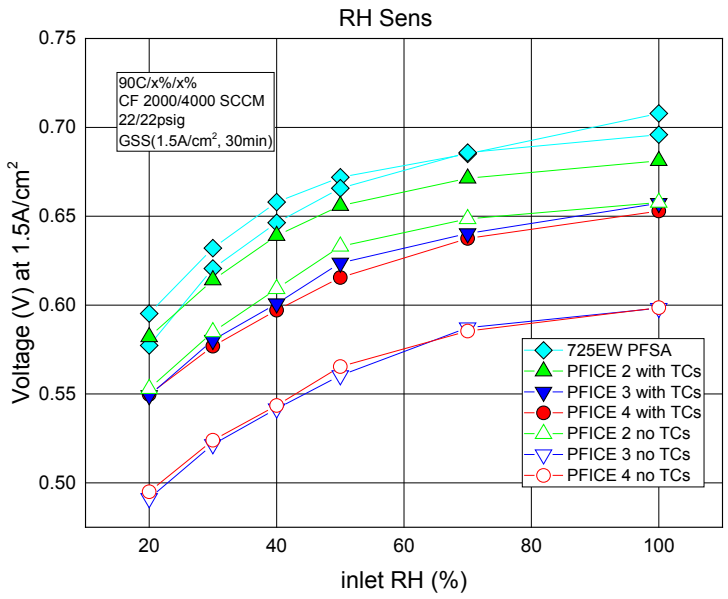

Figure 84 – Relative humidity sensitivity for PFICE materials compared to 725EW PFSA. Open symbols represent MEAs that did not receive thermal cycles during activation. Filled symbols represent MEAs that received six thermal cycles during activation.

During performance testing with decreasing RH, high frequency resistance was also measured. It was observed that the MEA resistance was greatly improved for the PFICE materials compared to the 725EW PFSA membrane. It was also observed that thermal cycling had little impact on the measured cell high frequency resistance.

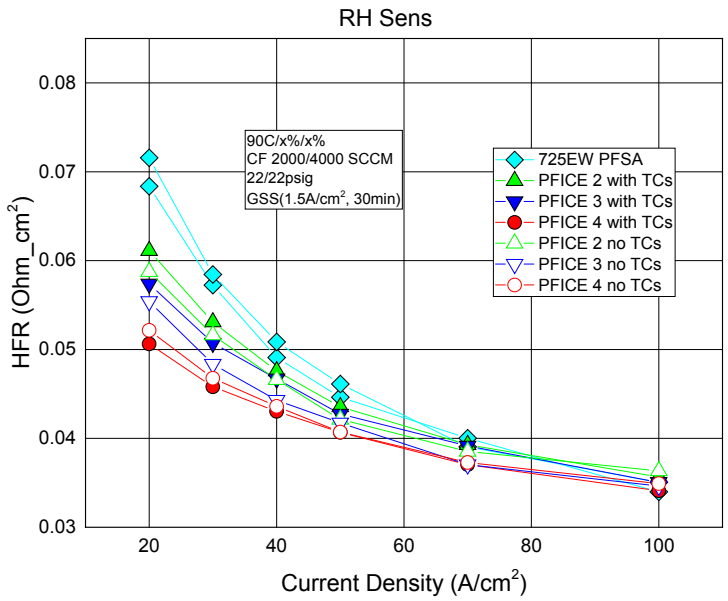

Figure 85 – MEA resistance sensitivity to relative humidity. Open symbols represent MEAs that did not receive thermal cycles during activation. Filled symbols represent MEAs that received six thermal cycles during activation.

Performance testing of Milestone Membranes

Performance testing of the two Go/No Go milestone membranes and a 3M control were all run using the same electrodes and test protocol. The details of these membranes are described in Table 19.

Table 19. Membranes used in performance and accelerated test comparisons.

3M ID	Milestone	Ionomer	Fiber type	Additive	Fiber (vol%)	Thickness (um)
0513277A	Control	3M 725EW	B1	Type 1	20.6	14
0514218A	#4	PFIA – Lot#1	FC1	Type 1	17.2	14
0515079D	#8	PFIA – Lot #1	FC1	Type 1	18.0	10

When operated at fully saturated conditions there is a very small performance difference only at the highest current density (Figure 86) and when the polarization data was corrected for resistance the IR free lines are nearly identical (dashed lines).

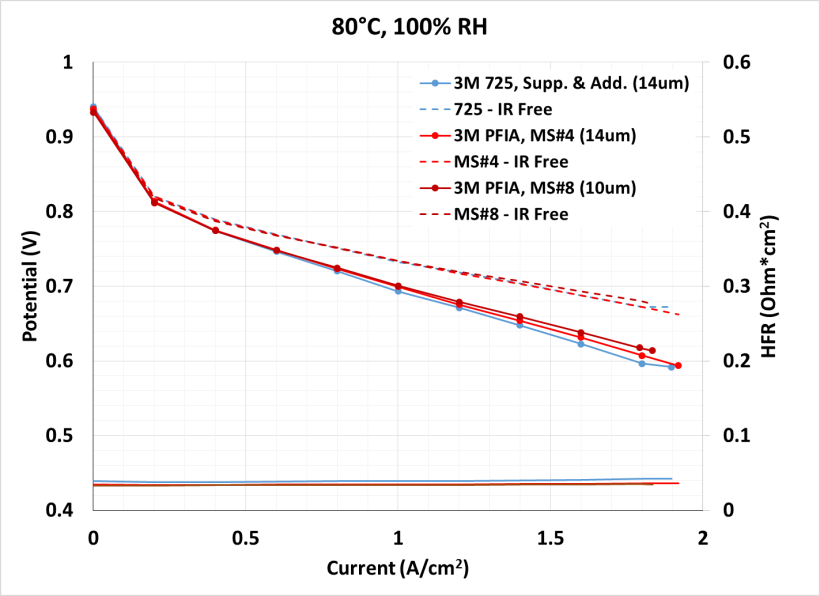

Figure 86. Polarization and HFR curves for 3M 725EW supported control, Milestone #4 and Milestone #8 membranes at 80°C and 100% RH.

The same membranes tested at 95°C and 50% RH (Figure 87) show higher performance for the MS #8 membrane followed by the MS#4 and then the control. In addition, the IR free curves show slightly higher performance with the thinner MS#8 membrane using PFIA ionomer. This suggests that the performance gain may also include additional factors such as enhanced water diffusion under these dry conditions.

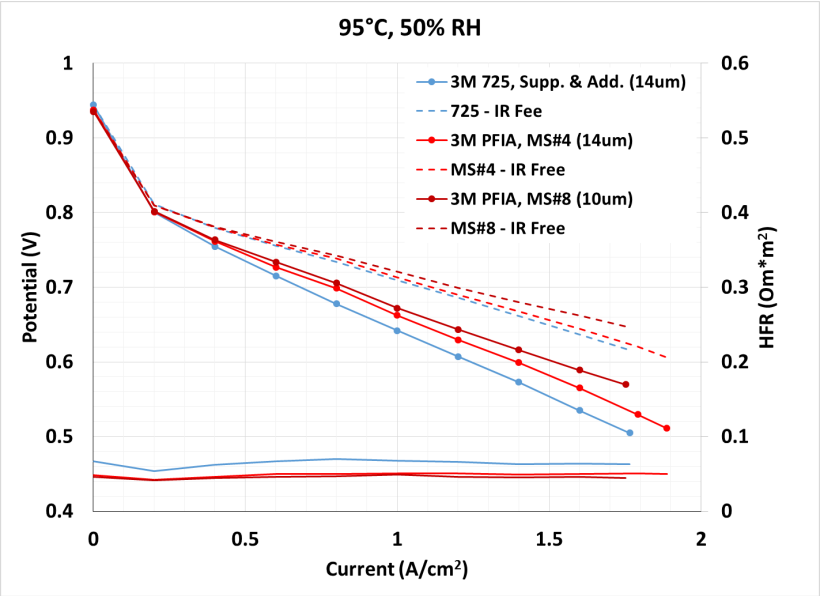

Figure 87. Polarization and HFR curves for 3M 725EW supported control, Milestone #4 and Milestone #8 membranes at 95°C and 50% RH.

Perhaps the best measure of the performance differences with the new PFIA based membranes is a performance versus relative humidity experiment (Figure 88). In this case the MS#8 membrane shows greater than 100mV higher performance at 1.5A/cm^2 compared to the state-of-the-art PFSA based control. It is important to note that the control membrane is fabricated using a 725EW 3M ionomer and that the more traditional PFSA ionomers with EWs in the range of 800-1000 would show even lower performance at the very dry conditions.

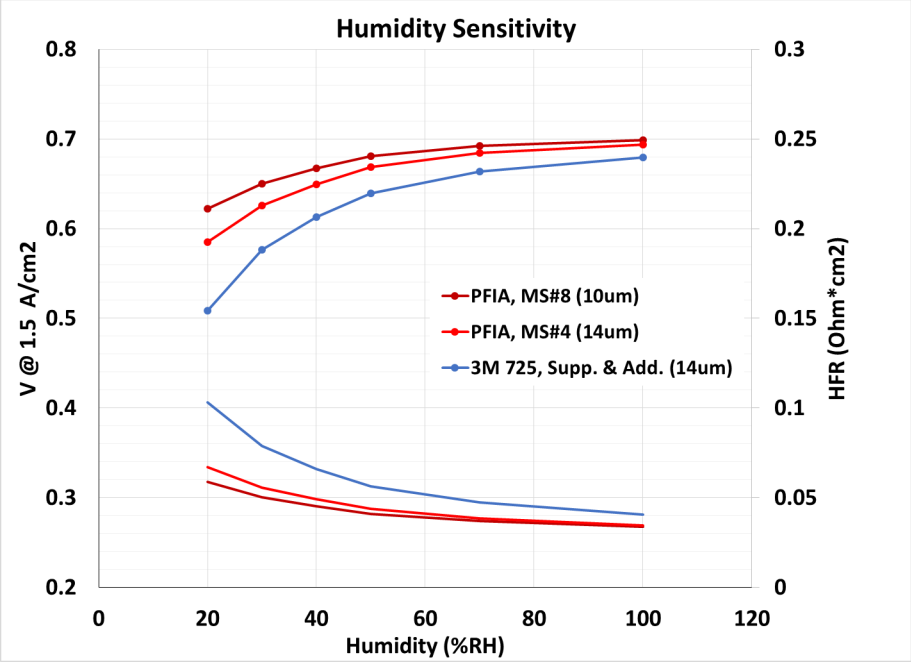

Figure 88. Voltage at 1.5A/cm2 and HFR for Milestone membranes #4, #8 and 3M 725EW supported control.

Subtask 4.2.2 50cm2 performance testing at GM

Membranes evaluated at GM for fuel cell performance used 50 cm^2 active area cells with graphite flow fields designed to mimic automotive hardware pressure drop and flow distribution. MEAs were prepared using GM's automotive competitive electrodes with 0.2 mg Pt /cm^2 cathodes and 0.05 mg Pt /cm^2 anodes. All tests were run in counterflow orientation. The MEAs were tested for performance using the test conditions shown in

Table 20. The first three tests are polarization curves where the current density is increased stepwise at constant cell operating conditions (temperature, pressure stoichiometry) and the voltage is recorded. In the temperature ramp tests, the current density and inlet reactant gas dew points are help constant, and the cell temperature is increased stepwise. All tests are run with pure H_2 on the anode and air on the cathode. Triplicate samples were run for each test. The average results are plotted with error bars representing one standard deviation.

Table 20. Fuel Cell Test Conditions

Protocol	Cell T	An / Ca RH %	P	H2/Air Stoic.
Standard Pol Curve	80°C	32% in	150 kPa	1.5/2.0
Wet Pol Curve	80°C	100% in	170 kPa	1.5/2.0
Dry Pol Curve	95°C	26% in	150 kPa	2.0/1.8
Temperature Ramps	60-120°C, 62°C dew pt.: 1.2, 1.5 A/cm^2	110→10% in	150 kPa	2.0/2.0

The results for the standard and dry polarization curves for the 0514218A supported PFIA membrane compared to 14µm thick supported PFSA PEMs are shown in Figure 89 and Figure 90, respectively. The cell voltages (upper curves) and the high frequency resistances (HFR) (lower curves) are plotted for each membrane type. In the standard polarization curves, all of the PEMs show similar performance. At these conditions, the ionomer type or equivalent weight does not appear to have any effect on performance. At the drier condition, the performance difference between the different ionomer types becomes apparent. The lower equivalent weight (725 EW) membrane outperforms the 825 EW membrane. Also the supported PFIA PEMs outperforms the PFSA PEMs at the dry conditions. The new supported PFIA PEM (0514218A) outperforms the previously received sample (05123102A). The differences in the cell potential can be explained by the difference in the membrane proton transport resistance, as seen in the HFR curves for the various samples. The temperature ramp test results at 1.5 A/cm^2 are plotted for the 14µm thick supported PFSA and PFIA membranes in Figure 91. Here, the PFIA PEM shows a clear advantage over the PFSA PEMs at higher operating temperatures above 90°C. Again, the differences in the cell potential can be explained by the difference in the membrane proton transport resistance, as seen in the HFR curves for the various samples.

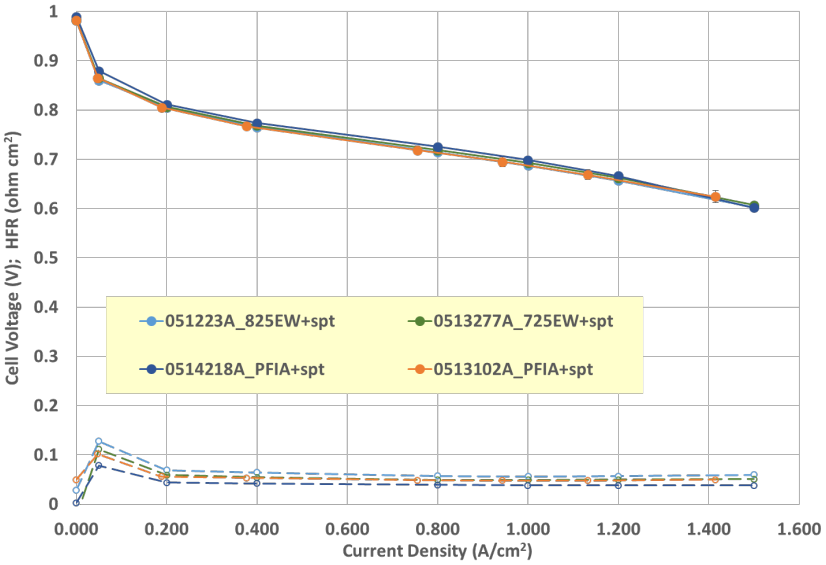

Figure 89. Standard Polarization Curves

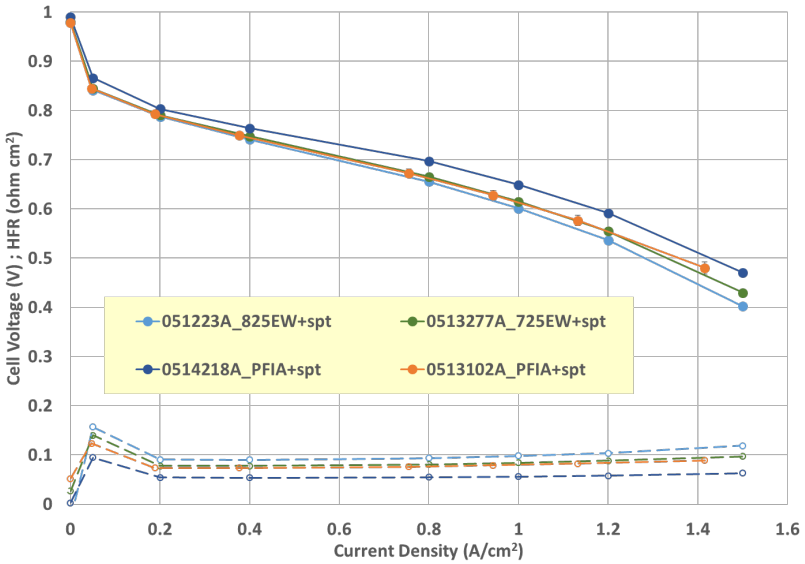

Figure 90. Dry Polarization Curves

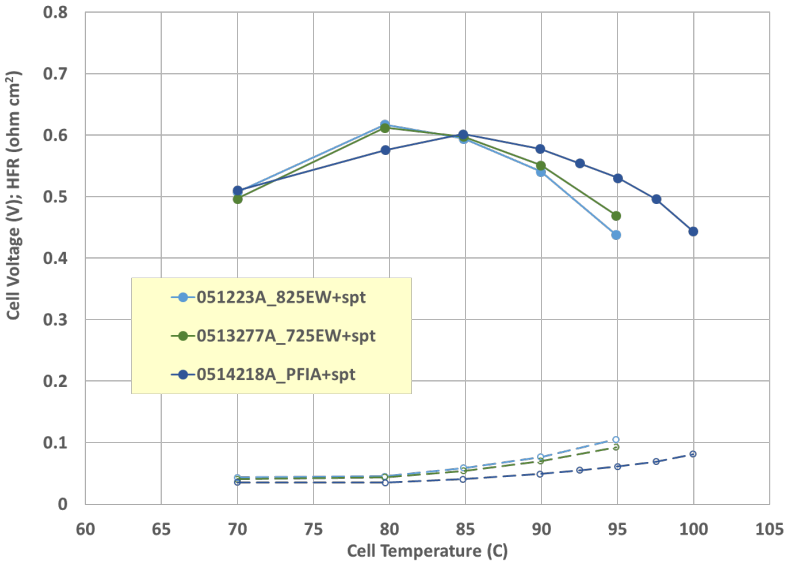

Figure 91. Temperature Ramp at 62°C inlet dew point and 1.5 A/cm2

Short Testing

GM measured shorting resistance on MEAs made using several of the supported and non-supported PEMs prepared at 3M. The measurements were done in a 50cm^2 cell with a 20% strain applied to the gas diffusion media (GDM) to assure good contact resistance yet to not induce localized shorts in the membrane[ix]. Resistance is measured at 25°C with fully humidified H_2 gas flowing through the anode and fully humidified N_2 through the cathode side of the cell. The shorting measurement was done after the MEAs had completed a series of performance tests which take less than one day. Results shown in Table 21 are averages of at least two MEAs. All MEAs had shorting resistances which exceed the DOE target of 1000 Ω•cm2. The only observation of note is that the thicker non-supported PEMs have higher shorting resistances than do the thinner supported PEMs. There is no clear difference in shorting resistance of the PFSA & PFIA ionomers.

Table 21. Shorting resistance of MEAs made using 3M membranes

Membrane	Ionomer	Thickness (µm)	Support	Resistance (Ω•cm2)
0512320E	725EW PFSA	20	no	16100
0513277A	725EW PFSA	14	yes	5600
0514177D	PFIA	20	no	9900

0514218A	**PFIA**	**14**	**yes**	**5700**

Subtask 4.3 Accelerated Stress Testing (AST)

Accelerated durability testing (AST) is one of the most important tasks for this project. The two main ASTs are the mechanical (RH cycle) and chemical (OCV hold) tests. For the RH cycle test, a membrane is rapidly cycled between wet and dry conditions until failure by cross-over or meeting the target of 20,000 cycles. In the open circuit voltage (OCV) test, a cell is held at OCV until membrane breach is detected through crossover or by rapid voltage loss as a result of membrane failure. Typically an OCV value of less than 80% of the original potential (~800 mV) is indicative of failure. Multiple tests were run on several candidate membranes using each test. A few of the key results will be summarized in this section.

Two samples of the milestone 8 membrane were run on the RH cycle test. One sample was removed after about 25,000 cycles when the leak rate of the membrane in the dry state exceeded 5 sccm (note; the leak rate of this same membrane under the DOE designated wet condition had not yet shown signs of increased leak rate). The second sample was allowed to run beyond the 20,000 cycle target. The leak rate of this sample for both the wet and dry condition is shown in Figure 92 for over 60,000 cycles. While it was our intention to run this sample to failure, we decided to remove it from test at about 69,000 cycles and test for hydrogen cross over. Consistent with the leak data, the crossover was less than 2 mA/cm^2 and in agreement with the beginning of life measurements of an identical MEA.

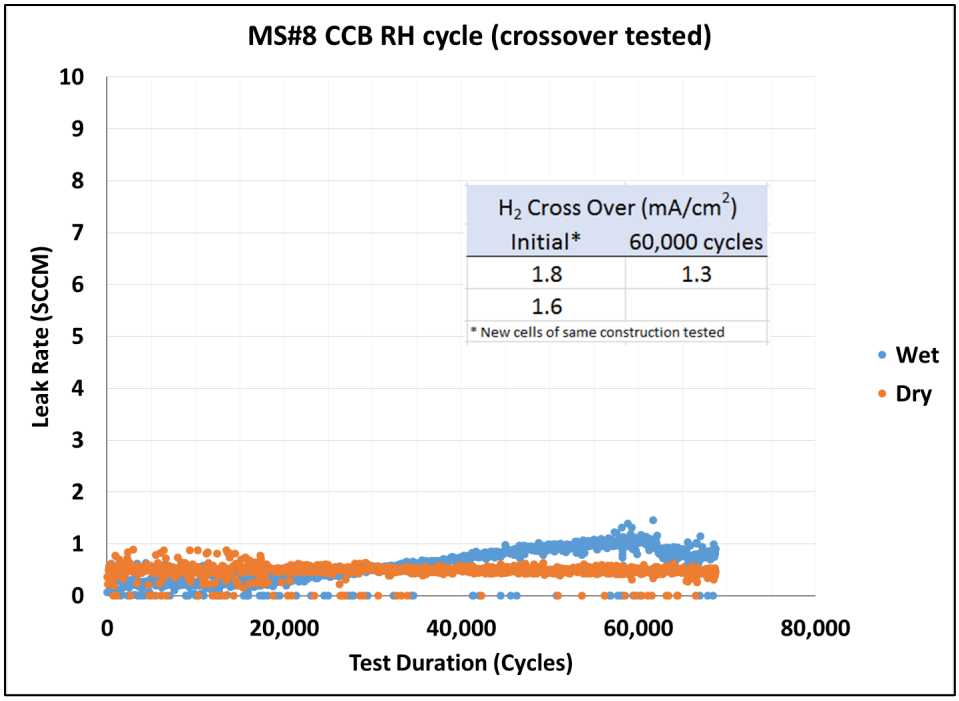

Figure 92. Humidity cycle accelerated stress test for Milestone #8 membrane. Blue symbols indicate leak rate when tested in the wet condition, orange symbols represent the dry condition.

The OCV hold test was also completed for the milestone 8 membranes using additive type 1 and 3M's commercial electrodes and additive package. In this set using commercial electrodes and additive, four MEAs were run and, to ensure that the 500 hr target was meet, removed from test and measured for hydrogen crossover. The potential and resistance are plotted in Figure 93 with arrows indicating the times when the cells removed to collect the crossover data shown in Figure 94. As expected the crossover remained low during the period where the OCV stayed above about 0.8V and all four samples passed the 500 hour target with the first cell shown signs of failure at about 1000 hours. For this set, the average lifetime exceeded 2,000 hours using the 80% of the original OCV to define end of life which is in qualitative agreement with the crossover results.

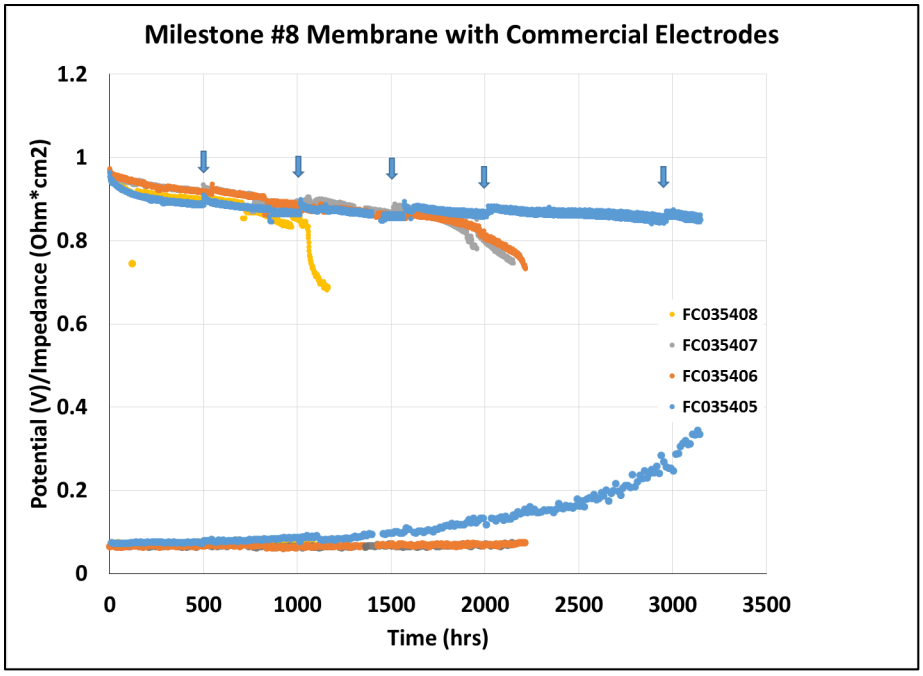

Figure 93. OCV versus time for four MEAs made using Milestone #8 membrane and 3M commercial electrodes and additives. Arrows indicate times when cells were removed and tested for shorts and cross over.

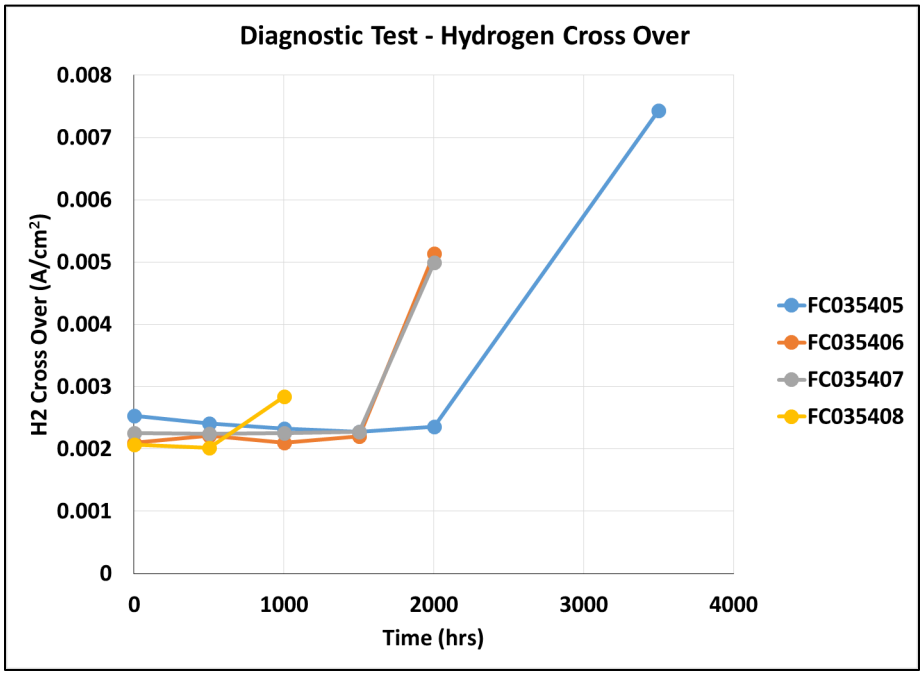

Figure 94. Hydrogen Cross over data for Milestone #8 membrane measured every 500 hrs of test time.

Peculiar to the PFIA containing membranes is an increase in the resistance near the end of life in the OCV test. This effect is evident in the data for MS#8 OCV test results reported using lab electrodes and additive type 1 and shown again by red lines in Figure 95. Interestingly this effect is not seen in every cell and is significantly reduced or eliminated by using commercial electrodes and additive levels. This observation became the focus of work in the final year of the project. Nevertheless, a comparison between PFSA and PFIA membranes is made in Table 22 where the lifetimes and standard deviations are similar between membranes when run with the same electrodes.

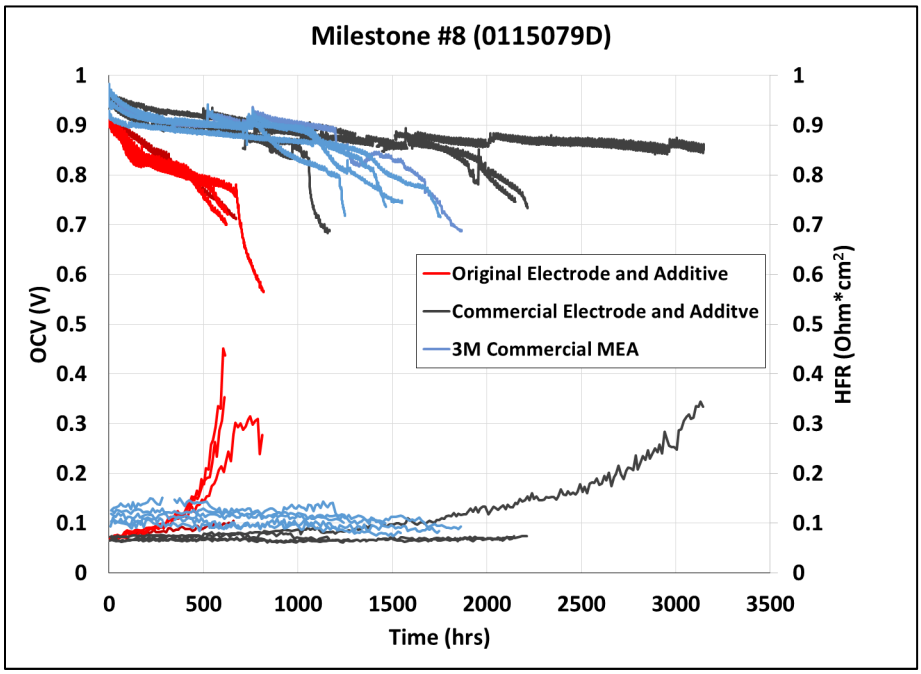

Figure 95. OCV and HFR data for milestone #8 membrane tested with original lab electrodes (red) and commercial electrodes (black) compared to 3M commercial control (blue).

Table 22. OCV lifetimes (80% of original OCV) for Milestone #8 membranes tested using two different electrodes and a 3M Control.

Membrane	Electrodes	Lifetime (hrs) 80% OCV
MS#8	Lab control	614 ± 55

3M 725EW with Support	**Lab Control**	**894 ± 226**
MS#8	**Commercial**	**2105 ± 851**
3M Commercial	**Commercial**	**1484 ± 209**

Multilayer MEA studies.

In order to analyze membranes at the end of life, we developed a multi-layer membrane test method. This method allows for the separation of membranes from the electrode layers at the end of life to analyze the polymer for structural changes. A schematic of this MEA construction is shown in Figure 96.

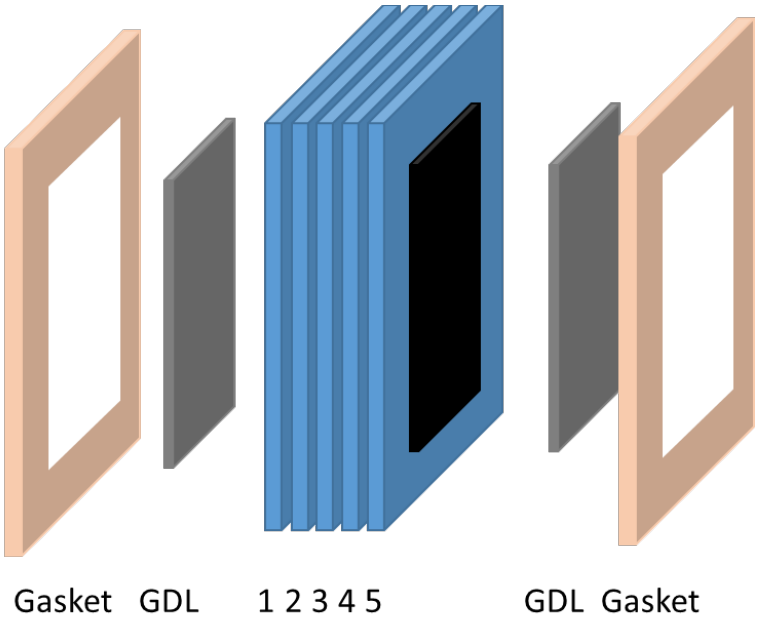

Figure 96. Schematic of multilayer membrane experiment. Anode is laminated to layer 1 and cathode to layer 5.

In one series of experiments, we made cells with 5 layers of PFIA membranes The OCV data and fluoride release rate (FRR) are shown in Figure 97 below for three types of membranes; a 20micron PFIA with no additive and no support and two supported membranes with additive, one with electrospun FC1 and one with ePTFE. One objective of this test was to assess the influence the support fibers may have on the observed decay in the OCV test. Unfortunately, these membranes could not be separated at the end of life.

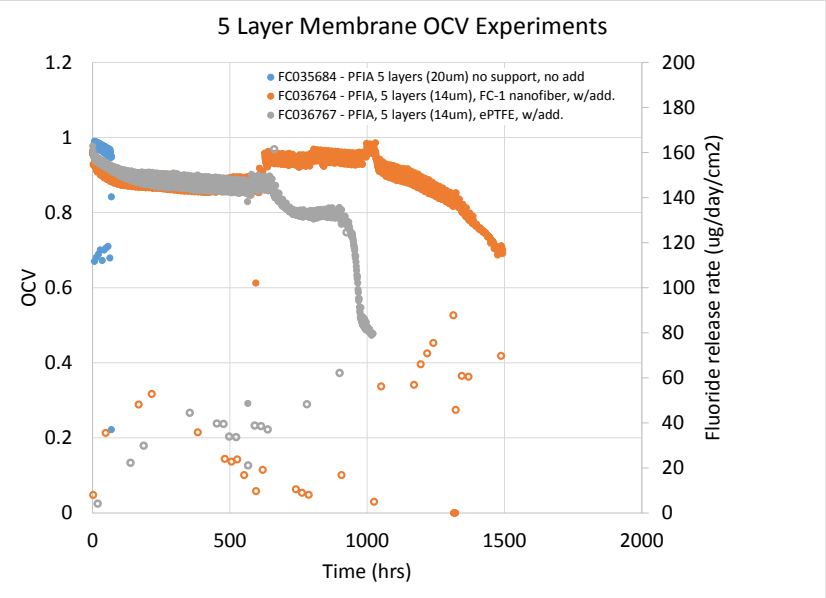

Figure 97. OCV lifetime plot for three multilayer membrane experiments. PFIA based membranes with no additive or support (blue), with additive and FC-1 nanofiber (orange) and with additive and ePTFE (grey). Samples were subjected to a recovery protocol at 600 hrs. Fluoride release numbers shown with open symbols.

The data shows a decay on the OCV values during the first 200 hours followed by a plateau for both of the supported membranes. The discontinuity in the data at about 600 hours represents the implementation of a recovery protocol (thermal cycles and hydrogen pump) in an effort to recover the performance as previously reported. The OCV data shows that the ePTFE sample exhibited a recovery nearly to the original OCV where the FC1 supported membrane had a sharp decay. It is our judgment that mechanical failure is responsible for the FC-1 sample decay and that the electrodes would have recovered to the original OCV in the absence of this failure. During the recovery, the effluent water was collected and concentrated about 30x and analyzed for chemical fragments using liquid chromatography coupled with mass spectroscopy (LC-MS). The results of this analysis are shown in Figure 98 below. Fragment assignments were not immediately obvious for all the peaks observed but when unambiguous assignments can be made the structures are associated with the data in the figure.

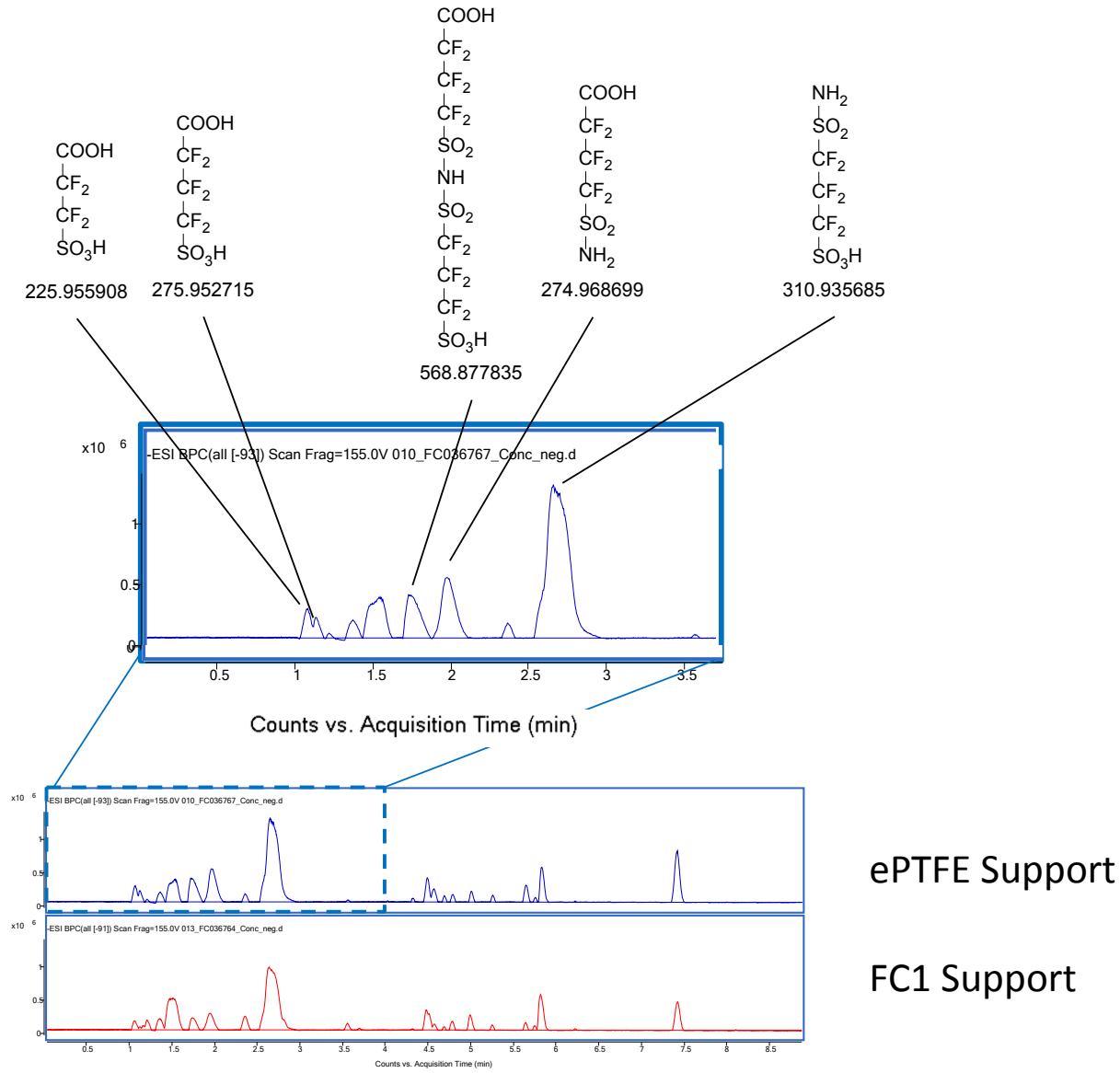

Figure 98. LC-MS data with relevant peaks identified (above). Traces for both ePTFE and FC1 support shown no difference (below).

There are two important observations with this data. First, the LC-MS traces for each sample are nearly identical regardless of the support used. This data, along with the OCV and FRR values, would suggest that the observed OCV decay is unlikely due to the nature of the polymer in the support. The second observation is that several fragments are identified that can be associated with the cleavage of one or more carbon-sulfur bonds in the PFIA sidechain.

In order to better understand the possible decomposition fragments for PFSA and PFIA ionomer we have the structures shown in Figure 99 and Figure 100 respectively. For the PFSA case, it is commonly accepted that degradation from the polymer chain-end is the predominate decomposition mechanism and that a secondary decomposition is possible by oxidative attack on the carbon-sulfur bond[1]. As shown in Figure 99 back-bone degradation can lead to the

release of a sulfonic acid-carboxylic acid fragment based on release of a side chain due to loss of the backbone. All other decomposition path ways will result in the evolution of sulfate ions, carbon dioxide, and hydrofluoric acid. It should be noted that decomposition pathways that originate at the side chain will procced up the chain and cleave the backbone thus further accelerating the overall polymer decomposition.

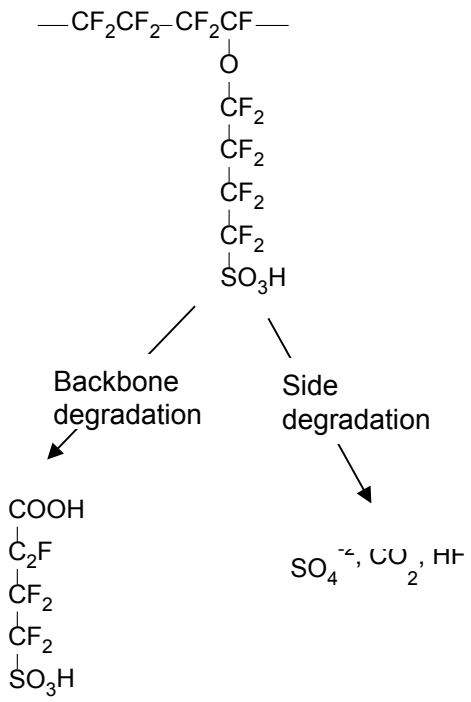

Figure 99. Possible decomposition pathways based on either backbone degradation through end groups (left) or side chain degradation originating at the terminal carbon-sulfur bond. Note that side chain degradation is expected to cleave the backbone resulting in greater backbone degradation.

In the PFIA case, however, there are more carbon-sulfur bonds with similar chemical environments to those of the PFSA cousin and there are new nitrogen-sulfur bonds that may also be subject to cleavage. Figure 100 shows the fragments expected for both backbone and side chain decomposition assuming one or both of the C-S or N-S bonds are vulnerable to cleavage in the presence of peroxide or peroxide radicals. The backbone fragments include the full PFIA side chain or the case where the side-chain has already been cleaved and the backbone is then degraded releasing the shortened fragment.

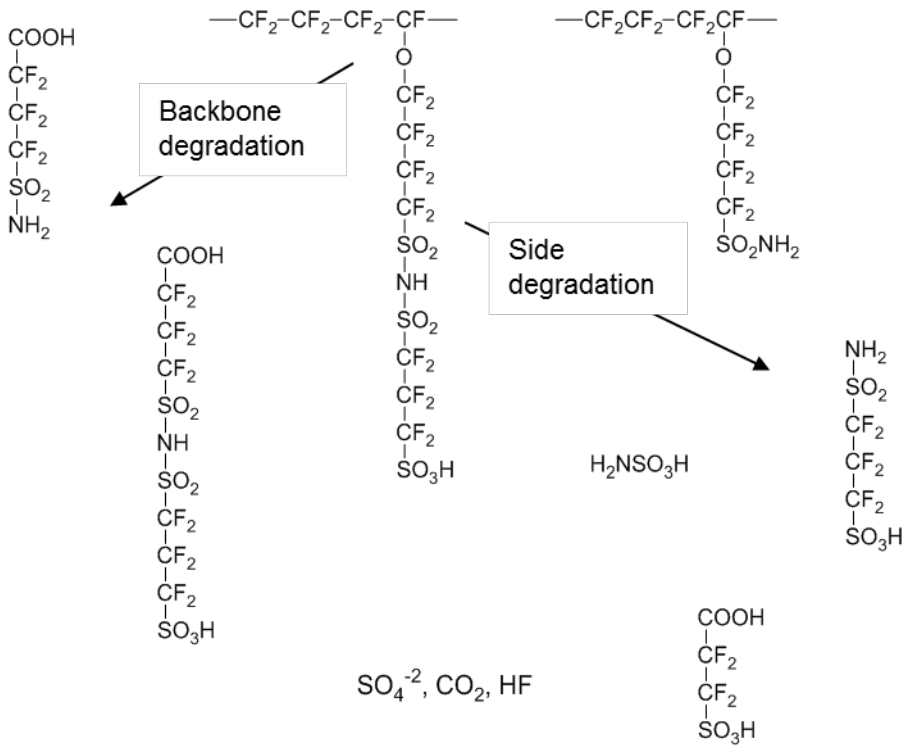

Figure 100. Possible decomposition fragments with PFIA ionomer based on cleavage at the C-S bonds.

Fragments in the effluent water provide some insight into the ionomer degradation in the OCV test but ideally analysis of the aged membranes would provide complimentary data. Obtaining a sample of degraded ionomer is exceedingly difficult from a normal MEA made with 10-14 micron thick membrane. Bonded electrodes along with significant mechanical degradation and thinning prohibit isolation of a membrane from a conventional cell. A simplified three layer construction was adopted to include a 10 micron supported 725EW PFSA membrane as the outer layers of the sandwich and a single membrane of interest in the center layer. A schematic of the construction is shown in Figure 101

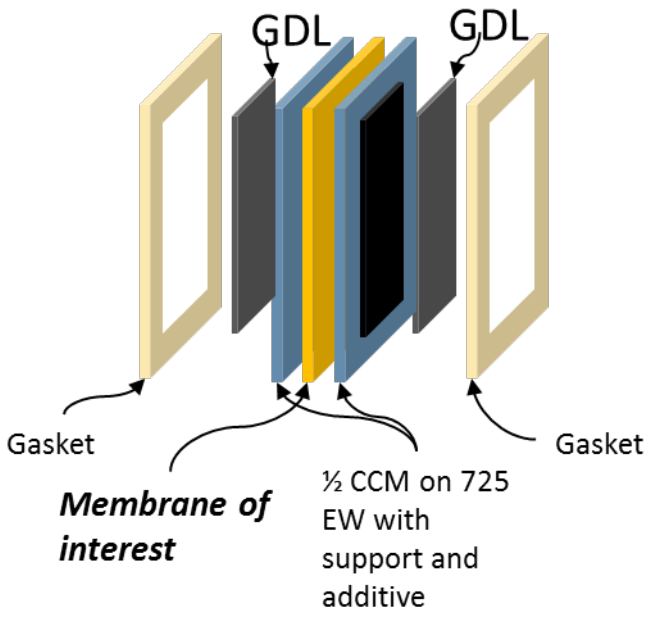

Figure 101. Schematic of a multilayer membrane MEA. The membrane of interest is placed in the center (shown in yellow) while the membranes containing electrodes (1/2 CCMs) are keep constant (shown in blue).

Two membranes of interest were run; the first was a 20 micron PFIA with no support and no additive, the second was a 725EW PFSA control with no support and no additive. Three PFIA cells were run and two PFSA controls.

Based on previous publications, we would expect the side chain of the PFSA control to degrade at the carbon-sulfur bond in a way that ultimately cleaved the backbone of the ionomer. The formation of carboxylic end groups on the polymer (~COOH) would be evidence of this pathway. The PFIA ionomer would be expected to exhibit a similar backbone cleavage if the carbon-sulfur bond closest to the backbone were to degrade. However, if either of the two carbon-sulfur bonds near the terminal end of the PFIA side chain were to cleave there is the possibility of a sulfonamide side chain (~SO_2NH_2). An outline of the proposed reactions are shown in Figure 102.

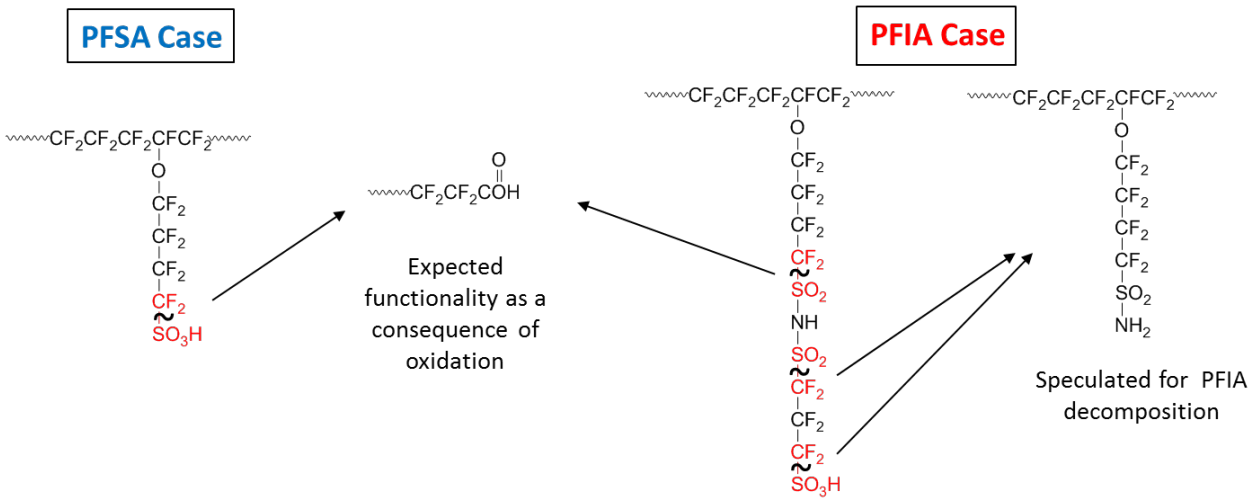

Figure 102. Proposed consequence of side chain oxidation through reaction at the carbon-sulfur bond.

Representative OCV data from one of the three cells that contained a 20 um PFIA membrane in the center layer is shown in Figure 103. This graph shows the OCV data (blue symbols), the performance at 0.2 A/cm^2 (orange), the resistance (yellow) and the resistance corrected 0.2A/cm^2 data (grey). The 0.2A/cm^2 condition is necessary in order to effectively measure the high frequency resistance.

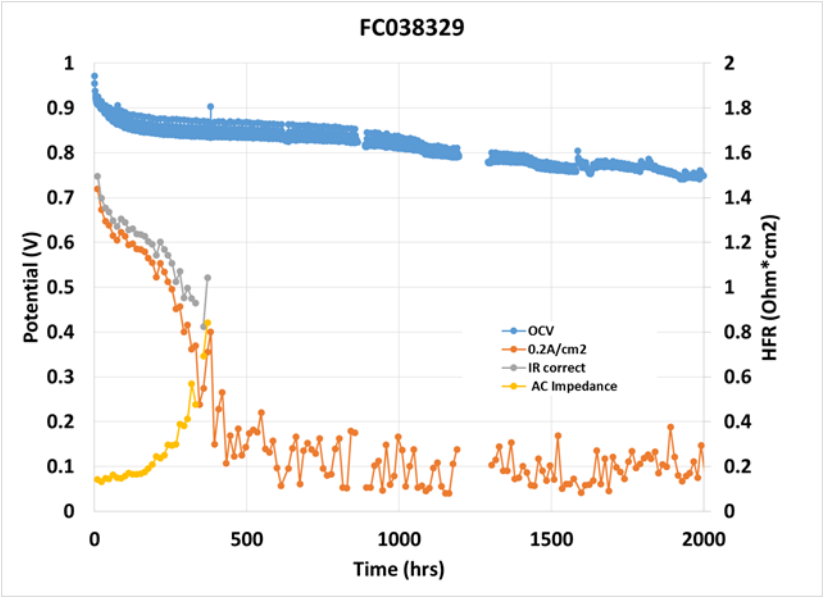

Figure 103. Typical OCV data for three layer membrane where a 20um PFIA membrane is in the center layer.

This cell ran for over 2,000 hours where it is evident that there was a rapid decrease in the initial OCV followed by a more gradual decay in the values. At the same time, the potential at 0.2 A/cm^2 was rapidly decaying as the resistance increased. The resistance corrected data shows that this loss in performance cannot be attributed to the increase in resistance only.

After 2,000 hours the MEA was removed from the station and an attempt was made to separate the membrane layers for analysis. The MEA was placed in a tray of deionized water and allowed to hydrate for at least 2 hours, the layers were carefully peeled apart while underwater. Two images of the center membrane are shown on white and black backgrounds (Figure 104). While it was not possible to spate all the layers cleanly, we were able to remove the outer half CCM from a large section of the center membrane as shown in the upper left of these images.

Figure 104. Image of the three membrane MEA after separating layers. Fully separated PFIA center layer can be seen in the top right image with the black background.

A similar experiment was run on the 725EW PFSA control with representative OCV data shown in Figure 105 and the separated membrane shown in Figure 106. Unlike the PFIA sample, the resistance did not increase in a significant way for this membrane. Interestingly, there is a slow decay in OCV and also a marked decay in the potential at 0.2 A/cm2 that plateaus at about 500hours. Like the PFIA case, the resistance corrected data showed little difference. Again, a section of the center layer of the membrane sandwich was able to be removed for analysis.

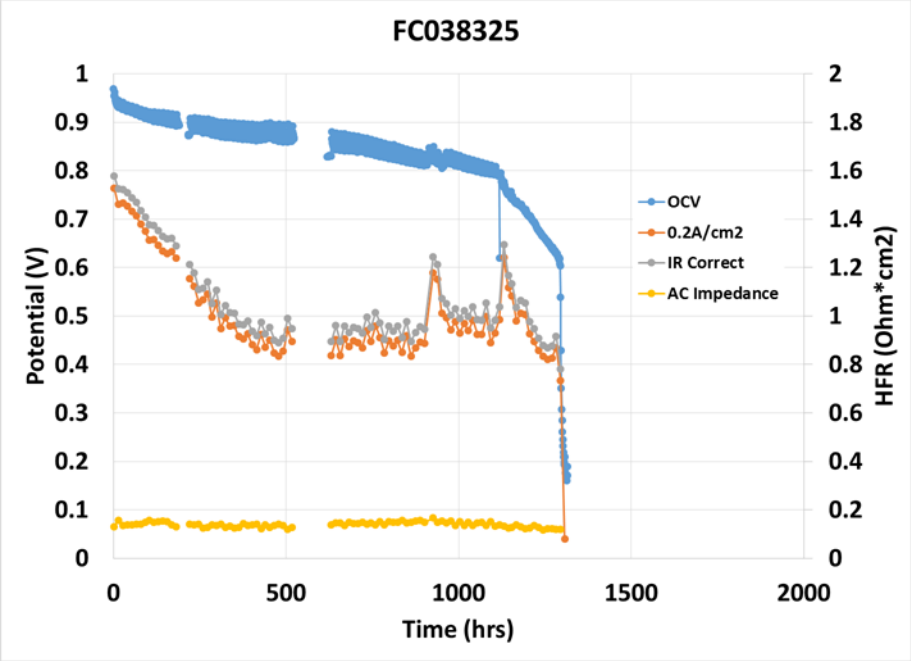

Figure 105. Typical OCV data for three layer membrane where a 20um 725EW PFSA membrane is in the center layer.

Figure 106. Image of the three membrane MEA after separating layers. A section of the fully separated 725EW PFSA center layer can be seen in the center/right section.

Infrared spectra were taken of the active are and edge areas of the membranes. Prior to the experiment, samples were soaked in 1M potassium chloride in order to form the potassium salt of the sulfonic acid side chain or the carboxylic acid end groups. This pre-treatment minimizes the interference from absorbed water when imaged in the proton form. The PFSA data is shown in Figure 107 and the PFIA data in Figure 108. In both figures the spectra from the edge is shown in green and the active area in red. For the PFSA case, the spectra are nearly identical with the exception of the peak at 1692 cm^{-1} that is assigned to the C=O bond in the carboxylic acid end group. The formation of this group has been reported before and is an expected result of long term OCV testing.

The PFIA sample however, shows significant differences between the spectra from the membrane edge and the active area. The peak at 1692 cm^{-1} appears as expected but another, new peak, shows up at about 1387 cm^{-1}. This new peak is attributed to the SO_2 group in the

sulfonamide side chain (~SO_2NH_2). Furthermore, the peaks associated with the imide functionality (1347, 1087, and 1060 cm^{-1}) have all decreased.

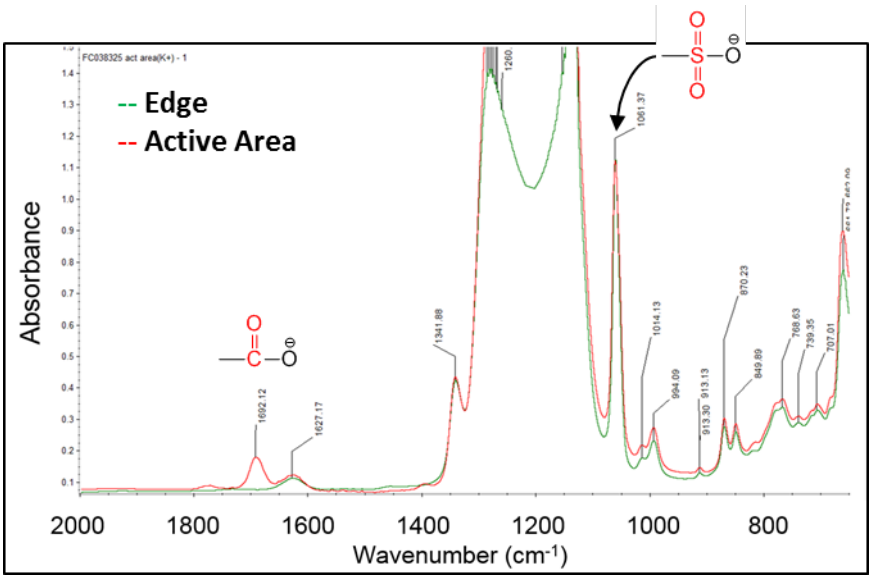

Figure 107. FTIR spectra for three layer membrane where a 20um 725EW membrane is in the center layer. Spectra from the edge is shown in green and from the active area is shown in red.

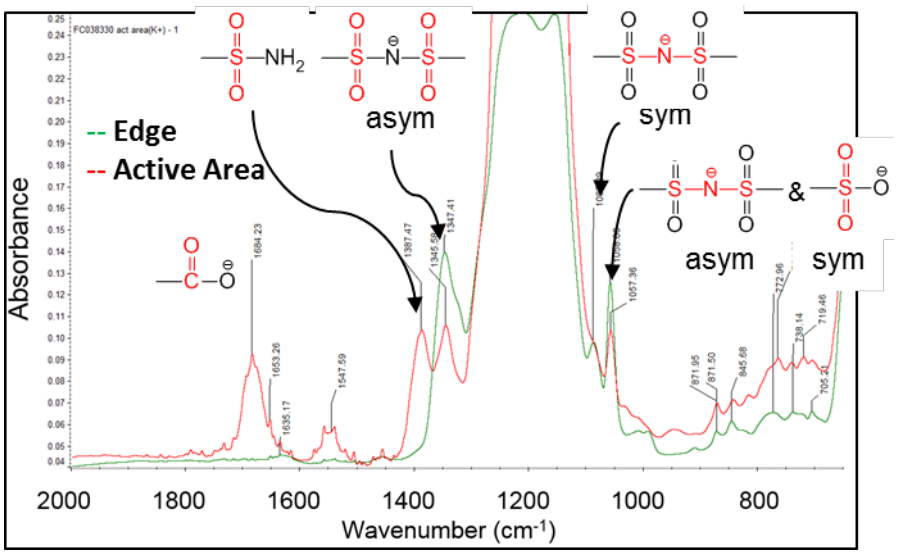

Figure 108. FTIR spectra for three layer membrane where a 20um PFIA membrane is in the center layer. Spectra from the edge is shown in green and from the active area is shown in red.

In addition to the FTIR data, ^{19}F NMR samples were prepared by dispersing a small amount of the membrane in deuterated water. The samples were converted to the lithium form for better peak resolution. A series of spectra are shown in Figure 109 where the original PFIA spectra is

on top, a sample that contains 10% of the sulfonamide (~$CF_2SO_2NH_2$) in the middle, and the OCV aged sample on bottom. Fluorines next to the SO_2 group are the most distinct signals for the purposes of structural assignments. The CF_2's associated with the imide are indicated with arrows at about -113.1 ppm, -113.9 and -115.2 ppm. The CF_2 next to the amide is about -115.5 and the CF_2 next to the standard PFSA acid is about -115.8 ppm

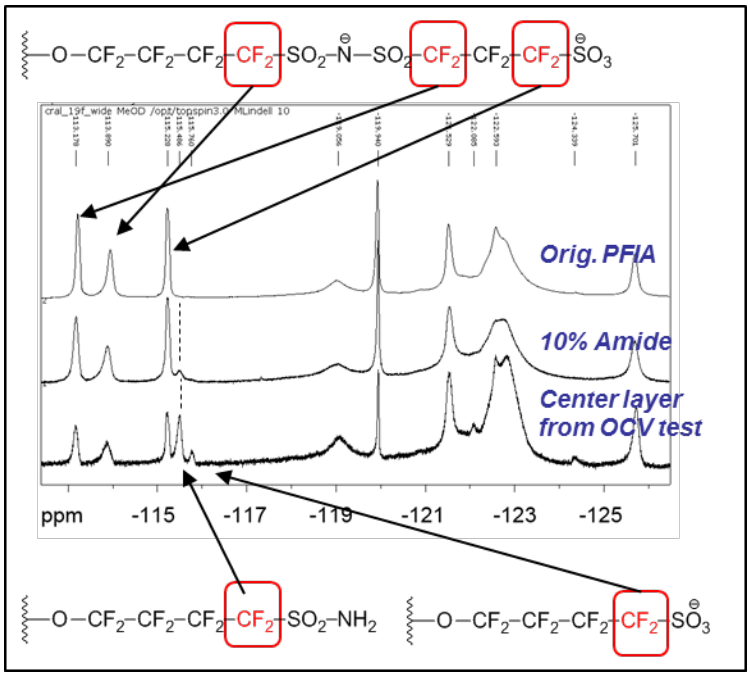

Figure 109. ^{19}F NMR data for three layer membrane where a 20um PFIA membrane is in the center layer (bottom), original NMR spectra (top) and a sample containing 10% of the sulfonamide (middle).

The spectra of the membrane from the multilayer shows a reduction in the intensity of the peaks associated with the imide and the appearance of the peak due to the sulfonamide. The peak associated with the sulfonic acid (-115.8) is likely die to residual ionomer form the outer layers membranes which were made with standard PFSA.

This work represents a significant advance in understanding of the stability issues in imide based ionomers. It should be noted that these ionomers are still remarkably stable and it was only after a great deal of durability testing and analytical effort that we were able to detect new decomposition pathways.

Task 5 Stack Testing

Membranes were provided to GM for MEA fabrication and fuel cell testing. Four samples were 10 microns thick and used PFIA ionomer and electrospun nanofiber support developed under this project. Additive type and level were varied for each of the four membranes. In addition, a 3M control and GM control membrane were also run resulting in a rainbow stack with six types

of membrane. A 14μm thick PFSA membrane was made with a hydrocarbon/fluorocarbon blend (B1) support layer and a chemical stabilization additive (Type 1 additive). Experimental, 10μm thick, PFIA membranes were made with a fluorocarbon (FC-1) support layer and a chemical stabilization additive (Type 1 additive). The PFIA membranes were made with various levels of chemical stabilization additives: 0, 1X and 2X of Type 1 additive. The PFSA membrane contains chemical stabilization additive of 1X level of Type 1 additive.

A GM additive (Type 2) was applied to the received membrane samples from 3M. A GM state-of-art membrane was also included in the fuel cell stack. The GM state-of-art membrane has a PFSA ionomer, an ePTFE mechanical support and a chemical stabilization additive package. Table 23 shows the membrane layout of the stack. The column of "3M + GM additive" explains the type and level of chemical stabilization additives applied for each type of MEA. This stack was tested for performance and durability using a GM automotive fuel cell test protocol that has an approximate acceleration factor of 4 compared to a non-accelerated drive cycle.

Table 23. GM short stack membranes layout

Membrane Types	Ionomer	Ionomer EW (g/mol)	thickness	Support	3M + GM additive
3M 0513277A	3M PFSA	725	14μm	B1	1X Type 1 additive, 2X Type 2
3M 05160081A	3M PFIA	650	10μm	FC-1	0X Type 1 additive, 2X 2 Type 2
3M 05160081B	3M PFIA	650	10μm	FC-1	1X Type 1 additive, 2X Type 2
3M 05160081D	3M PFIA	650	10μm	FC-1	2XT ype 1 additive, 2X Type 2
3M 05160081D	3M PFIA	650	10μm	FC-1	2X Type 1 additive, 1X Type 2
GM state-of-art PFSA				ePTFE	yes

Beginning of Life Testing

The fuel cell stack was broken-in and evaluated for beginning of life (BOL) performance. The fuel cell stack has full active area bipolar plates designed for automotive stacks with optimized pressure drop and flow distribution. The MEAs were prepared using GM's automotive

competitive electrodes with 0.1 mg Pt /cm^2 cathodes and 0.025 mg Pt /cm^2 anodes and state-of-art gas diffusion layers (GDL). The fuel cell stack was tested using a GM developed automotive polarization test for BOL performance. The automotive polarization test was conducted where the current density is increased stepwise from 0.05 to 1.5 A/cm2. The stack temperature and pressure increase with current density, with operation at 85^{o}C and 40% inlet RH at 1.5 A/cm^2. All tests are run with pure H_2 on the anode and air on the cathode. Four samples of each type of membranes were tested in the stack. The average results of cell voltage are plotted in Figure 110, and high frequency resistance (HFR) are plotted in Figure 111, with error bars representing one standard deviation. The polarization curves show all of the MEAs with PFIA membranes performing similarly to each other and to the GM PFSA benchmark. The 3M PFSA shows lower performance that the other membrane types. The BOL performance is partially explain by the HFR results. The PFIA MEAs show the lowest resistance, with no separation in HFR of the MEAs with different stabilization additive types and levels. The GM PFSA benchmark has higher HFR than the PFIA MEAs, but lower than the 3M PFSA. Note that these results agree with the 50cm^2 performance data shown in Subtask 4.2.2.

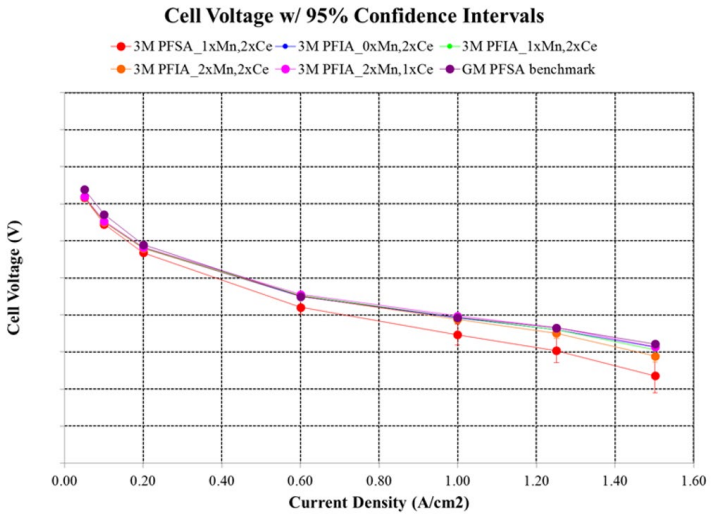

Figure 110. Stack cell voltage of GM automotive fuel cell polarization curves

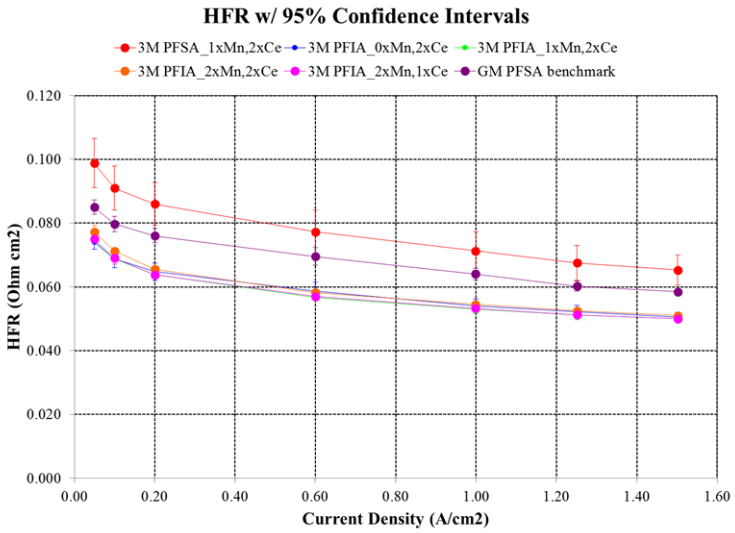

Figure 111. High frequency resistance (HFR) of GM automotive fuel cell polarization curves

After the MEAs were made and before the stack was assembled, each MEA went through a quality check (QC) during which the laminated MEAs were tested for shorting resistance. The QC resistance results are shown in Figure 112. The red line indicates the GM requirement of 5.8Ω. MEAs with lower resistance are at risk of early membrane failure due to local hot spots during operation. The GM state-of-art PFSA MEAs and the MEAs made with the 3M PFSA membrane pass the QC test, but all of the PFIA MEAs had resistances slightly below the specification. The reason for this is unclear, but it may be an issue with the quality of the incoming membranes or possibly the PFIA membrane experiences more creep during the MEA lamination conditions. Nonetheless, we opted to continue with the stack test as planned and MEAs with the highest resistance values were selected from among each MEA type to include in the stack the rest were saved for spares.

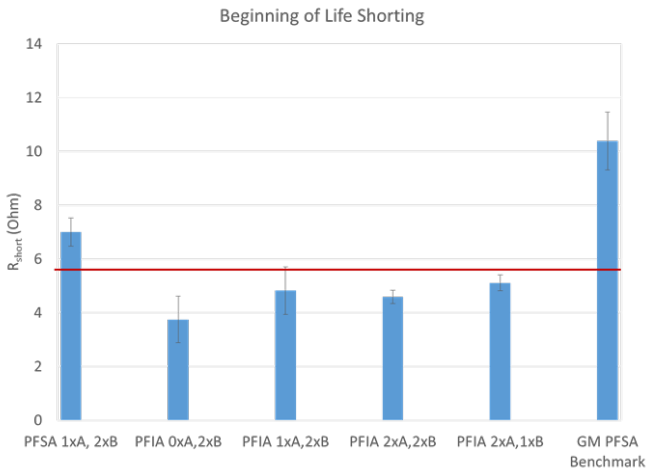

Figure 112. MEA Resistance Quality Check. Red line is GM specification.

Figure 113 shows the voltage over the first 830 hours of durability testing. The first 100h of testing includes a stack break-in protocol after which the durability protocol began. The performance of all of the MEAs rises during the break-in part of the protocol. The 3M 725EW PFSA MEAs show the greatest performance increase during the break-in period. The reason for the low initial performance and significant voltage rise of the 3M PFSAs is unclear. Once the durability protocol starts the voltage of all MEAs decreases. The degradation rates of the 3M 725EW PFSA MEAs and the GM state-of-art PFSAs are similar. All of the 3M PFIA MEAs, regardless of the stabilization level, degrade faster that the PFSA PEMs over the first 250h of durability testing. The reason for this higher degradation rate is unclear, but one hypothesis is that the PFIA MEAs are experiencing chemical degradation during the accelerated durability protocol and the degradation byproducts are adsorbing onto the cathode catalyst. This hypothesis is supported by OCV testing at 3M in subtask 4.3 and GM peroxide vapor cell tests in subtask 3.3. This hypothesis is also supported by the evidence of recoverable voltage loss as can be seen during the voltage recovery steps of the durability protocol at approximately 170 and 400h. There is no clear difference in decay rates for the PFIA PEMs with the different levels of stabilizer additives, although the MEAs with the higher stabilizer content have the lowest performance of the PFIAs at beginning of life. This suggests that these additives, which have both proven to be effective with PFSAs may not be effective for PFIAs. There is one PFIA MEA with 0x type 1, 2x type 2 stabilization that is degrading faster than the other MEAs after 450h, which is likely due to an increasing crossover leak in that MEA (see below). Note that two cells, one (cell 7) was a PFIA MEA with 0xA, 2x type 2 stabilization and the other (cell 16) was a PFIA MEA with 2x type 1, 2x type 2 stabilization, were removed after 471 hours of durability testing due to increasing crossover leak.

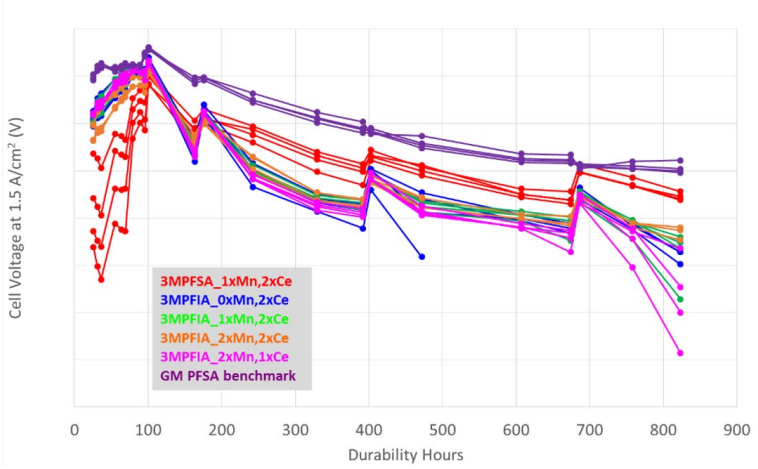

Figure 113. Cell Voltage at 1.5 A/cm2 over the first 830h of durability testing

A second set of failed cells were replaced at 890h and durability testing was continued on the remaining cells. At this point only two original PFIA MEAs were still in the stack. Figure 114 shows the voltage degradation of only the original cells in the stack after the 2nd repair. After nearly 1000h, the 3M PFSA MEAs and the GM benchmark PFSA MEAs are showing similar

performance. Note that there was a recovery procedure done at 980h. The two remaining PFIA MEAs still have lower performance than the PFSA MEAs. After 980h one of the remaining PFIA MEAs (cell 6 with 0x type 1, 2x type 2 stabilization) exhibits a rapid performance loss, whereas the other PFIA cell shows more stable performance. However, both cells show severe shorting at this time (data not shown). Thus, the remaining two PFIA cells have failed, indicating that all of the PFIA MEAs have failed in under 1000h of durability testing. Note that there does not appear to be any correlation with stabilization amount or type and failure time. One strategy to attempt to improve the PFIA stability would be to add even more manganese or cerium additive. This approach, however, has a fundamental limit in the form of ion exchange capacity. Since the additive cations neutralize a fraction of the acid groups in the membrane, there is no advantage to adding an excessive amount of these cations to a low EW PFIA material such that the EW is comparable to a traditional PFSA at the normal loading levels.

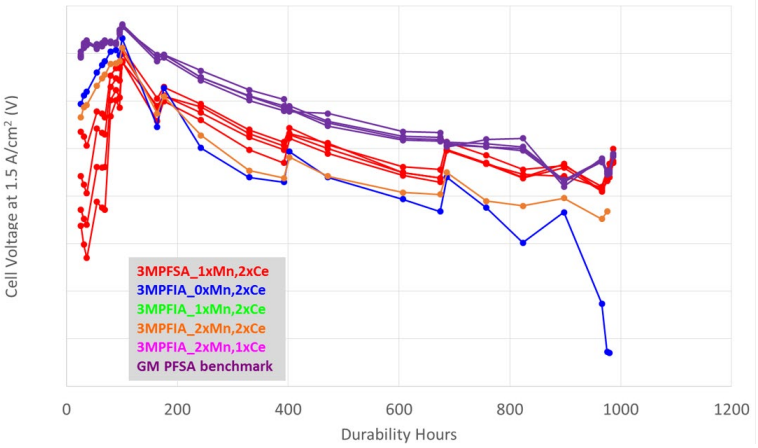

Figure 114. Cell Voltage at 1.5 A/cm2 over the first 980h of durability testing or original cells still in the stack

The HFR of each cell during the entire durability protocol (not shown) remains fairly constant over nearly 1000h of testing. This shows that the high degradation rate of the PFIA MEAs is not due to increasing membrane resistance. The lower ionomer EW and thinner PFIA membranes demonstrate lower HFR values than the 3M PFSA membranes throughout the test. The HFR of the GM state-of-art PFSAs are higher than the 3M PFIAs and lower than the 3M PFSA MEAs.

Postmortem Analysis

After 471h of testing, two of the MEAs had failed due to hydrogen crossover leak. One (cell 7) was a PFIA MEA with 0xType 1, 2x type 2 stabilization and the other (cell 16) was a PFIA MEA with 2x type 1, 2x type 2 stabilization, which is the MEA type with the highest amount of stabilizer additive. Postmortem analysis was conducted on theses MEAs.

In order to determine where there are leaks in the cells, a bubble test was conducted during which the MEA is submerged in water and air pressure is applied to the bottom surface of the MEA. Locations of crossover leak can be determined from where bubbles appear on the top side of the MEA. The bubble test results for the two failed cells are shown in Figure 115. Both cells show one region with a high rate of bubbling indicating a large leak. Cell 7 shows a large

leak near the cathode outlet port. Cell 16 has a large leak near the anode outlet port. Note that the stack is operated with anode and cathode flows in counterflow flow directions. Samples were cut from several regions of the MEAs to see if we could determine the failure mode and to look for thickness changes of the membrane during the durability test.

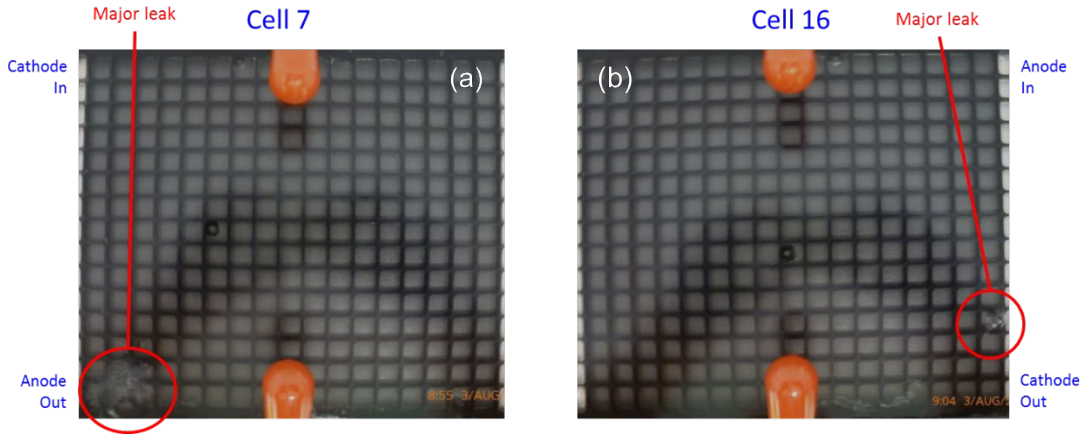

Figure 115. Bubble maps of cells 7 (a) and 16 (b) removed from durability stack after 471h

Cross-sections from cell 7 were taken from locations as shown in Figure 116. The sections were mounted in epoxy and polished in order to take optical cross-sectional images. Each sample near the edge extends from the active area to an inactive region which was beneath a subgasket where the MEA was not exposed to reactant gases or electric current. The region beneath the subgasket is assumed to be representative of the fresh membrane. Cross-section images from the region with the highest bubble rate (section 8 in Figure 116) are shown in Figure 117 along with the thickness of the membrane at distances of 1 mm, 5 mm, 9 mm, 15 mm, 19 mm and 23 mm from the subgasket edge. At 1mm from the subgasket the membrane thickness ranges from 6-10 μm, suggesting that some membrane thinning has started to occur in that region after 471h of durability testing, as the initial membrane was closer to 12 μm thick. At 5 mm from the subgasket edge significant local membrane thinning is observed and there is a region where the membrane is only 4μm thick, suggesting the ionomer is mostly gone and only the support remains. At 9mm and 15mm from the subgasket edge there is significant ionomer loss and separation of the anode and cathode sides for the membrane is observed. At 19mm from the subgasket edge the measured membrane thickness is less than 2μm, suggesting that, not only is there loss of ionomer, but the support layer appears to have disappeared as well. At 23mm from the subgasket edge the entire membrane has disappeared, with no evidence of either the ionomer or the nanofiber support. These images suggest that the failure mode observed in the PFIA membrane is chemical degradation. No significant thinning was observed in the other regions of the cell.

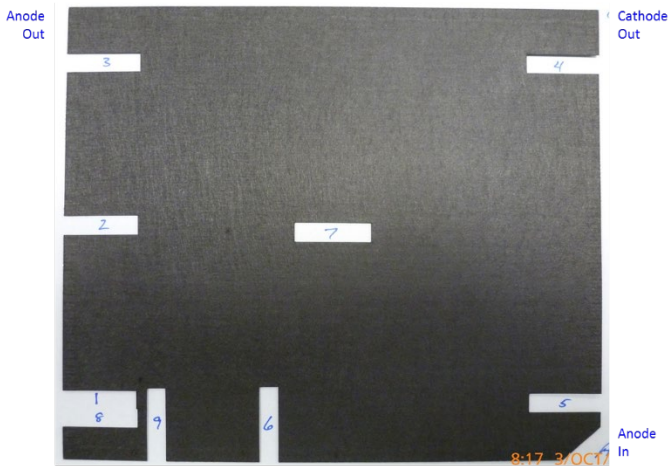

Figure 116. Punch-out regions from cell 7 for cross-section imaging.

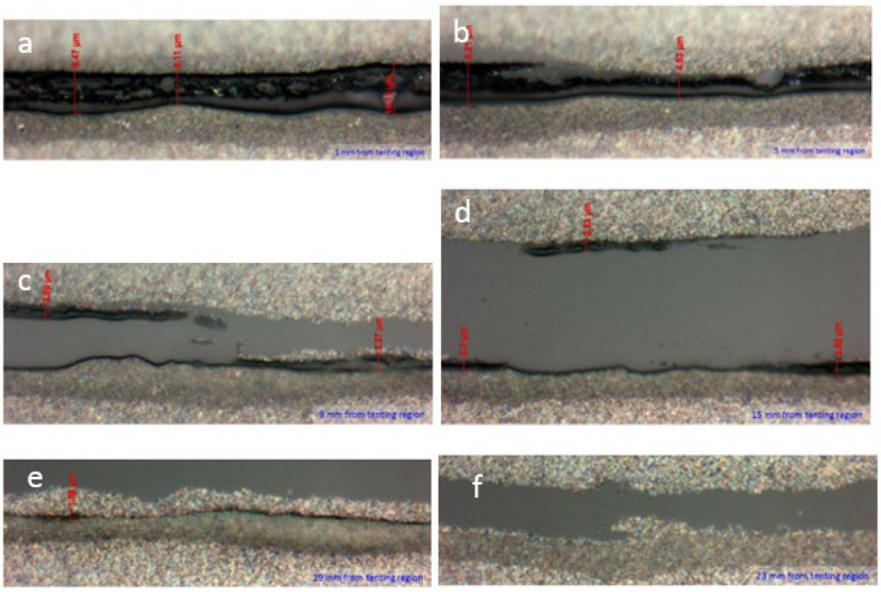

Figure 117. Cross-section images from cell 7 from samples 8: (a) 1 mm, (b) 5 mm, (c) 9 mm, (d) 15 mm, (e) 19 mm and (f) 23 mm from the subgasket edge

Task 6 Project Management and Reporting

The project was managed through regular teleconferences among team members and in-person meetings approximately one a year. A milestone driven project plan was followed and reported quarterly to the DOE. Both Go/No Go decision points were met at the ends of the fourth and eight quarters. Two no cost extensions were sought for this project resulting in a completion date of September 30th, 2017.

Conferences or Meetings Attended

1. Yandrasits, Michael; FC109 at DOE's Annual Merit Review in Washington DC on June 17, 2014
2. USCAR Fuel Cell Tech Team Presentation; "New Fuel Cell Membranes with Improved Durability and Performance" August 13th, 2014, Southfield, MI
3. "Electrospinning PFSA + PVDF Nanofibers for Fuel Cell Membrane Fabrication" R. Wycisk, J. W. Park, D. Powers, and P. N. Pintauro, 226th meeting of the Electrochemical Society, October 8th 2014, Cancun Mexico
4. Project Review Meeting with DOE Staff on November 4, 2014, St. Paul, MN.
5. Peter N. Pintauro, Ryszard Wycisk, and Jun Woo Park, "New Membrane Morphologies for PEM Fuel Cells" American Institute of Chemical Engineers Annual Meeting, Atlanta, GA, November 2014 (invited talk).
6. "Engineering a Proton Exchange Membrane for Automotive Fuel Cell Applications", Craig Gittleman, Advances in Polymers for Fuel Cells and Energy Devices Asilomar Conference Grounds Pacific Grove, California, February 8, 2015.
7. M. Yandrasits, "New Fuel Cell Membranes with Improved Durability and Performance" FC109 at DOE's Annual Merit Review in Washington DC on June 9th, 2015 http://www.hydrogen.energy.gov/annual_review15_fuelcells.html#membranes
8. Leslie Dos Santos, Jun Woo Park, Ryszard Wycisk, Peter N. Pintauro, Graeme Nawn, Keti Vezzù, Enrico Negro, Federico Bertasi, Vito Di Noto; *"Membranes from Blended Ionomer/PVDF Nanofibers: 1. PFSA/PVDF and PFIA/PVDF Fiber Spinning and Membrane Fabrication"* Fall ECS meeting Phoenix Arizona October 2015
9. D. M. Peppin, M. A. Yandrasits, A. S. Fochs ; *"Resistance Measurements for Multilayer Supported Membranes"* Fall ECS meeting Phoenix Arizona October 2015
10. M. Yandrasits *"New Fuel Cell Membranes with Improved Durability and Performance"* US DRIVE Fuel Cell Tech Team review October 7th, 2015 US DRIVE - Southfield, MI
11. Yandrasits, Michael; "*Fuel Cell Membranes based on Perfluorsulfonic Acids and Imides*", North American Membrane Society, May 23rd, 2016, Seattle WA
12. Yandrasits, Michael; FC109 at DOE's Annual Merit Review in Washington DC on June 7th, 2016
13. Mike Yandrasits "Perfluoro Imide Acid (PFIA) Ionomers for Fuel Cell Membranes" Gordon Research Conference Stonehill College, Easton, MA, August 8th 2016
14. Mike Yandrasits, Matt Lindell, Mike Kurkowski, Mark Schaberg "Ultra-Low EW Ionomers and Membranes for Fuel Cells" PRiME 2016, Fall ECS Conference, Honolulu Hawaii, October 5th, 2016
15. Mike Yandrasits, US DRIVE, Fuel Cell tech Team presentation, Nov 16th, 2016, Southfield Michigan.
16. Yandrasits, Michael; FC109 at DOE's Annual Merit Review in Washington DC on June 8th, 2017

Publications, Patents, or Presentations

1. “New Fuel Cell Membranes with Improved Durability and Performance” 2014 DOE Hydrogen and Fuel Cells Annual Progress Report
2. “New Fuel Cell Membranes with Improved Durability and Performance” 2015 DOE Hydrogen and Fuel Cells Annual Progress Report
3. D. M. Peppin, M. A. Yandrasits, A. S. Fochs *; “Resistance Measurements for Multilayer Supported Membranes”* ECS Transactions, 69 (17) 1105-1110 (2015)
4. “New Fuel Cell Membranes with Improved Durability and Performance” 2016 DOE Hydrogen and Fuel Cells Annual Progress Report
5. M. Yandrasits, M. Lindell, M. Schaberg and M. Kurkowski, *Electrochem. Soc. Interface Spring 2017* **26**(1) P. 49-53
6. “New Fuel Cell Membranes with Improved Durability and Performance” 2017 DOE Hydrogen and Fuel Cells Annual Progress Report

List of abbrivations

AC	Alternating Current
CW	Cross Web
DI	De Ionized
DW	Down Web
ePTFE	expanded poly(tetrafluoroethylene)
EW	Equivalent weight
Lb	pound
M	Molar
MASC	Multi acid side chain
MEA	Membrane electrode assembly
mm	millimeter
um	micrometer
MPa	Mega Pascal
MW	Molecular weight
nm	nanometer

NMP	N-methyl pyrolidone
PAI	poly(amide imide)
PEM	Proton exchange membrane
PEO	poly(ethylene oxide)
PFIA	Perfluoro imide acid
PPSU	poly(phenylene sulfone)
PVDF	poly(vinylidene fluoride)
SEM	Scanning electron microscope
STC-	Spinner to collector
THF	Tetra hydro furan

Acknowledgment

This material is based upon work supported by the U.S. Department of Energy's Office of Energy Efficiency and Renewable Energy (EERE) under the Fuel Cell Technologies Office (FCTO) under Award Number DE - EE0006362

Disclaimer

---

[i] Jiang, R., Mittelsteadt, C. K. and Gittleman, C. S., *J. Electrochem. Soc.,* **156** (2009) B1440-B1446

[ii] J. Zhang, H. A. Gasteiger, and W. Gu, *J. Electrochem. Soc*. 2013 160(6)

[iii] C.K. Mittelsteadt, H. Liu, Conductivity, Permeability, and Ohmic Shorting of Ionomeric Membranes, in: W. Vielstich, H. Yokokawa, H.A. Gasteiger (Eds.), Handbook of Fuel Cells: Advances in Electrocatalysis, Materials, Diagnostics and Durability, Volumes 5 & 6, John Wiley & Sons, Chichester, 2009, pp. 345-358

[iv] Dillard, D. A., Li, Y., Grohs, J., Case, S. W., Ellis, M. W., Lai, Y. H., Budinski, M. K., and Gittleman, C. S., "On the Use of Pressure-Loaded Blister Tests to Characterize the Strength and Durability of Proton Exchange Membranes". Journal of Fuel Cell Science and Technology, Vol 6 (3), pp. 031014-1 – 031014-8, 2009.

[v] S. Hommura, K. Kawahara, T. Shimohira, Y. Teraoka, *J. Electrochem. Soc.,* **155**, A29 (2008)

[vi] W. E. Delaney, W. K. Liu, *ECS Trans.,* **11**(1), 1093 (2007)

[vii] F. D. Coms, H. Xu, T. McCallum, C. Mittelsteadt , *ECS Trans.,* **50**(2), 907 (2013)

[viii] F. D. Coms, H. Xu, T. McCallum, C. Mittelsteadt , *ECS Trans.,* **64**(3), 389 (2014

[ix] C.S. Gittleman, F.D. Coms , Y-H Lai, "Membrane Durability: Physical and Chemical Degradation", in: M. Mench, E. C. Kumbur, and T. N. Veziroglu (Eds.), *Modern Topics in Polymer Electrolyte Fuel Cell Degradation*, Elsevier, 2011, pp. 15-88.